Publishing Office: *Department of Industrial Engineering, Engineering Faculty, King Abdulaziz University, P.O. Box: 80204 Jeddah 21589 Saudi Arabia*; Tel: +966 533 107628; Fax: +966 2 2486695.

Frequency: Journal of International Environmental Application & Science (ISSN 2636-7661) is published 4 times per year.

Aims and Scope: Journal of International Environmental Application & Science is dedicated to detailed and comprehensive investigations, analyses and appropriate reviews of the interdisciplinary aspects of renewable sources, municipal and industrial solid wastes, waste disposal, environmental pollution, environmental science and education, biomass, agricultural residues, energy sources, hazardous emissions, incineration, environmental protection topics included experimental, analytical, industrial studies, hydrological recycling, water pollution, water treatment, air pollution, gas removal and disposal, environmental pollution modelling, noise pollution and control. Suitable topics are also included regarding the efficient environmental management and use of air, water and land resources.

Publication information: Please address all your requests regarding orders and subscription queries to: *Dr. S. Dursun*, Environmental Engineering Department, Engineering Faculty, Selcuk University, Konya, TURKEY. Tel: +90 3332 2232057, Fax: +90 332 2410635, Mobil: + 90 536 5954591.
E-mail: jieas@jieas.com

Guide for Authors

Submission of Papers: Manuscripts for publication may be sent to the Editor-in-Chief, a member of the Editorial Board. Submission address is: Editor-in-Chief, Dr. S. Dursun, Environmental Engineering Department, Engineering & Natural Science Faculty, Konya Technical University, Konya, TURKEY. Manuscripts can also be sent to any member of the Editorial Board (see inside front cover for addresses). Although this journal is international in scope, all articles must be in the English language. Potential contributors whose first language is not English are urged to have their manuscript competently edited prior to submission. Papers should be written in the third person in an objective, formal and impersonal style.

Manuscript Preparation:

General: Manuscripts must be typewritten, double-spaced with wide margins on one side of white paper. Good quality printouts with a font size of 12 pt are required. The corresponding author should be identified (include E-mail address, Telephone and Fax number). Full postal addresses must be given for all co-authors. Two hard copies of the manuscript should be submitted by regular mail.

Abstracts: Each manuscript must be including a brief abstract and a short list of keywords.

Text: Follow this order when typing manuscripts: Title, Authors, Affiliations, Abstract, Keywords, Introduction, Main text, Conclusion, Acknowledgements, Appendix, References, Vitae and Figure Captions followed by the Figures and Tables. Pages should be numbered consecutively. The corresponding author should be identified with an asterisk and footnote.

Symbols and Units: All Greek letters and unusual symbols should be identified by name in the margin, the first time they are used. SI units should be used wherever possible, as recommended in ISO 1000 and BS 5555.

References: All publications cited in the text should be presented in a list of references following the text of the manuscript. In the text refer to the author's name (without initials) and year of publication (*e.g.* "since Dursun (1993) has shown that..." or "This is in agreement with results obtained later (Boddy, 1984)". For three or more authors use the first author followed by "*et al.*", in the text. The list of references should be arranged alphabetically by authors' names. The manuscript should be carefully checked to ensure that the spelling of authors' names and dates are exactly the same in the text as in the reference list.

References should be given in the following form:

Boddy L, (1984) The micro-environment of basidiomycete mycelia in temperate deciduous woodlands. In: *The Ecology and Physiology of the Fungal Mycelium* (Ed. by D.H. Jennings & A.D.M. Rayner), pp. 261-289. British Mycological Society Symposium 8, Cambridge University Press, Cambridge.

Dursun S, Ineson P, Frankland JC, Boddy L, (1993) Sulphite and pH effects on CO_2 evolution from decomposing angiospermous and coniferous tree leaf litters. *Soil Biology & Biochemistry* **25**, 1513-1525.

Ergas SJ, Schroeder E, Chang D, Scow K, (1994) Spatial distributions of microbial populations in biofilters. In: Proceedings of the *78th Annual Meeting and Exhibition of the Air and Waste Management Association*, pp. 19-24, Cincinnati, OH.

Hickey M, King C, (1988) *100 Families of Flowering Plants*. Cambridge University Press, Cambridge.

Littlejohn D, Wang Y, Chang S-G, (1993) Oxidation of aqueous sulphite ion by nitrogen dioxide. *Environmental Science & Technology* **27**, 2162-2167.

Illustrations: All illustrations should be provided in camera-ready form, suitable for reproduction (which may include reduction) without retouching. Photographs, charts and diagrams are all to be referred to as "Figure" and should be numbered consecutively in the order to which they are referred. They should be accompanying the manuscript, should be included within the text.

Tables: Tables should be numbered consecutively and given a suitable caption and each table should be included within the text. Footnotes to tables should be typed below the table and should be referred to by superscript lowercase letters.

Electronic Submission: Authors may submit electronic copy of their manuscript by e-mail or online submission on WEB site of the JIEAS. The final version of the manuscript should be submitted on floppy disk or CD. The electronic copy should match the hardcopy exactly. MS Word is recommended for software for article submission.

Proofs: Proofs will send to the author and should be returned 48 hours of receipt. Corrections should be restricted to typesetting errors; any others may be charged to the author. Any queries should be answered in full.

Subscription: Subscription for the issue contains author's article published in "*Journal of International Environmental Application & Science*" is €100.00 which will be sending to the corresponding author.Journal of International Environmental Application & Science (ISSN 1307-0428) is published since 2006. Subscription rates for a year are: Institutions: € 300.00 (four issues per a year) Individuals: € 150.00 (four issues per a year)

Copyright: Papers are considered for publication on the understanding that they have not been submitted to any other publisher. With the exception of review papers, the work described must be original and, generally speaking, not previously published. Authors who wish to reproduce illustrations that have been published elsewhere must obtain the permission of the copyright holder.

Correspondence: Papers should be sent to: *Dr. S. Dursun*, *Environmental Engineering Department, Engineering Faculty, Selcuk University, Konya, Turkey*. It may also be sent by e-mail to jieas@jieas.com in Microsoft Office Word 2007 format.

Website**:** *http://www.jieas.com;* ***E-Mail****: jieas@jieas.com, info@jieas.com*

"Journal of International Environmental Application and Science" is indexed in:
"**Global Impact Factor**, **EBSCO, CAS Source Index (A Division of the American Chemical Society), Index Copernicus, ProQuest, CABI, Ulrich's™ Serials Analysis System, SCIRUS, ArgosBiotech, NAAEE, The University of Queensland's Institutional, The NAL Catalog (AGRICOLA), WORLDCAT Catalog, LexisNexis, The National Library of Finland, National Library of Australia, Dergipark Turkey"** *Journal Indexing List.*

C O N T E N T S

J. Int. Environmental Application & Science, Vol. 14(4): 122-131 (2019)

Research Paper

The Use of Technology Opportunities with Terrestrial Laser Scanning Image for 3D Bridge Modelling and Monitoring

Ethem Bejko[1], Rrapo Ormeni[2,*], Gezim Gjata[3]

[1]*Department of Geodesy, Faculty of Civil Engineering, Polytechnic University of Tirana, Albania*,
[2]*Department of Seismology, Institute of Geosciences, Energy, Water and Energy, University of Tirana, Albania.*
[3]*Department of Geodesy, Faculty of Civil Engineering, Polytechnic University of Tirana, Albania*,

Received December 12, 2018; Accepted March 04, 2019

Abstract: 3D modelling and monitoring of engineering objects, based on the use of Terrestrial Laser Scanning image, provides ideal opportunities for the study, design and monitoring of these infrastructure works. The object of the study is the Bridge on Shkumbini River, an integral part of the existing railway infrastructure Rrogozhinë-Lushnje. This study reflects the necessity of using this technology due to the very high rates of development of instrumental measuring geodetic technologies, the need to increase monitoring rates, guaranteeing maximum operational safety in all projects where these facilities are applied. This method, due to its application in geodetic motorization technology, distance receiving information technology, without being required to provide the facility, digital photography technology through the digital cameras installed in them and due to advanced processing programs with photogrammetric graphics, results efficient, fast and incredibly accurate. As a result, the product offered entirely based on cloud-point pixels with a resolution of the millimetre order is a 3D format drawing rendered with maximum and complete dynamic accuracy needed for studies, monitoring, and rehabilitation projections of these very important infrastructural engineering works.

Keywords: *Modelling, Plotting, Monitoring, Digital Photo, Laser Image Scanner, Resolution, Points' cloud,*

Introduction

3D Laser scanning of existing bridge structures provide to civil engineering and contractors with very high accurate situations of bridges, it helps them for inspection, to determine exact measurements of bridge components and creating inspection models to planning, testing etc or of proposed building sites. The maintenance and reconstruction of these infrastructural engineering objects, of particular importance and directly related to the lives of their users, in order to keep under control, the functionality and the revitalization of these objects through the relevant specialists, had as a request to provide geodetic a finite graphic model as exact and real as possible. This requirement has been linked not only to the particular constructive elements in itself, of which these engineering objects are composed, but also to the geometry of their mutual positioning of these constructive elements in relation to one another. Often, this information becomes more important if offered in the dynamics of their changes in time. As a consequence of these high demands, the previous detection methods were not able to provide such information, important for the reconstruction or monitoring of existing bridges.

Also, given the long-time of their construction, around 70 years, these objects are of particular importance because they are directly related to the safety and quality of rail transport and not only that. The modernization of plotting methods through such numerical surveys creates a good basis for proper analysis, interpretation and action in the proper time with the ultimate goal to preserve the lives of users of these infrastructural engineering facilities. The instrumental technology used to accomplish these plotting processes ensures not only high precision, but also short plotting or monitoring time. These techniques guarantee the obtaining of complete dynamic information even in areas inaccessible to the operator as a result of applying them to laser rays technology (Remondino, 2011).

Compared to the classical modelling and monitoring method, which maximally provides a 3D model based on a number of reduced points and for a long-time realization, the modelling and monitoring method with the Terrestrial Laser Scanning image through specialized software provides

**Corresponding: E-Mail: rrapo55@yahoo.com; Tel: +355 68 26 28 492; Fax: +35542250601*

extra visual information with a resolution of millimetre order in a very short time. So we can say that the final graphical material is a "3D metric digital photography" in full dynamic. In this article we intend to look at how these techniques and technologies are applied.

Materials and Methods

The engineering object we have taken in the study belongs to the group of long-term facilities since it was built in the 1960s at the time of the railway line Rrogozhinë-Lushnje. It is a dual rail and motorway bridge about 270m long, 9.5m wide and 16m high, its beams are supported on two support walls and 7 piles. This object was constructed as an engineering solution for the passage of this Railway Line over the Shkumbin River, one of the country's largest rivers, which is distinguished for immediate changes in its hydropower regime. These changes give impacts to its bed, increasing erosion, increasing or decreasing the amount of alluviums and consequently increasing its destructive potential to engineering works built beside it. Added here and the impact of the factor on the inexcusable use of this bed for the production of construction inertia and climate changes which constitute an unforeseen destructive potential for these engineering works.

Probably the low level of maintenance necessarily requires the advancement of modelling and monitoring methods, programmed on the scientific basis of these objects, allowing for the control of the work and intervention to revitalize it within the technical design parameters. The cause for the monitoring and assessment of the sustainability of this bridge has been the collapse of 2008 in the motorway that was 70m in the eastern part of the bridge in the study (Fig.1, a, b, c), its seniority and not a very good current state of the structural formation of the river bed in which two of its main feet are incinerated.

This article we are introducing is an integral part of a geodetic monitoring project being implemented on this engineering work from the moment of the fall of the above-mentioned motorway bridge until now.

Figure 1. a) Position of the fallen bridge, **b**) Position of the bridge in the study, **c)** Incision of the feet at the riverbed

Data Base Admission

For the realization of this part of this geodetic project, we have been obliged to gather concisely existing graphic and engineering data from the archives of the respective institutions, old photos and drawings related to the realized and implemented project, topographic plans and maps, geological and tectonic information of the area in which this engineering object is built and continues to function.

From a geological point of view, the foundations of the bridge are located in Quaternary QH formations, which are represented by gravel deposits ranging from 3 to 20m in space. Deposits of the "Rrogozhina" formation are normal sequences with the "Helmesi" formation and have a sparse character. They are represented by sandblast, conglomerate and gravel thick and middle layer with silty clays and clay layers. The sandy areas are layered, mostly semi-sloping to compact. Conglomerates are an important element of this pack and meet in pockets, lenses of various sizes and mainly layers, from friable to poor cemented. The clays are silty clays type. The sandy areas are massive, mainly small grains, large grains, often sandy-gravels mixtures. Thickness in some sectors goes up to 1500m. Gravel is large from some mm to 5-6 cm of sedimentary and magmatic composition. Sandy areas are mostly compact to half compact. Clays, several times silty clays type,

compact with many carbonates, are beige in white colour. Conglomerates are massive with thick grain matrix. Within the conglomerates we find clay - silty clays type and sandstone layers. Thickness is up to 500 - 900 m (usually about 300 m). All this information has served us to build a full engineering and visual chronology, in order to better understand the situations that this object has been through for years. The process of acquiring the database for geodetic purposes has been carried out in two main phases:
A-Build a geodetic support base for the purpose of plotting and monitoring the object.
B-Numerical plotting of the object.
A- Construction of a geodetic supporting basement for the purpose of detecting and monitoring the object.
The ground geodetic support network is materialized as the main network, such as scanning stations and as a monitoring and plan marker. The network points are materialized on the ground steadily with concrete and the observations for the determination of their coordinates have been performed with post-position method with observation point ST-50 at not less than 3 hours observation (Figure 2).

Figure 2. Presentation of the geodetic supportive points used in the object.

Measurements for obtaining geodetic network coordinates (Fig.4) have been realized using the GNSS satellite system, through measurements with the TopCon GR-3 Satellite Receiver. This instrument, which uses DSP technology and a new UHF radio system, is designed to build strong geodetic bases using two satellite systems, GPS and GLONASS. The accuracy of the point coordinate designation (static method) is of the order:

3mm ± 5ppm in plan, 5mm ± 5ppm in height.

Below is an overview of the coordinates of the main geodetic network in the UTM Zone 34N system (Table 1).

Table 1. The coordinates of the main geodetic network in the UTM Zone 34N system.

Nr.	COORDINATES X(N)	COORDINATES Y(E)	QUOTA H
ST_10	4 546696.7010	386861.2260	22.5150
ST_50	4546860.1184	386944.5209	15.3354
ST_60	4546719.6199	386838.0197	15.9413
ST_70	4546736.7914	386926.3432	17.5180
ST_80	4547007.7102	386956.0703	22.8464
ST_90	4546904.0353	386883.8306	14.7719
ST_100	4546944.6994	386989.8299	14.0095

B- Numerical object plotting.
In 2008, when the first measurements were carried out at this object for plotting of the area and the bridge, as well as for its monitoring, were used classical measurement and geodetic monitoring methods based on the TopCon IS 203 instrument with the following parameters:

2mm + 2ppm distance designation accuracy,

Angle measurement accuracy 3”
together with the GNSS satellite system TopCon GR-3, the data of which is given below in Figure 3.

Figure 3. Presentation of the geodetic support network used.

The classical measurement technology used in this period, in this engineering object, provided an enough precision because the information received on the terrain does not have the required density of plotted points. The classical plotting method has a nearly zero chance of getting the necessary information on the characteristic points of the object or requires a lot of engagement in the staff and tools to make it possible to get this information. The cause is the necessity of physical presence at the desired point without which the method cannot function.

The necessity of a greater frequency of information on the points plotted in this type of object in order to obtain a more accurate form and metric relationship in the object, has conditioned us on the use of Terrestrial Laser Scanning image. With this instrument it is realized plotting through (point cloud), with a very high accuracy （Topcon, 2008). The frequency of the points is determined in function of the element and purpose of the survey. In our case, it has reached several million scanned points directly into the object. TopCon IS owns an excellent robotic technology; it has 2 integrated digital cameras that provide colour images in real time in two different positions (Fig. 6). Until now the data for obtaining a more fully model was reached with passive techniques based on images obtained through the photogrammetric method (Remondino & El. Hakim, 2006). The photogrammetric materials obtained offer realistic low cost, but the high quality of the 3Dato model requires well-known distances between points or some checkpoints on the terrain. (Barsanti et al, 2014) Active Techniques Using Classical Scanners (Vosselman, & Maas, 2010) somewhat meets some of the observed deficiencies in the first method since it provides accurate metric relationships between the plotted 3D points, but remains behind the inconvenience of receiving the visual information. As a result, in order to obtain a complete finishing material that can extract a lot of important engineering information; we thought the application of 3D modelling of the object based on the Laser Scanning Image technology. The result we obtain is a data matrix in space where the laser point coordinates reflected in the object can be calculated from this matrix equation:

$$\begin{pmatrix} X \\ Y \\ Z \end{pmatrix} = \begin{pmatrix} x0 \\ y0 \\ z0 \end{pmatrix} + d * \begin{pmatrix} vx \\ vy \\ vz \end{pmatrix}$$

Where:

X, Y and Z	are the coordinates of the point where the laser is reflected.
x0, y0 and z0	are the center coordinates of the instrument from which the laser measurement is performed.
vx, vy, and vz	are the components of the vectors of the laser's directions.
d	is the distance measured by the instrument at the point reflected in the object.

Exactly the systematic provision of this matrix makes this method effective (Boquera *et al* 2012) Thanks to this technique also based on the accuracy of angular measurements which is of the order of 3 "this instrument realizes the acquisition of information through a large and frequent number of points in the object with a resolution of up to millimetre order even for its specific constructive and damaged parts(Figure 5).

Figure 5. Scan times from a scanning temporary station.

Figure 7. Damaged structure

In this way, through scanned points cloud in the object with 4-dimensional coordinates (X, Y, H, Color), the problems previously displayed as a result of the application of the classical method were rebuilt as the object was plotted with a frequency of order points 3 -10cm for the whole object and up to 1mm for special elements such as the support of the beams on the bridge feet and supportive walls, in the vicinity of each other's beams on the same foot, as well as in the space between the beams .
There were 7 basic scanning stations and about 6 temporary scanning stations, with average plotting distance from object 5-50m. As a result of the intelligent measurement technology "iSCAN Feature Plotting", which creates the ability of the instrument to identify the characteristic points by means of previously taken pictures and then scan them. Also, Grid Scan technology provides an ideal opportunity to plot the object according to a cloud of distance points between the points previously set by us. Each pixel plotted in this way, based on the colour photos realized by the cameras that owns the instrument itself or from the external camera, you attach the fourth attribute that is related to the colour of the point. A summary overview of the main parameters of the realized scanning (Table 2).

Table 2. The main parameters of the realized scanning

Nr. of scans	Nr. Of scanned points	Scanning resolution	Scanning distance
7+6	24 861 214	1mm-3cm	5-50m

Elaboration of DATA-Acquisition of the 3D model

Numerical material obtained from terrain measurements is necessary to be filtered and purified from unnecessarily recorded information. The obtained file is the database that through the program TopCon Image Master Pro, a program specializing in photogrammetric processing and scanning, are used to describe desirable drawings up to the final 3D object model. Through this program, measurements are performed on the numerical photograph, ortho-picture is generated and 3D models are created using the images taken from the numerical cameras installed on the instrument. The program also performs 3D measurements from stereo images (Figure 6).

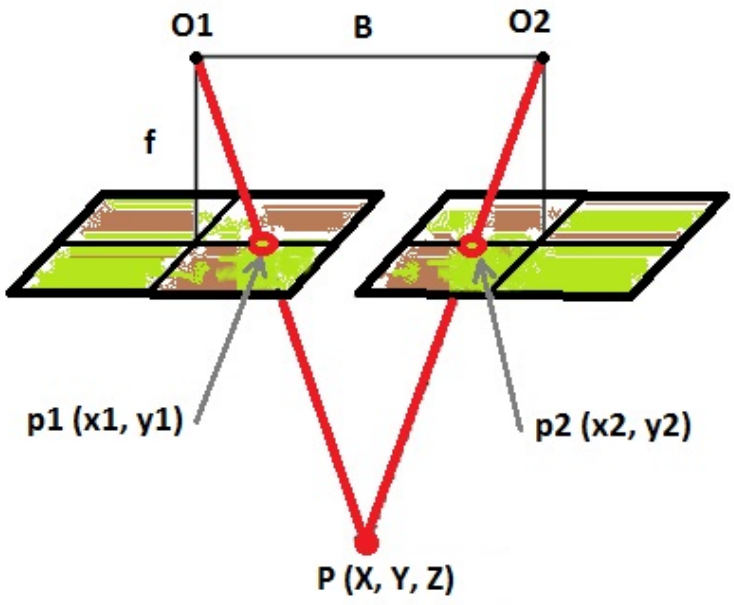

Figure 6. The basic concept for measuring 3D from the images is based on the stereo image.

The terrain resolution from 3D measurements on the image is given according to these formulas:

$$\Delta XY = \frac{H}{f} x\ \delta p$$
$$\Delta Z = \frac{H}{B} x\ \Delta XY$$

Where: Δ XY: planar resolution, Δ Z: height resolution, f: focal distance, δp: image resolution, H: photograph distance, B: photo base.

We can also create 3D panoramas. Image Master Pro has an important function that allows the creation of a unique object model from the image control point coordinates, calculated from terrain instrumentation points. Then it is also obtained the contour line, profiles, sections, triangular network and finally the 3D model of the plotted object. The material obtained along with ortho-photos can be stored in various graphics formats that can be edited by drawing programs like AutoCad or MicroStation, while the 3D model can be exported to VRML format. Registered and acquired files from the Master Pro Image Program also provide an excellent opportunity for use by GIS applications (ImageMaster 2008).

Final Numerical Product in 3D

We can say that what we have gained from the use of this method and technology is not compared with the previous classical methods of surveying and obtaining the final numerical material. The following figures show the 3D model of the object obtained with the classical modelling method, a bridge photo, and the 3D model obtained with the plotting earth scanning image method (Figures 7-9).

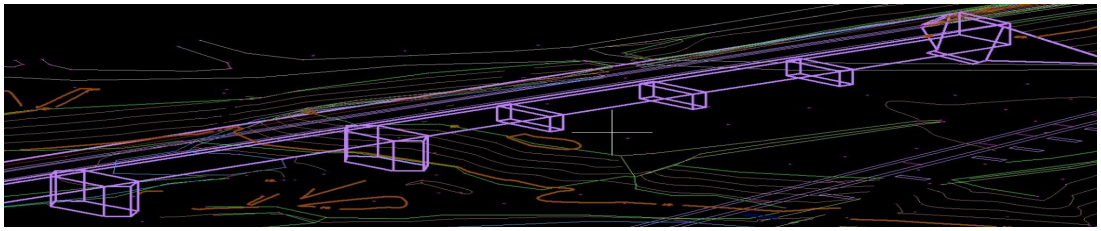

Figure 7. Isometric view of the bridge obtained according to the classical plotting method with Total Station and GNSS System.

Figure 8. Photo of the bridge.

Figure 9. Isometric view of the bridge obtained from the cloud of colored points with terrestrial laser scanner image.

Isometric view of the bridge obtained from the cloud of colored points with *terrestrial laser scanner.* The numerical products that we took from the 3D model obtained through the scanning program are different. Among them, we can mention the plan and longitudinal or cross-section of any kind of desirable position in the object (Figure 10).

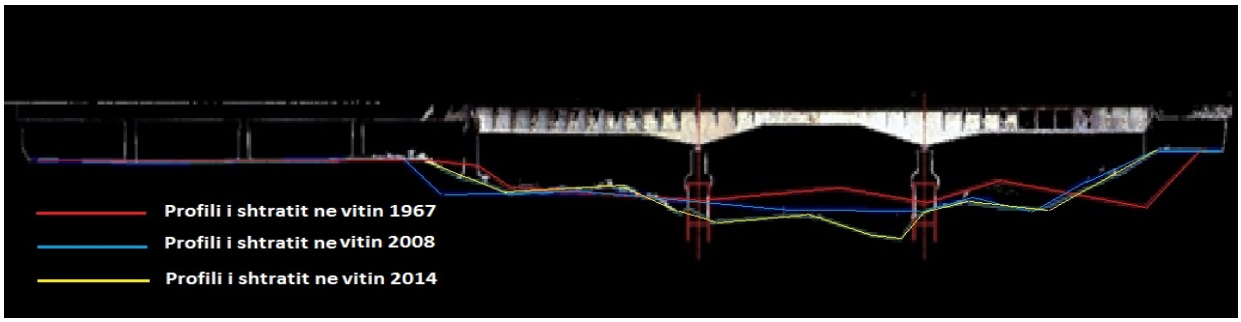

Figure 10. Longitudinal cut of the bridge.

Also accurate 3D and 2D models of important constructive engineering details were obtained with great value for analyzing the actual situation of the object, designing reconstruction projects or monitoring it with the aim of maintaining the engineering parameters of functioning, of vital importance (Figure 10).

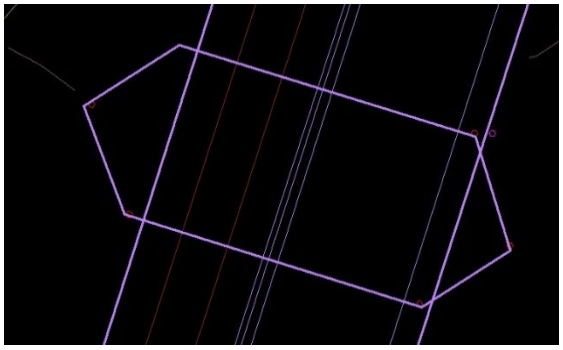

A. Top-view classic method of modelling

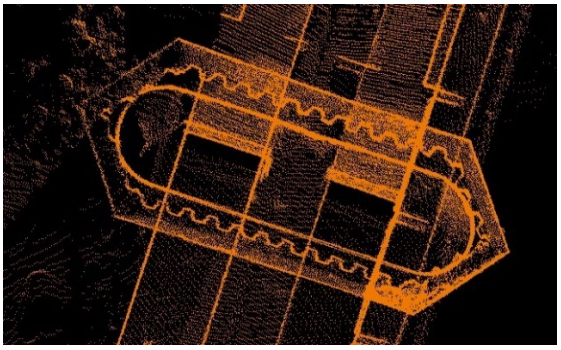

b. Top-view.laser scanner of modelling method

Figure 11.a, b. top-view presentation of the bridge's foot according to the classic method and ILST.

Due to the large number of points plotted in the object and the 3D modelling of the obtained surface, we can deduce up to the details in relation to the various constructive elements of the important object as for the design phase for its reconstruction as well and for the monitoring phase in order to keep within the engineering parameters of its functioning (Figure 12, 13).

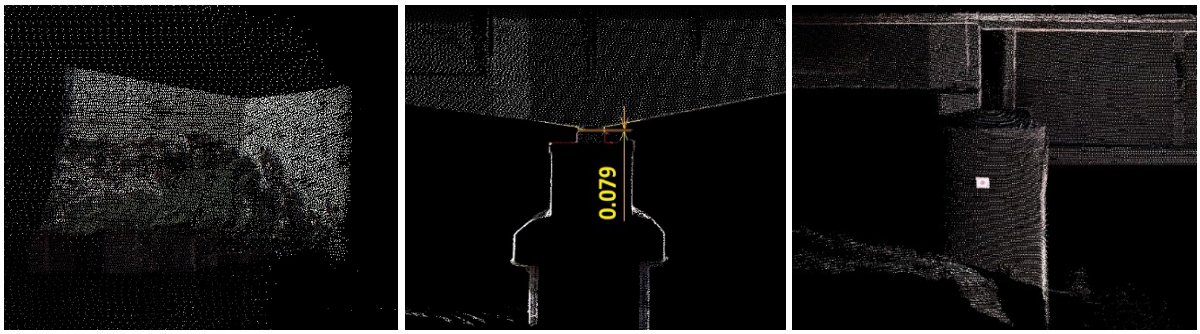

a. ***b.*** ***c.***

Figure 12. Important monitoring elements (a. Constructive damaged parts, b. Vertical monitoring brand, c. monitoring between the constructive elements).

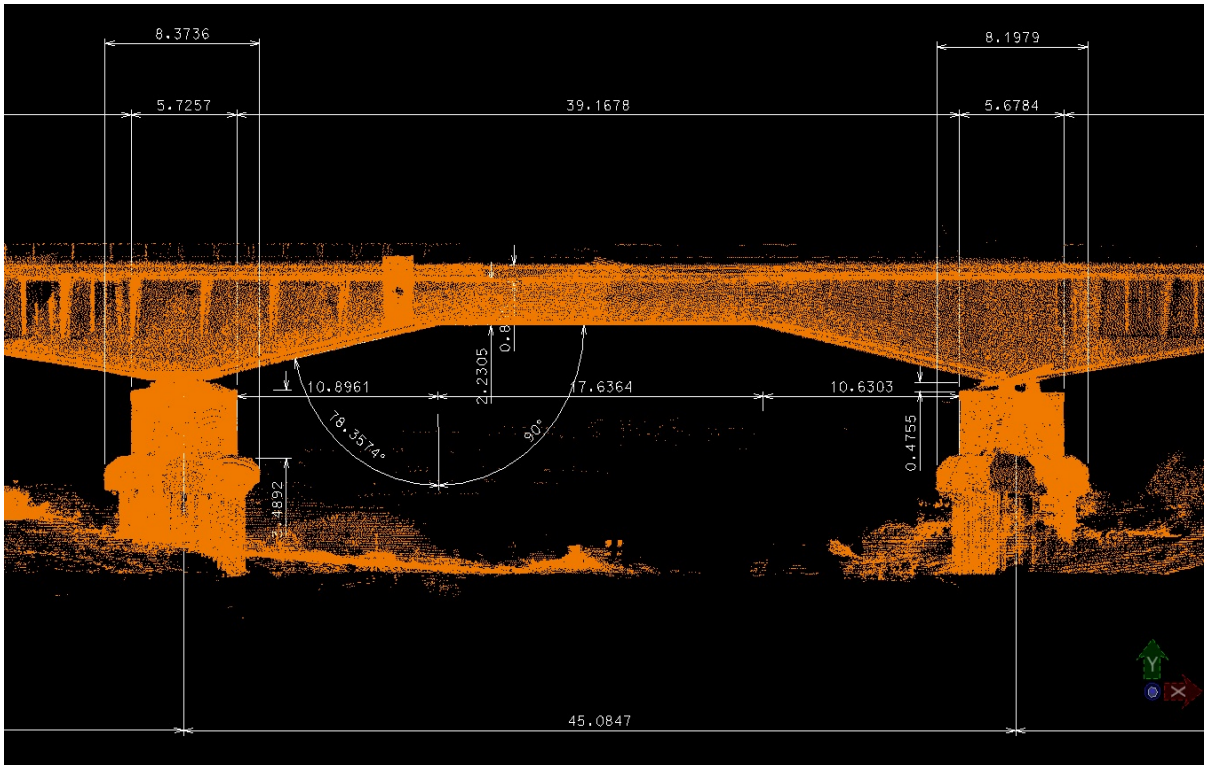

Figure 13. Presentation of some of the dimensions realized...

But the main product we have achieved to realize from this type of survey is to outline the 3D graphic model of the entire object, in which are clearly and accurate defined reciprocal metric relations between the constructive elements of the object itself, as in the developments in the plan and the altitude, also enriched with an accurate information of the object in terms of its visual state, i.e. the colour of each point (Figures 14, 15).

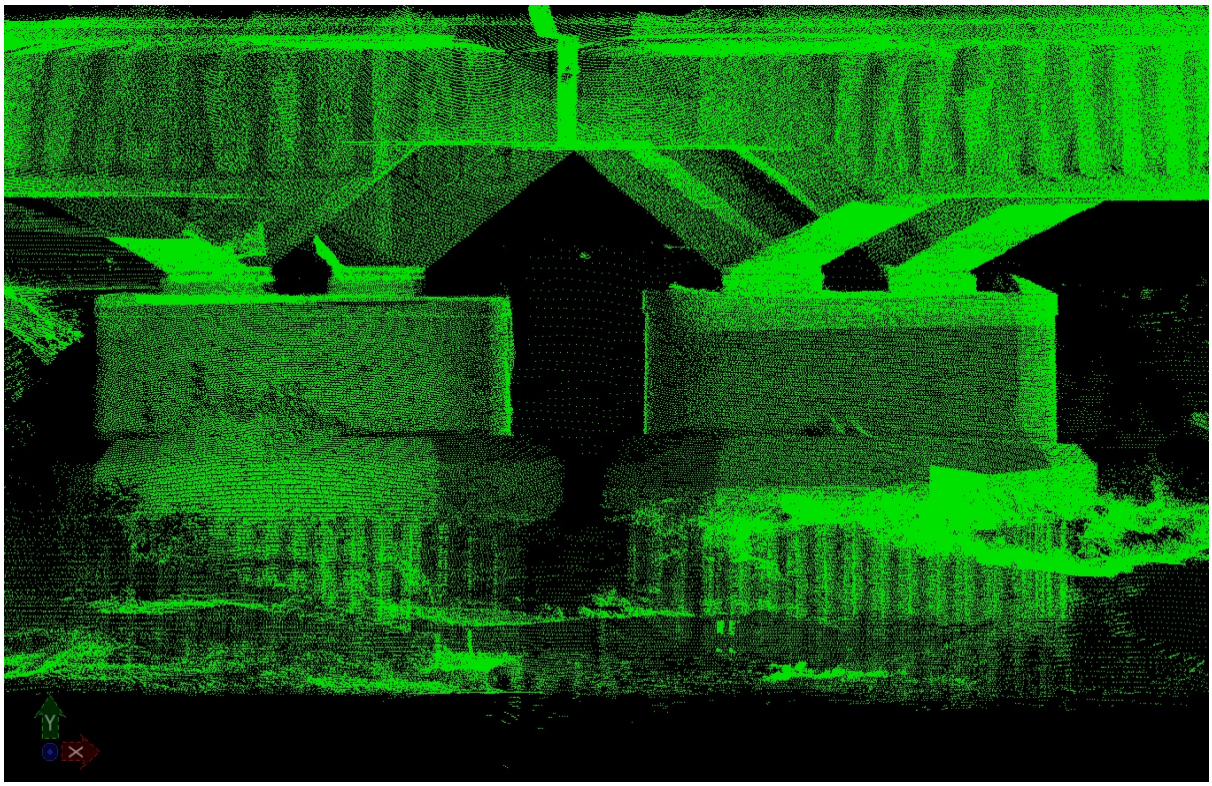

Figure 14. Right-view Presentation of the scanned object.

Figure 15. On the left, Object's Photographic Model, on the right Object's Scanned Model.

Conclusion

Using technology relevant engineering objects with Terrestrial Laser Scanning Image enables creation of a perfect object model as the metric point of view, both in terms of positioning and visualization. Thus, in a very short time and in large numbers, accurate graphics can be obtained with respect to any engineering details such as: different profiles, different horizontal cut-outs, and dimensions in each important part of the object as well as Real-time, detailed visual information in the same graphical model. This information is accurately provided up to 1mm resolution. Plotting this object with Terrestrial Laser Scanning Technology showed that this technology is a powerful tool for reducing the time of receiving terrain information while providing high resolution. This technology generates massive numerical data and therefore requires no programming and computer accessories with maximum parameters. The data obtained also serves to archive the current state of the object as well as to create the possibility of realization with high precision of reconstruction projects in order to maintain the quality and safety of the operation of these types of objects. The use of this plotting method also provides ideal, not applied before opportunities for monitoring these engineering objects.

References

Barsanti SG, Remondino F, Visintini D, (2014). 3D surveying and modeling of Archaeological Sites-Some critical issues. ISPRS Annals of Photogrammetry, *Remote Sensing and Spatial Information Sciences*, **II-5/W1**, 145-150

Boquera JH, Ríos JLD, García EMG, Esteve PN, (2012) Applications del Láser Scanner a la ingeniería civil. Publishing online.

ImageMaster (2008) Pro _Manual.pdf. Publishing online.

Remondino F, El-Hakim, S, (2006) Image-based 3D Modeling: A Review. *Photogrammetric Record*, **21**, 115, 269-291.

Remondino F, (2011) Heritage Recording and 3D Modelling with Photogrammetric and 3D Scanning. *Remote Sensing*, **3**, 1104-1138.

Tpcon (2008) IS2EngRev2.pdf". Publishing online

Vosselman G, Maas HG, (2010) *Airborne and Terrestrial Laser Scanning*. CRC Press Book.

J. Int. Environmental Application & Science, Vol. 14(4): 132-137 (2019)

Research Paper

Overview of Valley Types Formed by Göksu River (Mersin, Southern Turkey)

Ahmet Turan*

Konya Tecnical University, Faculty of Engineering and Natural Science, Geology Department, Konya, Turkey

Received August 28, 2019; Accepted October 25, 2019

Abstract: There are varius valley types in the rock groups formed from Ordovician to Miocene at the mouth of the Göksu River. Basement rocks in the area are coposed of mainly low resistant Miocene mudstone-shale-marl and high resistant chalkarenites and an important or lesser amount of low resistant Ordovician metamorfic rocks; medium to high resistant Upper Devonian-Upper Cretaceous clastic and carbonateceous rocks. The types of valley with wide and gentlement floor (broad valley) is dominant in the Langhian- Tortonian low resistant mudstone-shale-marl-clayey limestone in the Mut and surrounding area. These rock groups have cropped out in the ondulated morphology and as low dipping stratas. The deposition of the thick alluvial materials in the bottom of the Göksu River caused the developing of the many small-scale planes along the Göksu Valley. A canyon valley in 2.5 km long was also developed in the Miocene chalcarenites showing plentiful joints and strongly porous nature that were observed in the Evkafçiftliği and Kargıcak villages, in the central part of the study area. A very thin alluvial cover composed of pebles-sands and muds was deposited at the bottom of the canyon. The valleys developed on the Paleozoic-Mesozoic clastic and carbonateceous rocks in the main valley of the Göksu River at the surrounding area of the Değirmendere and Karakaya villages in the western part of the Silifke are narrow floor, anticline and cutting through type valleys. Terrace deposits are clearly observed in the main valley slopes while recent alluvial materials deposited in the bottom of the valley are in the shape of narrow and thin strips. The meander valley types can distinctly be distinguished in the Langhian-Tortonian mudstones-shales- marls and very wide spread and very thick Holocene alluviums of the Göksu delta at the center of the Silfke and surrounding area in the eastern-south-eastern part of the study area.

Keywords: *Valley types, broad valley, canyon valley, delta of the Göksu, Holocene alluviums,*

Introduction

Göksu River arises from the east of the Söbüçimen Yayla in 2900 m altitude, which is in the Geyik Dağı mountain between Gündoğmuş and Hadim towns of the Central Taurides Orogenic Belt (Demirtaşlı, 1984; Özgül, 1984; Figure 1). It reaches to the Mediterranean Sea in the Silifke Delta after taking a 245 km long road in a hilly terrain, extending NW-SE direction. Mut and Silifke towns are important settlements in the Göksu River route. Valley forms, which are the subject of study, are ground down of the Göksu River. In this part of the river, broad-based-flat, meandering, canyon, with narorw floor, cutting through and anticline valley types and different geological-geomorphological formations and structures are observed (Russel, 1954; Whitten and Brooks, 1972; İzbırak, 1977, 1979; Ardos, 1994; Yalçınlar, 1996; Hugget, 2010, Lutgens and others, 2013; Poort and Carlos, 1992). Broad-based–flat and meandering valleys are predominantly seen in Mut area. This areas characterized by less rugged, flat over which partially flattened hills, ridges and shallow cover as broad valleys. Narrow-based, canyon, cutting through and anticline valleys are more common around the Silifke district showing more high relief. This field consists of hills and ridges that has been deeply splited with Göksu main valley and its arm valleys.

Material and Method

The valleys in the ground down of the Göksu River have been studied in a detail. Stratigraphical and lithological properties of the rocks, which is hosting valleys, were carefully observed during the field works. Geometric dimensions, rock types and the position of strata (according to Roberts, 1989) in the

*Corresponding: E-Mail: aturan@selcuk.edu.tr; Tel: +90 332 223 2176; Fax: +90 332 2410635

valley slopes and valley floors were determined during the observational assessments. Scientific interpretation of the data from the study area has been done with this research. The valley types in the region were also distinguished based on the valley systematic. Important valley types in the study area and their characteristic properties will be present below as sistematically.

Figure 1. Location map and Google Earth image of study area.

1. Valleys with wide and gentlement floor (broad valley): They were observed in rather Mut region. The valley floor wide is between 500-1000 m. Valley slope is about 10-12 degrees. Langhian-Serravalian formations are located in the valley slopes. This type of valley has been observed in the rather Mut region. The wide of valley floor is between 500-1000 m. These formations are ductile and less rigid layers interbedded claystone- shale and marl-clayey limestone. Average strike and dip values of the layers in area about N 70^{o}W and 20-30^{o}E directions (Figure 2). Slope aspects are to southward and to northward at the northern and southern parts of the Göksu valley, respectively. Miocene rocks in this area therefore show a synclinal structure. The thickness of the Holocene alluvium at the bottom of the valley floor and broad-based valley is about 30-35 m. These alluvial sediments are composed of mainly calcareous well-rounded gravel (20%), sand (10-15%) and silt to clay sized materials (65-70%).

2. Meandering valleys: This type valley can also be seen around the Silifke although it is common in Mut region. The valley floors are 300-500 m wide. Meandering valleys were predominantly formed in the Middle Miocene rocks. The dips of slope in alluvium side, are between 10 and 12 degrees while in the autochthonous rock side, ranges from 20 to 25 degrees. The strikes of the layers are in variable directions in the valley slopes and the dips of the strata are also between 20 and 25 degrees (Figures 3, 4). Valley bottoms were filled with alluvium in the 10-15 m thick. 55-60% of these deposits are mostly well-rounded limestone gravel and sand, while 40-45% is made up of silt and clay sized materials.

3. Canyon valleys: Important canyon of the region is southwest of the village of Kargıcak and Evkafçiftliği of the Silifke towns. This canyon was developed in the Middle Miocene aged, medium-thick bedded, abundant fractured and strongly rigid clastic limestone. Here the wide of the valley floor is 40-50 m, and they have 90-100 m altitude and steep slopes. Strike and dip values of the strata

on the edge of the canyon is close to N 30-40 W/20NE position. The canyon in this region continues nearly 2,5 km NNW-SSE direction (Figure 5).

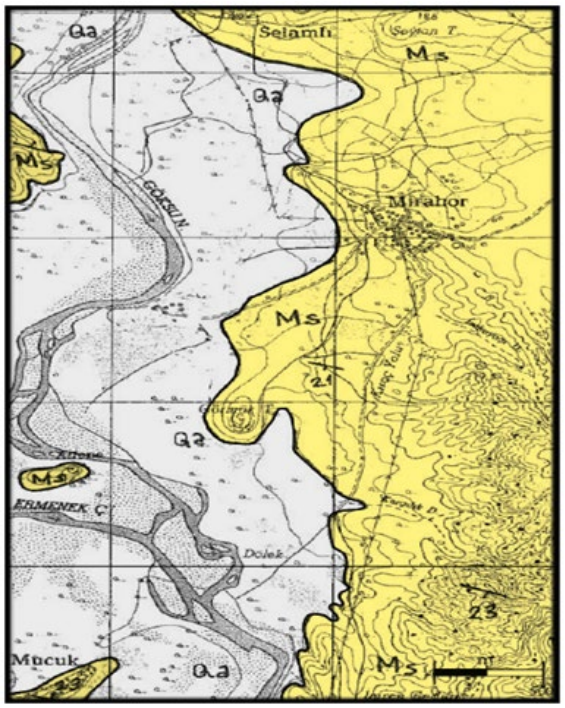

Figure 2. Broad valley and simplified geological map of the Suçatı village of Mut (Ms: Miocene aged claystone-shale and marls, Qa: Quaternary alluviums. The scale line is 500 m and geological map was modified from Akarsu, 1960 and Niehof, 1960).

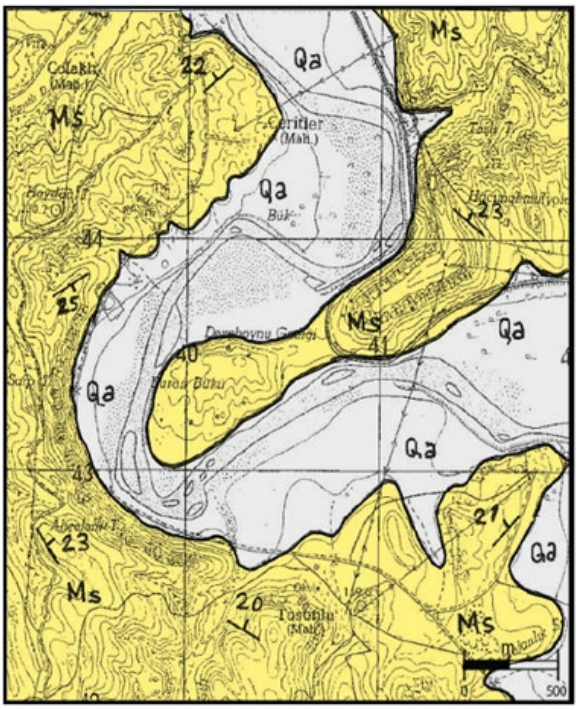

Figure 3 Meandering valley and simplified geological map of the Köselerli village of Mut (Ms: Miocene aged claystone-shale and marls, Qa: Quaternary alluviums. The scale line is 500 m and geological map was modified from Akarsu, 1960 and Niehof, 1960).

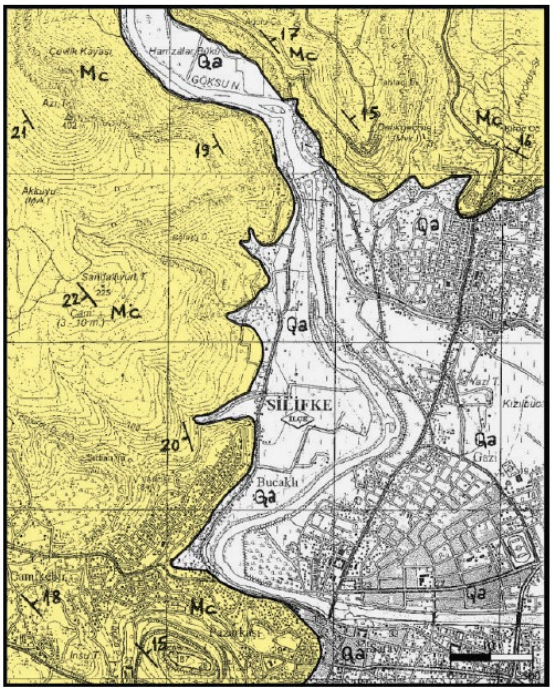

Figure 4. Meandering valley and simplified geological map of the Silifke city centre (M: Miocene aged claystone-shale and marls, Qa: Quaternary alluviums. The scale line is 500 m and geological map was modified from Gökten, 1976).

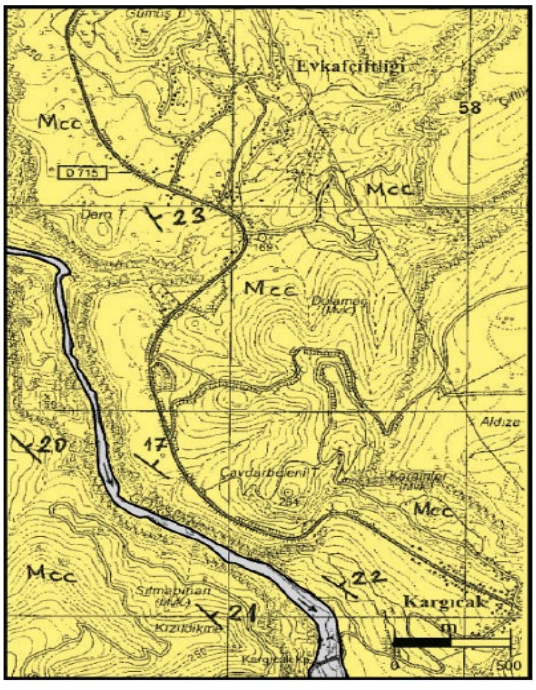

Figure 5. Canyon valley form and simplified geological map of the Kargıcak village of Silifke (Mcc: Miocene aged clastic limestones, Qa: Quaternary alluviums. The scale line is 500 m and geological maps were modified from Akarsu, 1960 and Niehof, 1960).

4. Cutting through valleys: Göksu River between Bilalli distric and Meteris gap passes through a narrow chute of Jurassic-Cretaceous recrystallized limestone showing medium-thick bedded, intense jointed and extremely high strength. In this part, the wide of the valley bottom is 30-35 m. Also inclinations of the slopes are 60-65 degrees. Development of the valley floor is unqualified and in the bottom of the valley, recent sand and gravel deposits with 0,5-1 m thickness can be seen. The valley floor of the splitting valley expands towards both the upstream and the downstream and it takes a similar position to narrow based valley (Figure 7).

5. Anticline valleys: Göksu River flows along the axis of an anticline that is trending E-W in the east of the study area near Bademhayat and Ekşiler villages. Here it cut Upper Devonian-Carboniferous rocks. In this part of the valley floor width is 200-300 m. The valley bottom is covered by alluvial deposits with 5-10 m thickness. This recent cover materials consist of gravels and sands that were well rounded and are in predominantly limestone-dolomite-quartzite composition. There are fossiliferrous limestone-dolomite-shale-quartzite layers cropped out on the slopes of valley. In the northern parts of the anticlinal axis, strike and dip of the layers are N 40-50 W/ 50 NE, and also in the southern parts of N 35-40' W / 45' SW (Figure 8).

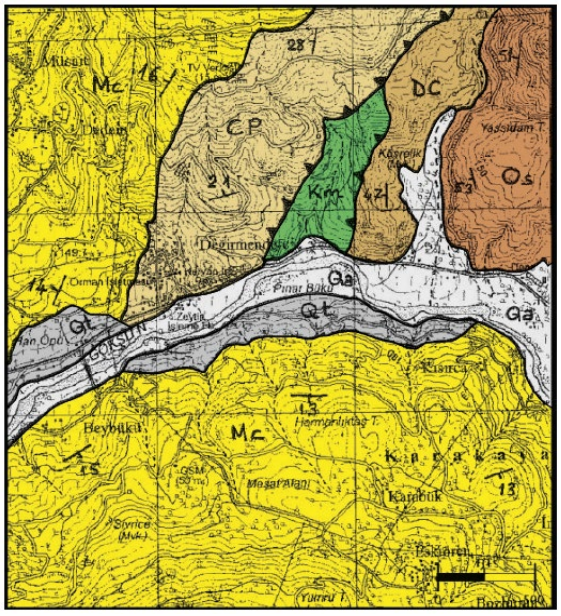

Figure 6. Narrow floor valley form and simplified geological map of the surrounding area (Os: Ordovician schist, DC: Devonian and Carboniferous detritics and carbonates, CP: Carboniferous and Permian sediments, JK: Jurassic-Cretaceous carbonates, Km: Upper Cretaceous ophiolitic melange, Mc: Miocene carbonates, Qt: Quaternary talus, Qa: Quaternary alluviums. The scale line is 500 m and geological map was modified from Turan, 1997 and Turan and others, 2005).

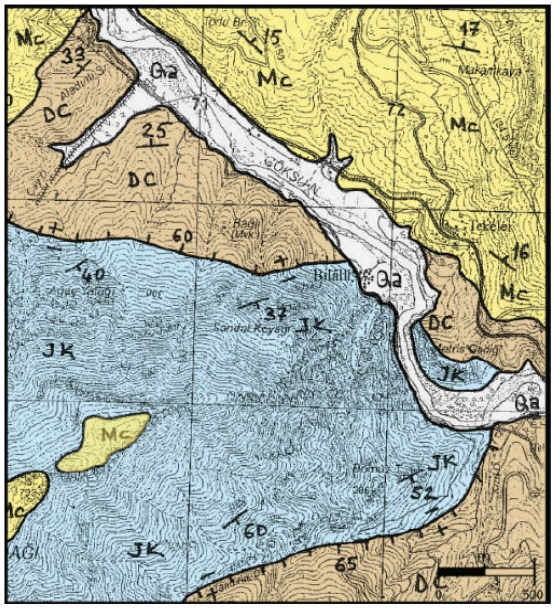

Figure 7. Cutting through and narrow floor valleys forms and simplified geological map of the Değirmende village of Silifke (DC: Devonian and Carboniferous detritics and carbonates, JK: Jurassic-Cretaceous carbonates, Mc: Miocene carbonates, Qa: Quaternary alluviums. The scale line is 500 m and geological map was modified from Turan, 1997 and Turan and others, 2005).

Conclusions:

Main type valleys observed in the valley of the Göksu River between Mut and Silifke towns have been identified by this study

1. Geometric shapes of the valleys located along the Göksu River and their dimensions were determined.
2. Lithology types and stratigraphic levels of the formations, in which the valleys in the area were developed, have been explained.
3. Information on the position of the layers in the formation of the valley (strike and dip values) were given.

4. Data about the width, thickness, particle size and composition of the recent alluvial materials on the bottom of the valleys were presented in the study.

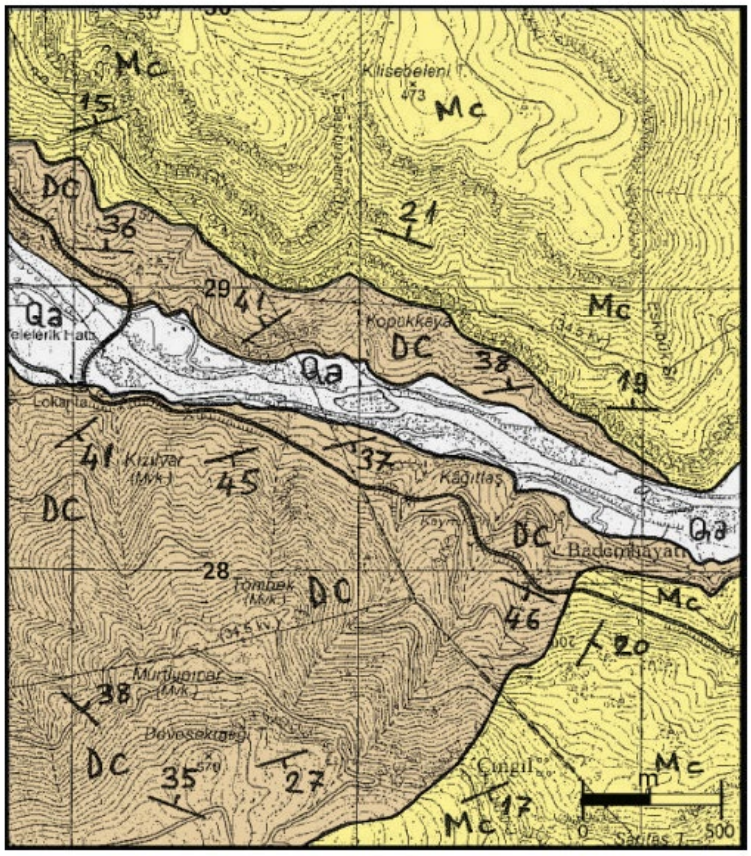

Figure 8. Anticline valley form and simplified geological map surrounding area (DC: Devonian and Carboniferous detritics and carbonates, Mc: Miocene carbonates, Qa: Quaternary alluviums. The scale line is 500 m and geological map was modified from Turan, 1997 and Turan and others, 2005).

References:

Akarsu İ, (1960) Geology of Mut Region; *J. Min. Res., Explor. Inst.*, **54**, 36-45, Ankara, Turkey

Ardos M, (1994) *Geomorphology Dictionary*; Çantay Bookstore, 326p., Istanbul, Turkey.

Demirtaşlı E, 1984, Stratigraphy and Tectonics of the Area between Silifke and Anamur, Central Taurus Mountains; *Inte. Sym. on the Geology of the Taurus Belt*, 101-118, Ankara / Turkey.

Dengiz O, (2010) Morphology, Physico-Chemical Properties and Classification of Soils on Terraces of the Tigris River in the South-east Anatolia Region of Turkey, *J.Agric. Sci.***16**. 205-212

Gökten E, (1976) Basic Rock Units and Miocene Stratigraphy of Silifke Region; Bulltein of the Geological Society of Turkey, **19**(2), 103-117, Ankara / Turkey.

Hugget RJ, (2010) Fundamentals of Geomorphology; Third Edition (Translation by Prof. Dr. Uğur Doğan); Nobel Offset Printing, 512p, Ankara / Turkey.

İzbırak R, (1977) Systematic geomorphology; Erol and Offset Printing, 327p, Ankara / Turkey.

İzbırak R, (1979) Analitic and General Geomorphology; Language-History-Geography Faculty of Ankara University Printing, 468p, Ankara, Turkey

Lisle RJ, (2004) Geological Structures and Maps A. Practical Guide. Cardiff University. Elsevier Butterworth-Heinemann, Linacre House, Jordan Hill, Oxford.

Lutgens FK, Tarbuck EJ, Tasa D, (2013) Essantials of Geology; Eleventh Edition (Translation by Prof. Dr. Cahit Helvacı); Nobel Offset Printing, 547p, Ankara, Turkey.

Niehof W, (1960) Report on Revision result of map sheet number Mut 126/1; Mining Research Exploration Institude, Report Number:3390, Ankara, Turkey

Özgül N, (1984) Stratigraphy and tectonic evolution of the Central Taurides; Intern. Symp. of the Geology of Taurus Belt, 77-90, Ankara / Turkey.

Poort JM., Carlos RJ, (1992) Historical Geology Interpretations and Applications; Macmillan Publishing Company, 241p, New York, U.S.A.

Roberts JL., (1989) Geological Structures; The Macmillan Press Ltd. 250 p., London, UK.

Russel RJ, (1954) Alluvial Morphology of Anatolian Rivers; Assoc. Amer. Geo. 44:361-391.

Turan A, (1997) Stratigraphy of Pre-Miocene Tectono-stratigraphic Units along the Göksu Valley; Geosound Earth Sciences Magazine, Number:30, 855-874, Adana / Turkey.

Turan A, Küpeli, Ş, Deli A, (2005) Pre-Miocene Geological Evolution of the Area among Karakaya-Değirmendere-Şeyhler (West of Silifke: South Turkey); *J. Faculty Engin. & Archit. Selçuk Un.*, **20**, 47-60.

Whitten DGA, Brooks JRV, (1972) Dictionary of Geology; Penguin Books Ltd. Registerted Offices, 495p., Middlesex, England.

Yalçınlar İ, (1996) Sutructural Geomorphology; Özeğitim Offset Printing, 480p, Konya / Turkey.

J. Int. Environmental Application & Science, Vol. 14(4): 138-144 (2019)

Research Paper

Conducting Hydrological Modelling in Mat River

Klodian Zaimi [1*], Sergio Fattorelli[2], Francesca Ramazzina[2]

[1]*Institute of Geosciences Energy Water and Environment, Tirana, Albania;* [2]*BETA Studio srl, Padova, Italy*

Received October 14, 2019; Accepted November 14, 2019

Abstract: Ulza Lake catchment is part of the Mat River basin and has a hilly and partially mountainous watershed. From the hydrographic point of view, it is distinguished for a dense network of watercourses, especially in the middle and lower part where ultrabasic formations are dominant. In order to analyse seasonal and annual water balance for Ulza Lake watershed, the HEC HMS hydrological rainfall-runoff model has been implemented in the Mat river. The hydrological model used as input daily hydrometeorological observed data for precipitation, discharge, and temperature in the period 2002-2011. The method used for transform was SCS Unit hydrograph and for the routing was used Muskingum Kinge. The observed meteorological data was validated through a basic integrity test for the identification of anomalous values. Ulza Lake catchment has been divided into 13 sub-basins in order to better calculate the inflow. The hydrological historical data in the period 2002-2011 was used for calibrating the model. HEC HMS result data series for Ulza Lake were processed and plotted using different methods.

Keywords*: hydrological model, water balance, discharge, rainfall-runoff, inflow*

Introduction

According to the geographical classification of Albania, the Mat River watershed belongs to the North Central Highland. The Mati River originates from Mount Kaptinës and has a hilly and partially mountainous watershed. The upper part of the Mati River watershed extends from the southern side of the Dhoksit Mountain and from Kaptinës Martaneshit to Klos. The Mat River watershed is bordered on the east and southeast by the Drini I Zi River basin, on the south and southwest by the Ishëm River Basin and on the north by the Fan River Basin. From the hydrographic point of view, it is distinguished for a dense network of watercourses, especially in the middle and lower part where ultrabasic formations are dominant. The watercourses that flow into the Mat River mention the Zalli i Liçonës, the Bejnit stream, and the Lusës (Kurdarise) stream from the right flowing stream, while the left flank mentions the Dishës, Xibri, Darsi and Batrës streams (IHM, 1984). The basin relief is hilly, and the valley height varies from 50 m to 700-800 meters. Elevations from 200 to 400 meters are predominate. The smallest heights are in the west while the highest is east of the basin. Mat river valley lies between 125-200 meters and 200-400 meters. According to the climate classification of Albania, the study area is part of the Northern Hilly Mediterranean climate zone. The average annual temperatures vary between 11ºC and 14 ºC, while the absolute minimum varies from -7ºC to -9ºC and in cold winters from -13 -C to -17ºC. The average temperature of January due to the relief forms is in the range of 2-4 ºC. Ice days vary between relief forms between 30 and 40 days and occur from November to March but can also be observed from October to mid-April. The annual rainfall varies from 1200mm to 1400mm which is approximately what is the average of the territory of Albania. Snow is mostly observed during November-March (IHM, 1985). The average maximum layer of snow reaches 15 to 30 cm. Ulza lake catchment basin is vulnerable to climate change hazards, particularly droughts and floods. Human pressure has adversely affected natural ecosystems causing significant erosion and sediment transport to the lake. A hydrological model, validated and calibrated, has been built to estimate the water resources for the Ulza Lake watershed.

The surrounding of Ulza lake watersheds is composed of different ecosystems (forests, lake ecosystem, water sources and rivers, pastures and agricultural land). The ecosystems provide services such as the natural cycles of nutrients, soil formation, and primary production, but are under considerable human pressure. They play an important role in carbon sequestration, water quality, biodiversity values, etc. Direct services are also provided, such as drinking water, firewood, medicinal plants, soil protection, fish, etc.

**Corresponding: E-Mail: klodianzaimi@yahoo.com; Tel: 00355672155234;*

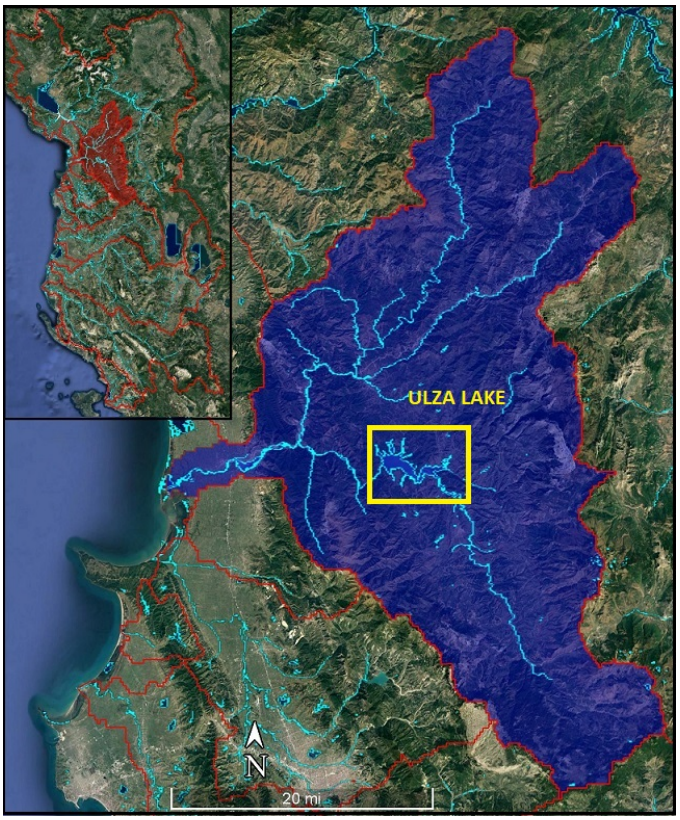

Figure 1. Mati river catchment and Ulza Lake

Materials and Methods

The hydrological conditions of the Mat River watershed in Ulza lake, depending primarily on climate, topography, geology, hydrology, soil type, and vegetation. In the study area, a series of streams and streams flow into the Mat River. From the Vasha Bridge to the Shoshaj Bridge, over the Mat River, the streams flow mainly from the left bank. As we said above, the hydrography of the Mat River consists of many streams, that characterize the terrain's orography. In the dry season of the year, most of the streams are dry, while in winter they have torrential flows. During the maximum discharges, they descend to the lower area Klos, Sucit, and Plezhës fields, eroding the banks of their valleys. Rainfall and snow are the main sources of water accumulation in the Mat River watershed. The average rainfall ranges from 1200 to 1400 mm per year, but in the upper parts of the basin, the rainfall has reached 2500-2700 mm in some years (IHM, 1985). About 82% of the annual precipitation falls in the colder year and 14% falls in the warmer year. In June, which is an intermediary month, falls 4% of the precipitation. The water supply of the Mat River and its tributaries in the warm season of the year is made of groundwater coming from limestone formations such as the case of the Benit stream flowing into the right bank of the Mat River in the town of Klos (IHM, 1984).

Table 1 Average monthly and annual temperatures

Stations /Months	1	2	3	4	5	6	7	8	9	10	11	12	Average
Fshat Klos	6	6.2	8.3	11.7	16	13	23	23	19	13	10	6.1	12.9
Bize	3.2	-2.4	0.2	4.5	10	12.5	16.4	14.3	12	6.7	2.9	-1.4	5.9
Lena Martanesh	1	2.3	4	8.4	13.9	16.6	19.1	19.1	15.6	10.8	6.8	2.6	10
Burrel	5.5	5.9	8.3	11.7	16.1	20.3	22.7	23	19	12.7	9.5	6.2	13.4
Kurbnesh	0.4	2	4.6	8.9	13.5	17.4	19.9	20	16.6	11.4	7.1	3	10.4

In this river, three hydrological stations in Shoshaj, Klos, and Darsi stream have been operating. For the purpose of the study, the water flow analysis of the Mat River at the Shoshaj site was initially conducted. It is noted that the catchment area of the Mat River at the Shoshaj site is 646 km^2 (IHM, 1984). While at the entrance to Ulza Lake it reaches 704 km^2. At the Ulza hydropower dam, the catchment area is 1186 km^2, which in addition to the lake itself (16 km^2) includes a series of important watercourses such

as the Uraka River (257.6 km^2), the Kurvaj River (61 km^2), the stream of Shuterise, etc. From the Ulza Dam to the Shkopet Dam the watershed extension is relatively small and the total area up to the Shkopet Dam reaches 1243 km^2.

Table 2 Average monthly and annual precipitation

Stations /Months	1	2	3	4	5	6	7	8	9	10	11	12	Annual
Burrel	142	130	116	107	86	60	42	47	78	113	161	159	1240
Fshat Klos	159	154	128	115	108	73	47	70	95	118	185	181	1430
Bize	191	170	153	147	137	79	50	67	134	185	240	194	1750
Q. Bulqize	130	136	108	104	84	68	38	60	60	100	172	173	1230
Martanesh	178	161	140	132	117	79	43	51	88	141	226	196	1550
Kurbnesh	129	124	138	131	97	62	76	101	136	136	189	170	1500

Table 3 Monthly average discharges in Shoshaj hydrological station

Station	1	2	3	4	5	6	7	8	9	10	11	12	Annual discharge
Mati Shoshaj	36.9	37.5	36.8	38.8	30.8	15.4	7.3	5.2	6.9	10.7	29.8	40	24.7

In order to provide seasonal and annual water balance for Ulza Lake watersheds, the hydrological rainfall-runoff model has been implemented. The software chosen was the open-source HEC-HMS of the US Army Corps of Engineers (USACE), which is designed to simulate the complete hydrologic processes of dendritic watershed systems, including the erosion and sediment transport. The Hydrologic Modeling System (HEC-HMS) is one of the most widely used simulation tools developed by the U. S. Army Corps of Engineers Hydrologic Engineering Center (HEC) and is designed to simulate the rainfall-runoff processes of the drainage basin. A soil moisture accounting algorithm has been used to evaluate the performance of the HEC-HMS model for many river basins. The software includes many hydrological analysis procedures such as event infiltration, unit hydrographs, and hydrologic routing. HEC-HMS also includes procedures necessary for continuous simulation including snowmelt, soil moisture accounting, and evapotranspiration. Advanced capabilities are also provided for gridded runoff simulation using the linear quasi-distributed runoff transform (ModClark). Supplemental analysis tools are provided for model optimization, forecasting streamflow, depth-area reduction, assessing model uncertainty, erosion and sediment transport, and water quality USACE (2018). The software features a completely integrated work environment including a database, data entry utilities, computation engine, and results reporting tools. A graphical user interface allows the user seamless movement between the different parts of the software. Simulation results are stored in HEC-DSS (Data Storage System) and can be used in conjunction with other software for studies of water availability, urban drainage, flow forecasting, future urbanization impact, reservoir spillway design, flood damage reduction, floodplain regulation, and systems operation. The software includes many traditional hydrologic analysis procedures such as event infiltration, unit hydrographs, and hydrologic routing, and includes procedures necessary for continuous simulation including evapotranspiration, snowmelt, and soil moisture accounting USACE (2018).

Results and Discussions

The physical watershed for Ulza Lake is represented in the basin model. Hydrologic elements are added and connected to one another to model the real-world flow of water in a natural watershed. In this study case the elements used to describe the watersheds are:

a. Sub-basin used to represent the physical watershed with given precipitation.
b. The outflow from the sub-basin element is calculated by subtracting precipitation losses, calculating surface runoff, and adding base-flow.
c. Reach used to convey streamflow in the basin model.
d. Inflow to the reach can come from one or many upstream elements.
e. Outflow from the reach is calculated by accounting or translation and attenuation.
f. Channel losses can optionally be included in the routing.
g. Junction used to combine streamflow from elements located upstream of the junction.
h. Reservoir used to model the detention and attenuation of a hydrograph caused by a reservoir.

Table 4 The mathematical models used in Ulza Lake catchment

Sub-basin	Surface	Simple
	Loss rate	Soil moisture accounting
	Transform	SCS Unit hydrograph
	Baseflow	Recession
Reach	Routing	Muskingum Kinge

Most hydrologic elements require parameter data so that the program can model the hydrologic processes represented by the element. The soil moisture accounting loss method uses three layers (soil, groundwater 1 and groundwater 2) to represent the dynamics of water movement in the soil and should be used with the canopy and surface methods. The soil layer will dry out between precipitation events as the canopy extracts soil water. The surface layer holds precipitation and allows it to infiltrate after the rain has stopped. Infiltration is generally reduced if no surface method is selected. The soil layer is subdivided into tension storage and gravity storage. Groundwater layers are not designed to represent aquifer processes but are used for representing shallow interflow processes (USACE 2018).

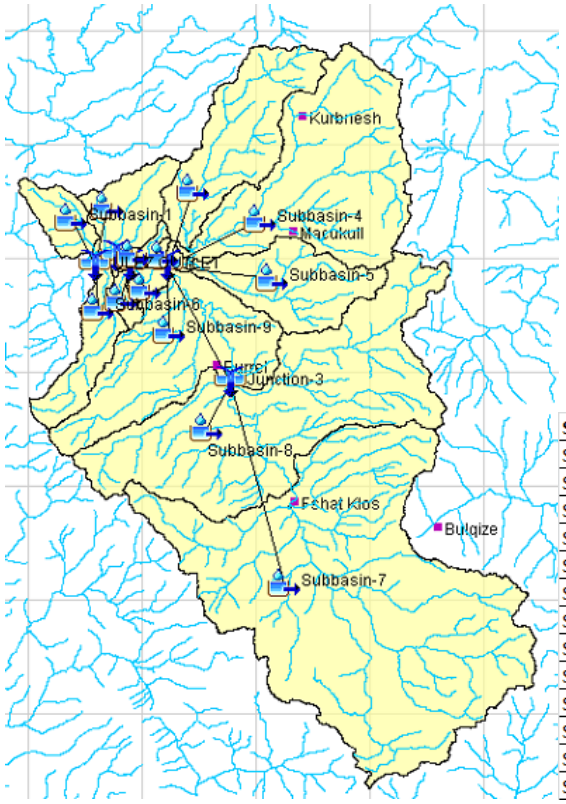

Subbasin ID	Area [km²]
Subbasin-1	20.74
Subbasin-10	6.66
Subbasin-11	7.26
Subbasin-12	2.86
Subbasin-13	8.9
Subbasin-2	33.81
Subbasin-3	84.82
Subbasin-4	168.08
Subbasin-5	62.79
Subbasin-6	33.87
Subbasin-7	438.44
Subbasin-8	237.85
Subbasin-9	116.48

Figure 2. Mat Basin model for Ulza Lake in HEC-HMS hydrological model

The initial condition of the soil is specified as the percentage of the soil that is full of water at the beginning of the simulation. It was assigned equal to 85% from calibration. It affects only the very first period of the simulation. The maximum infiltration rate sets the upper bound on infiltration from the surface storage into the soil: it has been set equal to 10 mm/hr (sandy soils). The percentage of the sub-basin which is subject to direct runoff (Impervious) was assigned equal to 30% from calibration. Soil storage represents the total storage available in the soil layer. Tension storage specifies the amount of water storage in the soil that does not drain under the effects of gravity. Percolation from the soil layer will occur whenever the current soil storage exceeds the tension storage. Water in tension storage is only removed by evapotranspiration. Tension storage must be less than soil storage. The soil percolation sets the upper bound of percolation from the soil storage into the upper groundwater. Groundwater 1 storage represents the total storage in the upper groundwater layer USACE (2000). The groundwater 1 percolation rate sets the upper bound of percolation from the upper groundwater to the lower groundwater. The groundwater 1 coefficient is used as the time lag on a linear reservoir for transforming water in storage to become lateral outflow. The lateral outflow is available to become base flow.

Similarly, for Groundwater layer 2, not used in this model. Parameters have been set based on the manual's range and calibration results. The available meteorological observational data for the daily precipitation and daily maximum and minimum temperature in the period 2002-2011 are meteorological stations: Macukull, Kurbnesh, Bulqize, Shengjergj, Fshat-Klos, and Burrel. It is important to underline that the application of the bias correction methods based on observed dataset shorter than 30 years period doesn't permit to completely remove the bias (Maraun and Widmann, 2018), in particular for what concerns the values in the tails of the distributions. Based on this concept, the observed data was validated through a basic integrity test and a test for the identification of anomalous values (Ray et al., 2016). On the base of these tests, the initial dataset was reduced. However, the completeness test over the whole period considered was passed (at least 75% of data are available) for the period 2002-2011 for each variable and station examined. This preliminary phase is essential for the evaluation of the bias and the following bias correction application. In order to verify how many observational data are not available, the percentage per year of the missing data for each station is calculated for each variable considering the observed period 2002-2011. The most different behavior can be noted for the Shengjergj station in 2002, where a very low value of the annual precipitation is reported; however, this can be explained with the very low number of data available during this year (missing data are about 79%) Furthermore, the generally low value of the annual precipitation for Bulquize and Burrel stations depends on the presence, in the observed data, of long periods of absence of precipitation. Also, the maximum and minimum temperature is characterized by a low annual value for the Shengjergj station in 2002 with respect to the other stations due to the presence of about 81% of missing data (from January to the middle of October) during this year. Moreover, for the same reason, a high value of the annual maximum and minimum temperature for Kurbnesh station in 2010 and above all in 2011 with respect to the other stations is reported. In fact, in those years, both variables are characterized respectively by about 25% of missing data (generally in February, November, and December) in 2010 and 28% of missing data (from January to the middle of April) in 2011.

Definition of the initial storage and cover factor in Ulza Lake

CORINE Land Use classes have been grouped in 8 families to which has been assigned a unique initial storage value (sum of canopy and surface storage) and cover factor value, based on literature data and calibration results. Ulza Lake catchment has been divided into many sub-basins in order to better calculate the inflow at the reservoir. The following Table 5 summarizes the main parameters adopted for each sub-basin, following the calibration of the model. Considering the simulated time period, the daily time step of the input data (precipitation, temperature) compared to the time of concentration of the flow (less than 1 day), the element reach is not included in the model because it would not influence the result but only extend the time of the simulation.

The hydrological historical data in the period 2002-2011 from Shoshaj station and data measured from Ulza hydropower operator was used for calibrating the model. Figure 3 shows the model calibration results for Ulza Lake, comparing the simulated water flow and measured water flow at the lake (recalculated from the available data). HEC-HMS result data series were processed and plotted using different methods (temporal distribution, aggregated distribution, probability density distribution, etc.). The following Figure 3, and Table 6 show the analysis of the hydrological model results for Ulza Lake in terms of simulated annual flow (daily values) using rainfall and temperature dataset.

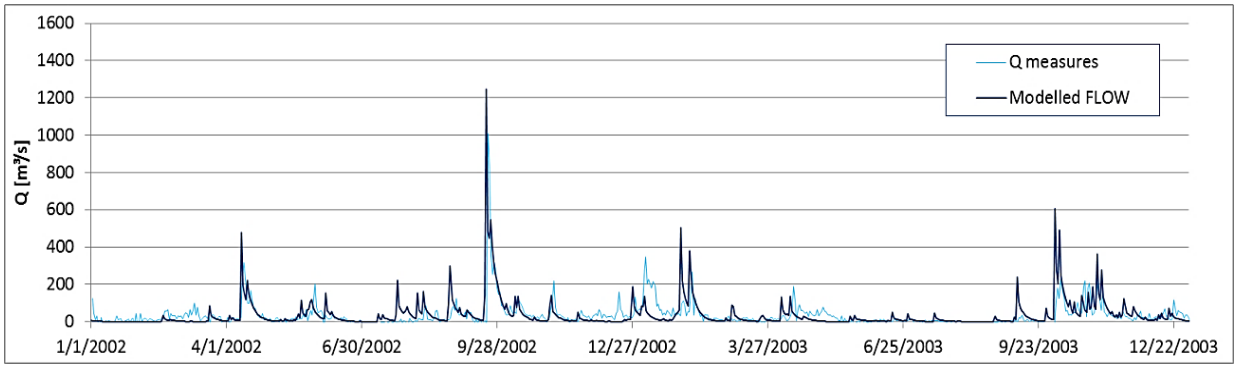

Figure 3. Model results for Ulza Lake (simulated water flow and measured water flow at the reservoir)

Table 5. Main parameters adopted for each sub-basin of Ulza Model, based on the model's calibration.

Component/Sub-basins		1	2	3	4	5	6	7	8	9	10	11	12	13
Canopy	Max. Storage (mm)	6.50	5.75	6.09	6.15	5.54	6.80	6.20	5.93	5.03	5.95	4.01	2.19	3.62
Surface	Initial storage	2	2	2	2	2	2	2	2	2	2	2	2	2
Transform SCS	Lag time	74	121	143	136	107	110	176	137	130	50	69	50	118
Soil Moisture Accounting loss	Soil [%]	85	85	85	85	85	85	85	85	85	85	85	85	85
	Ground water	95	95	95	95	95	95	95	95	95	95	95	95	95
	Max infiltration	7	7	7	7	7	7	7	7	7	7	7	7	7
	Impervious	5	5	5	5	5	5	5	5	5	5	5	5	5
	Soil storage	350	350	350	350	350	350	350	350	350	350	350	350	350
	Tension storage	330	330	330	330	330	330	330	330	330	330	330	330	330
	Soil percolation	3	3	3	3	3	3	3	3	3	3	3	3	3
	Ground water store.	350	350	350	350	350	350	350	350	350	350	350	350	350
	Ground water perc.	1	1	1	1	1	1	1	1	1	1	1	1	1
	Ground water coef.	240	240	240	240	240	240	240	240	240	240	240	240	240
Baseflow recession	Recession constant	0.8	0.8	0.8	0.8	0.8	0.8	0.8	0.8	0.8	0.8	0.8	0.8	0.8
	Ratio to Peak	0.4	0.4	0.4	0.4	0.4	0.4	0.4	0.4	0.4	0.4	0.4	0.4	0.4

Figure 6 Results for yearly water balance in Ulza Lake

Years	Annual Discharge Measured m^3/sec	Annual Discharge simulated with HEC-HSM m^3/sec	Difference %
2002	34.79	37.2	2.29
2003	32.57	34.1	1.41
2004	54.67	53.5	-1.19
2005	48.47	52.1	3.39
2006	28.33	30.2	1.99
2007	27.14	26.9	-0.39
2008	33.54	35.3	2.40
2009	61.64	66.7	5.45
2010	83.22	87.5	3.70
2011	21.35	20.2	-2.44

Conclusions

The hydrological conditions of the Mat River watershed in Ulza Lake are very important for the hydropower sector and the management of the water resources. In order to provide seasonal and annual water balance for Ulza Lake watersheds, the HEC-HSM hydrological rainfall-runoff model has been implemented. The hydrometeorological qualitative dataset is very important for the application of hydrological modeling in Mat River. The density of the watercourses with the change of the topography from 200 to 2000 meters above the sea level creates difficulties in the distribution of the hydrometeorological information in the catchment. Extending in time the database with the recent period 20012-20019 will improve the model results. Some type of testing has been performed to improve the

database. In some sub-basins, there is the need of having more information especially from the water users because of the agriculture some part of the discharge is stored in small reservoirs in the wet season and used in the period from May to October. The calibration and verification procedure of the hydrological model has very good results in most parts of the sub-basins.

References

Cyril Ray, Clément Iphar, Aldo Napoli. Methodology for Real-Time Detection of AIS Falsification. Maritime Knowledge Discovery and Anomaly Detection Workshop, Jul 2016, Ispra, Italy. pp.74-77 -ISBN 978-92-79-61301-2. hal-01421910

Maraun, D., & Widmann, M. (2018). Statistical Downscaling and Bias Correction for Climate Research. Cambridge: Cambridge University Press. Doi: 10.1017/9781107588783.

Hydro-meteorological Institute of Albania (IHM), Academy of Science of Albania, (1984) Hydrology of Albania. Albania**.**

Hydro-meteorological Institute of Albania (IHM), Academy of Science of Albania, (1985) Climate of Albania. Albania.

USACE (2000). HEC-HMS hydrologic modeling system user's manual. Hydrologic Engineering Center, Davis, CA.

USACE (2018). HEC-HMS hydrologic modeling system Quick Start Guide. Hydrologic Engineering Center, Davis, CA.

J. Int. Environmental Application & Science, Vol. 14(4): 145-151 (2019)

Research Paper

Determinants of Poverty among Smallholder Farms in Central District of Hatay Province, Turkey

Ugur Baser[1,*], Cevahir Kaynakci[2]

[1]*Department of Agricultural Economics, Faculty of Agriculture, Ondokuz Mayis University, Samsun, Turkey;*
[2]*Department of Agricultural Economics, Faculty of Agriculture, Kahramanmaras Sutcu Imam University, Kahramanmaras, Turkey*

Received October 15, 2019; Accepted November 28, 2019

Abstract: The aim of this study was to examine poverty and its determinants in smallholder farms in the central district of Hatay province, Turkey. Data were collected from 73 small farmers by questionnaire. In the study, Headcount Ratio (HCR) and the Poverty Gap Index (PGI) were used to measure poverty. The Logit model was used to reveal the determinants of poverty. The results show that HCR and PGI were determined as 17.8% and 49%, respectively. In addition, considering the 50% of the median income of all farmers, the poverty line was calculated as ₺3740.9 and 13 farmers were found below the poverty line. The most important factors affecting poverty in small farms were determined as retirement status of the householder, social security status, household equivalent size and land size. We concluded that the presence of retirement and social security situations decreases poverty whereas increasing the number of equivalent households' increases poverty. Early retirement programs for small producers and ease of payment of social security premiums may contribute to poverty reduction in small holder farms.

Keywords: *Poverty, smallholder farm, headcount ratio, poverty gap index, Hatay.*

Introduction

Poverty is one of the main problems of underdeveloped and developing countries. According to the most recent estimates, in 2013, 10.7% of the world's population lived on less than US$ 1.90 a day (World Bank, 2018) and many countries have taken some political measures to reduce poverty. The definition of poverty varies depending on the country, the target group, and even the type of settlement. Although there is no universally accepted definition of poverty, it is accepted as a humanitarian issue which must be considered worldwide. In its simplest definition, poverty is the inability of individuals to meet their basic needs as human beings (Caglayan *et al*., 2012).

Approximately 45% of the world population lives in rural areas; this ratio increases to 64% in Africa and falls down to 25.6% in Turkey (FAO, 2018). The effects of poverty are felt more in rural areas than in urban areas. There are many factors that directly or indirectly affect poverty in the countryside. Among these are wrong policies applied in rural areas, inadequate distribution of agricultural resources, lack of irrigation water, individual and socio-economic factors preventing the adoption of innovations, traditional structure and cultural barriers, inability to diversify rural employment, low yield and income resulting from plant and animal diseases, and marketing problems caused by intermediaries. All of these problems result in significant declines in incomes and well-being of rural people, especially among the smallholder farmers.

The householders or managers of small farms in developing countries have to cope with the risks of small farm despite these small farms continue to contribute significantly to agricultural production, food security, rural poverty reduction, and biodiversity conservation (Thapa & Gaiha, 2011). For example, the use of new technologies in a farm requires more capital input, mechanization and a high level of education. Therefore, these requirements may pose more severe challenges for small farmers (Hazell *et al*., 2007).

Numerous studies have been conducted to reduce poverty in rural areas. Some of these studies determined the current poverty situation (Apata *et al*., 2010; Mbanasor *et al*. 2013; Bogale, 2011; El-Osta & Morehart, 2008; Rotich *et al*., 2017; Naschold, 2009; Profitable, 2016). Some others investigated the effects of gender (Ike & Oboh, 2009; Oluwatayo, 2014), credit access (Obisesan, 2013; Asogwa *et al*. 2012), and the effects of non-farm income on poverty (Vatta & Sidhu, 2010).

*Corresponding: E-Mail: ugur.baser@omu.edu.tr; Tel: 0362 312119-1480; Fax: 0362 457 6091

Some studies have addressed small farmers, the most disadvantaged group in terms of poverty (Oluwatayo, 2014; Obisesan, 2013; Apata *et al*., 2010; Bogale, 2011). According to Oluwatayo (2014), age, gender, level of education, major occupation, household size, amount of remittances received, and extension services had a significant effect on the poverty status of the respondents. Obisesan (2013) examined the access of small farmers to credit and founded the significant determinants of credit accessibility as gender, age, main occupation, participation in off-farm activities, membership of farmers' association and crop yield. Apata *et al*. (2010) studied the determinants of rural poverty of small farmers in Nigeria and found that access to micro-credit, education, participation in agricultural workshops/seminars, livestock assets, and access to extension services significantly influenced the probability of households' existing chronic poverty. The findings of Bogale (2011) stated that poverty is location specific depending on access to irrigated land and access to non-farm income. However, this study also indicated that household wellbeing was negatively affected by household size, and positively affected by age of household head. Also, involvement in governance, social and production related networks are also found to be strongly associated with the probability of a household being poor. All these researches show that the poverty among small farmers was affected by the socio-demographic factors, access to extension services and credit, social and production related networks with governance.

The majority of people in absolute poverty have lived on small farms. Practices to reduce the poverty of small farms, which are the most disadvantaged group in terms of poverty, are of great importance. The aim of this study was to calculate poverty in the smallholder farms and to determine its affecting factors in the central district of Hatay province, Turkey.

Material and method

Material

The research was conducted in the central district of Hatay province of Turkey in 2018. The UNCTAD (2015) classified smallholdings as the farms with a low asset base and operating in less than 20 decares of farmland. The data of the study were collected by questionnaire from 73 small farmers who have 20 decares or smaller land sizes.

Method

Measuring of poverty

Poverty measures fall under two broad categories: those that examine poverty either in absolute or in relative terms (El-Osta & Morehart, 2008). Absolute measures of poverty compare household income with the cost of a basket of specific goods and services. Relative measure of poverty compares household income and spending patterns with income and spending patterns of the general population (El-Osta & Morehart, 2008). In the study, HCR and PGI were used to measure relative poverty. HCR is calculated as the ratio of the population below the poverty line to the total population. After the income of each poor is subtracted from the poverty line value, it is obtained by adding the obtained values and dividing them by the number of poor people. HCR gives information about the poverty deficit and the degree of poverty. HCR is the ratio of the number of people whose income falls below the poverty line to the population and it is expressed as follows (Ravallion, 1992);

$$H = \frac{q}{n}$$

Where H= Headcount ratio (Poverty incidence)
q= Number of poor smallholder farmers
n= Total number of smallholder farmers

The PGI is equal to the ratio of the average poverty gap to the poverty line in society. PGI usually measures poverty depth (Mbanasor *et al*. 2013) and in this study, the following formula was adopted (Ravallion, 1992);

$$I = \left[\frac{Z - Y}{Z}\right]$$

Where I = Poverty gap
Z= Poverty line estimated using median equivalence of household income
Y=Median income of the poor smallholder farmers

Fifty percent of the median income was taken to calculate the poverty line (OECD, 2018). As households are of different sizes and components, they should be standardized with the help of an equivalent person scale. OECD equivalence scale was used for the equivalent person scale. This scale assigns a value of 1 to the household head, of 0.5 to each additional adult member and of 0.3 to each child. The t-test was used to compare the means and the chi-square test was used to compare the groups.

Logit Model

In the study, the logit model was used to analyse the factors affecting poverty. The Logit model is expressed as follows (Gujarati, 1995):

$$P_i = F(Z_i) = F\ (\alpha + \beta X_i) = \frac{1}{1+ exp^{-(z_i)}} = \frac{1}{1+ exp^{-(\alpha+\beta x_i)}} \quad (1)$$

P_i is the probability of i[th] household to select a specific choice, F is probability function, α is constant coefficient, $Z_i = \alpha + \beta X_i$, where β is the estimation of parameters for each explanatory variable, X_i represents i[th] independent variable. The equation below has been found by rearranging Equation 1 and finding the natural logarithm of both sides of the equation;

$$L_i = Ln\left[\frac{P_i}{(1-P_i}\right] = Z_i = \alpha + \beta_0 + \beta_1 X_1 + \beta_2 X_2 + \cdots \beta_n X_n + \varepsilon_i \quad (2)$$

Marginal probability calculates the variation in the probability of poverty in accordance with the change in each explanatory variable (Greene, 2011). The estimated β-coefficients of Equation 2 do not directly represent the marginal effects of the independent variables on the probability P_i. In the case of a continuous explanatory variable, the marginal effect of X_j on the probability P_i is given by:

$$\frac{\partial P_i}{x_{ij}} = \frac{\left|\beta_j \ \exp(-\beta X_i)\right|}{|1 + \exp(-\beta X_i)|^2} \quad (3)$$

However, if the explanatory variable is qualitative or discrete in nature $\partial P_i / \partial X_{ij}$ do not exist. In such a case, the marginal effect is obtained by evaluating P_i at the alternative values of X_{ij}. For example, in the case of a binary explanatory variable X_{ij} that takes values of 1 and 0, the marginal effect is determined as:

$$\frac{\partial P_i}{x_{ij}} = P\left(X_{ij}\right) = 1 - P\left(X_{ij}\right) = 0 \quad (4)$$

The dependent variable in the study was taken as 1 for small farmer households living under the poverty line and 0 for households living above the poverty line. Factors affecting poverty in small farms are given in Table 1.

Table 1. Variables used in Logit model

The dependent variable	
POVERTY	**Poverty (1=Poor farm 0=Non-poor farm)**
The independent variables	
AGE	Age (year)
GENDER	Gender (1=Male 0= Female)
EDUCA	Education (Elementary school and above=1 other= 0)
SOCSEC	Social security (1=Yes 0= No)
EQUIVASIZ	Household equivalent size (Person)
LANDSIZE	Land size (Decares)
MEMUNION	Membership to the farmer organizations (%) (1=Yes 0= No)
RETIRE	Retirement (1=Yes 0= No)

Results and discussion

Socioeconomic and Structural Characteristics of Smallholder Farmers

According to the general level of society, individuals or households who have income or expenditure below a certain limit are considered to be relatively poor. Poor and non-poor farmers were defined by their annual incomes. Thirteen farmers living under the poverty line of ₺3740.9 were considered as poor and 60 farmers living above the poverty line were regarded as non-poor. The average age of the householders was 51.1 years old, 52.7% of the interviewees were women. It was also revealed that 41% of poor farmers and 30% of non-poor farmers have less than elementary education. Besides, 79.1% of farmers were married, 28.4% of the participants were retired, 69.3% of the participants had social security and the average household size was 4 people. Equivalent size can be calculated for the different consumption needs of adults and children in households and standardizes the number of family members. In the study, the equivalent household size was found to be 2.4 persons on average. According to the results of the survey, the most important income source for 72.6% of the households was agriculture and the average agricultural experience was 23.5 years. Maintaining physical or financial records in the farms is of great importance for controlling the management of the farms. As for the physical and financial records, while none of the poor farms hold any records, 6.2% of non-poor farms hold this kind of records. In addition, only 33.3% of the total income of the poor farms came from agriculture. Non-poor farms earned 43.2% of their total income from agriculture (Table 2). The results of the study showed that there were statistically significant differences between the poor farms and non-poor farms in terms of household size, the household equivalent size, membership to the producer organization, land size, total income, agricultural income, and non-farm income.

Table 2. Socioeconomic and Structural Characteristics of Smallholder Farmers

	Poor Farms (13)		**Non-poor Farms (60)**		**All Farms (73)**	
	Mean	**Std. Dev.**	**Mean**	**Std. Dev.**	**Mean**	**Std. Dev.**
Age *(year)*	54.2	8.9	50.6	11.5	51.1	11.2
Gender *(%)*	38.0	-	54.7	-	52.7	-
Education						
Less than elementary school (%)	41.0	-	30.1	-	32.1	-
Elementary school (%)	59.0	-	51.0	-	53.3	-
Secondary school (%)	-	-	9.1	-	7.2	-
High school (%)	-	-	5.6	-	4.1	-
University (%)	-	-	4.2	-	3.3	-
Marital status (%)	80.3	-	78.5	-	79.1	-
Retired *(%)*	13.3	-	30.4	-	28.4	-
Social security *(%)*	40.0	-	73.0	-	69.3	-
Household size *(person)**	5.5	2.2	3,7	1.8	4.0	2.0
Household equivalent size *(person)**	3.1	1.0	2,2	0.8	2.4	0.9
Main profession as farmer *(%)*	70.0	-	73.1	-	72.6	-
Experience on agriculture *(year)*	25.8	16.5	23.5	15.8	23.5	15.9
Record Keeping *(%)*	-	-	6.2	-	5.5	-
Membership to the farmer organizations *(%)* ***	16.2	-	65.0	-	39.7	-
Land size *(decare)**	1.3	1.1	4.8	4.0	4.3	3.8
Number of parcels *(unit)*	1.4	0.8	2.1	1.3	2.0	1.2
Credit use *(%)*	-	-	12.0	-	10.5	-
Total income *(₺/year)**[1]	6382.9	3996.0	21619.8	12392.0	18962.2	12763.9
Agricultural income *(₺/year)**	2126.9	2650.4	9340.7	9122.7	8082.5	8790.7
Non-farm income *(₺/year)**	4256.0	3539.1	12279.1	7503.6	10879.7	7603.2

** and *** indicate that the difference between the means are statistically significant at the level of 1 and 10%, respectively*

[1] *$1 equal ₺ 3.76 (TRCB, 2018)*

Determination of the Poverty Line and Gap in Smallholder Farmers

In this study, the average and the median income per equivalent person were found as ₺8884.7 and ₺7405.5, respectively. The median income per farm was ₺15897.5. The poverty line is the determination of a monetary amount to meet basic needs (Oztornaci & Demirdogen, 2015). The

poverty line was ₺3740.9 and 13 farms were determined below the poverty line. In Turkey, the poverty line for the rural areas was ₺3724, while the poverty rate and gap were 14.3% and 0.22% in 2013 (TurkStat, 2018). In this study, the HCR was calculated as 17.8%, which means that 17.8% of small farmers were poor. The poverty gap was calculated as 49%, indicating that the income of small farmers under the poverty line should be increased by at least 49%. The poverty rate and deficit in the small farms were found by Bogale (2011) as 35.6% and 9.1%, respectively. The poverty rate and deficit in the study of Ike and Oboh (2009) were found as 50.6% and 28%, respectively. Mbanasor *et al*. (2013) found a higher poverty rate (56%) and deficit (56.8%) However, Kan (2012) found that less poverty rate (17.86%) and the poverty gap (29%) in Turkey (Table 3).

Table 3. Estimates of Poverty Line, Gap and Incidence in Family Farm

Variables	Estimates
Average income per equivalent person (₺)	8884.7
Median income per equivalent person (₺)	7405.5
Median income per farm (₺)	15897.5
Poverty line	3740.9
Number of families under poverty line (unit)	13.0
HCR (Poverty Incidence) (%)	17.8
Poverty Gap (%)	49.0

Logit model results

The factors affecting the poverty of smallholder farmers are presented with the logit model. The likelihood ratio test shows a good fit for the model ($P < 0.001$). Among the variables included in the Logit model, the variable of the households' equivalent size, land size, retirement status, and social security status were found to be statistically significant at the level of 1%, 5%, and 10%, respectively.

The results of this research stressed that the most important factor affecting poverty is the retirement status of the farm householder. The retirement of the farm householder reduces the probability of households to be poor by 24.1%. In order to reduce poverty in the smallholder farmers, the government should give social aids to non-retired smallholder farmers and they encourage them to work part time non-farm business. Vatta and Sidhu (2010) also emphasized that non-agricultural income is an important factor in reducing poverty.

Another important factor reducing poverty is the social security situation of farmers. Social security is a set of policies and systems that protects individuals against occupational, physiological and socio-economic risks in their life. According to the results of the study, the probability of households with social security being poor reduces by 14.8% on average.

The household equivalent size was determined as another factor affecting poverty. Our study shows that when households' equivalent size increases by 1, the probability of being poor increases by 12.3%. The average number of households in rural areas is higher than in urban areas. Population growth in rural areas through family planning as government policy was determined as one of the measures to reduce poverty. Bogale (2011) stated also that increasing households' equivalent size will exacerbate extremely poor and moderately poor poverty. It has been found that increasing the number of households negatively affects poverty (Oluwatayo, 2014; Vatta & Sidhu, 2010).

The land is an important factor to reduce poverty. In our study, it was revealed that the increase in land size by 1 decare reduced poverty by 6.1%. Thus, it might be suggested that the size of the land should be increased to reduce the poverty of smallholder farmers. It has been supported by various studies that poverty could be decreased by increasing land (Apata *et al*., 2010; Vatta & Sidhu, 2010).

Gender is another important variable that affects poverty. In the study, it was found that being male farm manager decreases the probability of being poor by 9.8%. Oluwatayo (2014), Apata *et al*. (2010) and El-Osta and Morehart (2004) found similar results.

Education and organization in agriculture are of great importance in the adoption of innovations and cooperation. Thus, it was determined that the education level at least higher than elementary school reduced the probability of being poor by 8.9%, and membership of agricultural organizations reduced the probability of being poor by 8.7%. Apata *et al*. (2010) and El-Osta and Morehart (2004) found similar results which stated that education and organization reduce poverty

The population aging phenomenon of the transformation process also affects the rural population in Turkey. Urbanization, migration from rural to urban areas, and the elderly population remain predominantly in rural areas are among the main socioeconomic problems. It has been shown that increase in the age of householder by 1 year increases the probability of being poor by 0.1%. Oluwatayo (2014) found similar findings in their study, while Apata *et al*. (2010) found that age reduces poverty.

Table 4. Logit Model Results

Explanatory variables	Coefficient	Standard Error	P	Marginal effects
INTERCEPT	-0.072	4.037	0.985	-
AGE	0.018	0.063	0.771	0.002
GENDER	-1.174	1.092	0.282	-0.098
EDUCA	-1.064	1.047	0.309	-0.089
SOCSEC	-1.770	0.911	0.052	-0.148
EQUIVASIZ	1.479	0.527	0.005	0.124
LANDSIZE	-0.728	0.354	0.039	-0.061
MEMUNION	-1.050	1.107	0.343	-0.088
RETIRE	-2.882	1.359	0.034	-0.242
Number of observations	*73*			
Loglikelihood	*-23.151*			
χ^2	*0.001*			
Pseudo R^2	*0.418*			

Conclusions and Recommendations

Poverty is one of the main problems facing the world, especially the underdeveloped and developing countries. Especially the people in rural areas have suffered more from poverty due to their low value-added products. Developing new methods to combat rural poverty and increasing the works in this field are of great importance in reducing poverty.

According to the results of the research, the median income is below the average income which indicates the existence of income distribution inequality. The poverty line for farms was calculated as ₺3740.9 and it was founded that 17.8% of the producers lived below the poverty line. In addition, the poverty gap for the poor farmers was found as 49% and it was understood that the producers had to increase their income at least twice to get out of poverty.

The logit model concluded that age and the household equivalent size had an increasing effect on poverty, while gender, education, social security, land size, membership to producer organizations and retirement had a reducing effect on poverty. The most effective factors on poverty were the retirement status, social security situation, and household equivalent size, respectively. There are significant differences between the characteristics of the poor farmers and non-poor farmers in terms of education, retirement, social security, membership in cooperatives, land size and credit utilization. Elimination of these differences could play an important role in reducing poverty.

In the light of the conclusions of the study, it is recommended that policies such as increasing the education level of smallholder farmers through non-formal education, promoting social security and finding non-farm part time works, and allocating idle land to smallholder farmers can play an important role in reducing rural poverty. Policymakers should take efficient precautions to get social fairness in the mid-run and long-run to guide and reduce poverty among smallholder farmers.

References

Asogwa BC, Umeh JC, Okwoche VA, (2012) Poverty and efficiency among the farming households in Nigeria: A guide for poverty reduction policy. *Curr. Res. J. Econ. Theory.* **4**(1), 6-10.

Apata TG, Apata OM, Igbalajobi OA, Awoniyi SMO, (2010) Determinants of rural poverty in Nigeria: Evidence from small holder farmers in South-western, Nigeria. *Int. J. Sci. & Tech. Educ. Res*. **1**(4), 85-91.

Bogale A, (2011) Analysis of poverty and its covariates among smallholder farmers in the eastern Hararghe highlands of Ethiopia. *J. Dev. & Agric. Econ*. **3**(3), 157-164.

Caglayan E, Kosan NI, Astar M, (2012) An empirical analysis of the determinants of household poverty in Turkey. *Asian Eco. and Fin. Rev.* **2**(1), 181-191.

El-Osta HS, Morehart MJ, (2008) Determinants of poverty among US farm households. *J. Agri. App. Eco*., **40**(1), 1-20.

FAO, (2018) Food and Agricultural Organization. http://www.fao.org/faostat/en/#data/QC, Accessed on 20.08.2018.

Greene WH, (2011) *Econometric Analysis.* Seventh Edition. Prentice Hall, ISBN-10: 0131395386, New Jersey.

Gujarati DN, (1995) *Basic Econometric*s, Mc Graw-Hill Inc, U.S.A.

Hazell PB, Poulton C, Wiggins S, Dorward A, (2007) The future of small farms for poverty reduction and growth. *Int. Food Policy Res. Inst., Policy Brief*. **42**.75-76.

Ike PC, Oboh VU, (2009) A Gender Analysis of Poverty Gap among Farm Families in Ukwani Local Government Area of Delta State, Nigeria. *Agri. J.*. **4**(6), 254-259.

Kan A, (2012) Poverty in Agricultural Holdings and Evaluation of Poverty in the Framework of Gender Assessment in Rural Area: Konya Province, Hadim District Case, Doctoral Dissertation, Selcuk University, Social Sciences Institute 278 p.

Mbanasor JA, Nwachukwu IN, Agwu NM, Njoku MSE, Onwumere J, (2013) Analysis of income inequality and poverty dynamics among rural farm households in Abia state, Nigeria. *Int. J. Food & Agri. Eco*. **1**(2), 99-104.

Naschold F, (2009). Microeconomic determinants of income inequality in rural Pakistan. *The J. Dev. Stu.* **45**(5), 746-768.

Obisesan AA, (2013). Credit accessibility and poverty among smallholder cassava farming households in South West, Nigeria*. Gre. J. Agri. Sci*. **3**(2), 120-127.

OECD, 2018. http://www.oecd.org/eco/growth/OECD-Note-EquivalenceScales.pdf Accessed on 10.10.2017.

Oluwatayo IB, (2014) Gender dimensions of poverty and coping options among smallholder farmers in Eastern Nigeria. *Med. J. Soc. Sci.* **5**(27), 49-61.

Oztornacı B, Demirdogen A, (2015) According to Different Equivalence Scales, Change of Basic Poverty Indicators: The Case of Turkey. *J. Agri. Eco*. **21**(1), 7-15.

Ravallion M, (1992). Poverty Comparisons: A Guide to Concepts and Methods. World Bank LSMS Working Paper, 88.

Rotich JK, Odhiambo M, Ngeno V, (2017) Effect of tea farming household characteristics on poverty levels among tea farmers in Konoin Sub-County, Kenya. *Global J. Com. & Man. Pers.* **6**(3), 34-44.

Sarwar I, Ashfaq M, Bari A, Hafeez N, (2012) The contribution of various non-farm income sources in reducing income inequality across different farm sizes: A comparison of barani Punjab and cotton/wheat Sindh. *Pak. J. Agri. Sci*, **49**(3), 371-375.

Thapa G, Gaiha R, (2011) Smallholder farming in Asia and the Pacific: Challenges and opportunities. *International Conference on Dynamics of Rural Transformation in Emerging Economies*, April 14-16, 2010, New Delhi, India.

TRCB, (2018) The Central Bank of the Republic of Turkey. https://www.tcmb.gov.tr/wps/wcm /connect/ EN/TCMB+EN/Main+Menu/Statistics/Exchange+Rates. Accessed on 08.10.2018.

TurkStat, (2018) Turkish Statistical Institute. http://www.turkstat.gov.tr/Start.do;jsessionid= 0l2JZjQQyhzQ7Rv1hdFhSHk23bCJQzlLlJc9Vk2GXrkKbwdK13J9!-1513161628. Accessed on 10.10.2017.

UNCTAD, (2015) Smallholder Farmers and Sustainable Commodity Development. United Nations Conference on Trade and Development, Commodity and Development Report.

Vatta K, Sidhu RS, (2010) Rural non-farm employment, income distribution and poverty: Micro level evidence from Punjab. *Ind. J. Agri. Eco.* **65**(4), 693-709.

World Bank, (2018). http://www.worldbank.org/en/topic/poverty/overview Accessed on 10.10.2017.

J. Int. Environmental Application & Science, Vol. 14(4): 152-159 (2019)

Research Paper

Ornamental Plants Which Can Be Used in Visual Landscape Improvement in Cold Climate Regions

Feran Aşur*

**Department of Landscape Architecture, Faculty of Architecture-Design, Yuzuncu Yıl University, Zeve Campus, 65090 Tuşba, Van, Turkey*

Received October 07, 2019; Accepted December 04,2019

Abstract: Plants in cities; help to keep the balance of the ongoing interaction between the environment and the human system by its visual and functional effects. It is possible to develop alternative solutions to eliminate visual pollution by evaluating the colour, texture, form, size and similar properties of plant materials and the potential properties of the composition with other inanimate materials such as highlighter, background forming, harmonizing and concealer. The number of ornamental plant species that grow in cold climates is less than in warm climates. For this reason, especially in the landscaping works of urban spaces, it is difficult to create the desired visuality with aesthetically qualified plants that are suitable for the ecology of the area, without creating monotony, with colour variety. In this study, the importance of ornamental plant and their compositions in the solution of visual problems in urban environments in cold climatic conditions is emphasized. The potential of ornamental plants that can be used for this purpose in preventing visual pollution is given. In addition to the design group disciplines that are effective on planning or application basis in the city and its surroundings, the studies to be carried out in detail in terms of planting design as a discipline of Landscape Architecture can provide visual improvement.

Keywords: *Visual improvement, residential landscape, urban space.*

Introduction

Visual pollution, which is a phenomenon in general environmental problems, can be defined as all the irregular formations in the natural or artificial environment that leave negative traces in memory. It is possible to develop alternative solutions to eliminate various visual contaminations using soft scape, which is one of the important landscape design elements especially in urban spaces. However, weather conditions such as wind, snow, frost, ice, diminishing daylight and long-term cold in winter cities, which dominate the winter season, restrict the use of plants in public open spaces with many negative effects.

When the definition of winter city is examined, it is seen in the literature that the temperature is below 0 °C and below 0 °C, precipitation is generally in the form of snow, daylight is felt in limited time, these three factors are defined as the city with long time periods and harsh season passes. According to Erskine (1986), the winter city is generally located at latitudes of 45° and above and with a temperature of 0 °C or less in January (Henke, 2006). Public spaces connecting society as a common ground; It is one of the most important parts of the cities, ranging from streets to squares, parks and surrounding buildings (Erdönmez & Akı, 2005; Tandoğan & Şişman, 2018).

In this study, ornamental plants that in the resolution of visual problems in habitable urban spaces in cold climate regions have been investigated and the importance of plant compositions has been emphasized. At the end of the study, a list of ornamental plants that can be used to eliminate visual pollution in public space design for cities considered as winter cities and at the same time make the area more visually impressive is given.

Ornamental Plant Characteristics That Can be Considered in Preventing Visual Pollution

In the ornamental plant material to be selected in order to prevent visual pollution of the plant designs to be made in landscape architecture: Physical properties varying according to local conditions, Functional features such as shading, screening, wind protection, space modulation, colour, texture, form, size etc. Depending on the characteristics of the architectural and aesthetic potential of

* *Corresponding: E-Mail: feranekasur@gmail.com; Tel: 0090 505 8867677*

plants should be known properties (Austin, 1982; Yazici & Gulgun, 2017; Yazici et al., 2017). Ornamental plants play an active role in the sustainability of urban life and are one of the most versatile benefits of aesthetic, ecological, socio-cultural, psychological, hygienic and functional scope. Aesthetically, ornamental plants soften the solid and sharp lines of buildings in urban areas, create interesting shapes and textures by creating contrasting shapes and textures (Booth, 1996; Yildizci, 1988; Dirik & Ata, 2005; Scarfone, 2007: Gulgun *et al*., 2014; Yazici *et al*., 2018) and provide aesthetic and physical value to the city space with features such as line, form, size, colour and texture (Yildizci, 1986) also meets the psychological and socio-cultural needs of the citizen (Konijnendijk et al., 2004; Birisci et al., 2017).

The roles of plants in design; ecological / engineering, architectural and aesthetic functions are divided into three classes (Booth, 1996; Leszczynski, 1999). In addition, it requires good practice and maintenance work (Erbas, 2003). A person's desire to live in a place suitable for his desires and tastes; aesthetically and functionally, the creation of the most appropriate outdoor spaces, design and selection of the most appropriate elements can be realized by the conscious use (Kelkit, 2002). The visual quality of single or group plant compositions is examined in terms of the line, form, texture and colour concepts that make up the visual characteristics of the plants. Although these elements are more abstract than the special effects of fruits, flowers are essential for understanding the whole composition (Ayaslıgil, 2004; Robinson, 2004). It is possible to create positive effects on the urban landscape by choosing plant species that offer attractive winter features such as leaves, fruits and stem colours in public spaces in winter cities. It is possible to see examples of this in different winter cities in the world (Figure 1).

Figure 1. Plants in winter city (**a**: Oslo, URL-1); (**b**: Stockholm, URL-2), (**c**: Moscow, URL-3)

Material and Method

The main material of this study is cities that located in cold climate region in Turkey. In addition, winter city examples and literature studies on this subject were used as auxiliary materials. In the first stage of this study, based on the definitions made for winter cities, the world that have made the Köppen climate classification maps were examined and winter city in Turkey are determined. Examples of liveable winter cities were examined and literature studies on this subject were utilized. According to the Köppen-Geiger climate classification in Turkey is 10 sub-climate types. Based on the

definitions made for winter cities, cold climate areas (D) in terms of Köppen Classification (Figure 2), the winters are severe, the average temperature of the coldest month is below -3 °C, the average of the warmest month is above 10 ° C and the soil is covered with snow for months characterized by features. According to Köppen Classification, cold climatic zones are also separated according to certain criteria (Table 1) (Türkeş & Tatlı, 2011; Öztürk et al., 2017).

Table 1. Sub-climate types of cold climate areas (D)

Climatic areas	Features
Dwa:	Winter is severe and arid, summer is long and hot
Dwb:	Winter is severe and arid, the font is cool
Dwc:	Winter is severe and arid, writing is short and cool
Dwd:	Winter is very severe, writing is short and moist
Dfa:	Severe in winter, long and hot in summer, rainy in all seasons
Dfb:	winter severe, summer short and hot, rainy in all seasons
Dfc:	winter severe, summer short and cool, rainy in all seasons
Dfd:	Winter is very severe, summer is short, rainy in all seasons

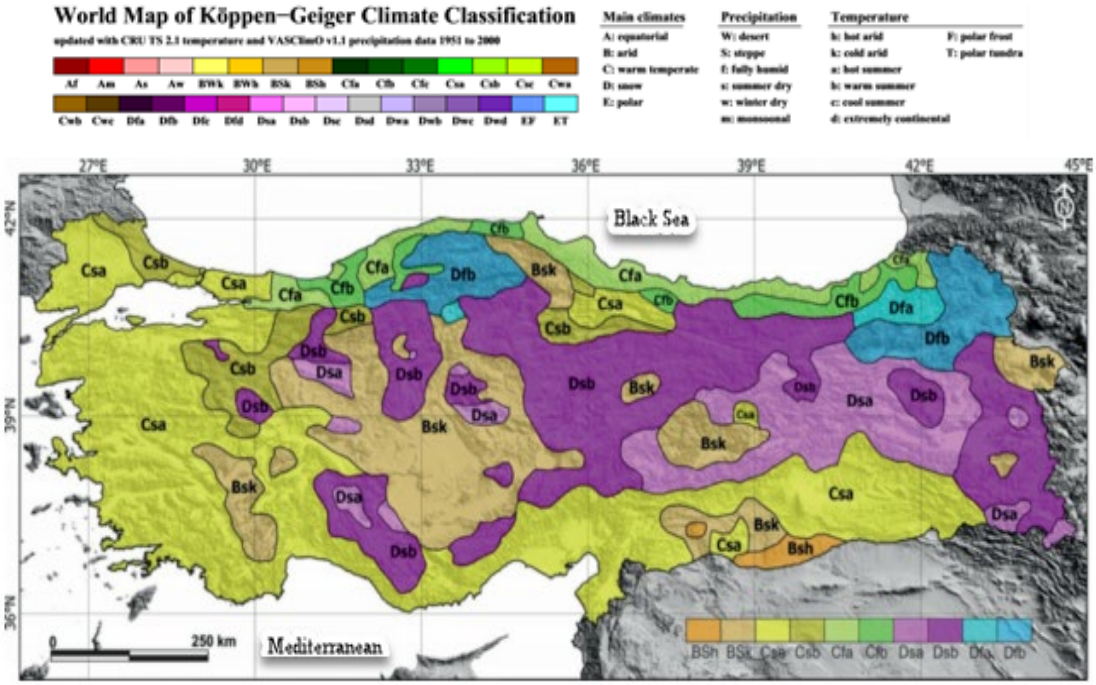

Figure 2. Köppen-Geiger sub-climate types of the Turkey (Öztürk *et al*., 2017; Kottek *et al*., 2006; Url-2)

When Köppen's world climate classification maps are examined, the provinces in Turkey corresponds to the eastern Anatolia region. For this reason, suggestions were made for Ardahan, Kars, Igdir, Agri, Van, Hakkari, Bitlis, Mus, Erzurum, Erzincan, Tunceli, Bingol, Elazig and Malatya (Figure 3). The area of Eastern Anatolian Region is 164 thousand km² and covered with high mountains. The altitude results in a cold and harsh climate, and more difficult living conditions for the people living here. Eastern Anatolian Region borders Georgia, Armenia, Azerbaijan, Iran and Iraq on the east. The cities that located in these provinces are not considered rich about ornamental plants.

In the second stage of this study, design criteria were proposed to make public spaces in winter cities more visually beautiful and liveable. In the third stage, suggestions were made for plant material that can be used in public places in winter cities. In determination of plant material, cold resistance criteria were taken into consideration. The plant material that meets these criteria are evaluated aesthetically (leaf colour, stem, fruit / flower, form) and a suggestion plant table is prepared for winter cities.

Figure 3. Region considered in the study: Eastern Anatolian Region

Findings

Plants Design in Public Open Spaces in Winter Cities

In plant design, plant selection should be made in which tolerances to hot and cold climatic conditions are appropriate. Ornamental plants that can be used in visual improvement and create effective images in winter were investigated, for Ardahan, Kars, Igdir, Agri, Van, Hakkari, Bitlis, Mus, Erzurum, Erzincan, Tunceli, Bingol, Elazig and Malatya that located in Eastern Anatolia Region (14 province).. In this direction the points to be considered in ornamental plants design in public spaces in winter cities are as follows:

- Cold and salt resistant species should be selected in terms of plant health when selecting plant material, which is the most important factor regulating urban ecology in winter cities (Pressman, 2016).
- Select vegetation for landscaping near roadways that can withstand exposure to salt, ice smelters, gravel and sand. Vegetation should be able to withstand snow loads, wind and require little maintenance throughout the year (Coleman, 2009; Pressman, 2016).
- Give preference to native plants, trees, grasses and shrubs that are colourful and/or look attractive covered with snow (Pressman, 2016).
- Use planting beds surrounded by curbs to lessen damage due to snow-clearing equipment.
- As they have an important role in providing sun and wind control around public open spaces and structures, the choice of plant should be made according to the size and character of the plant in summer and winter, and growth rate (Figure 4) (Candemir, 2009).
- Summer / winter green, evergreen plants should be selected on the northern front of public open spaces and structures. These plants will function as wind breakers and reduce heat losses, protect pedestrians from cold winds (Olgyay, 1962). Deciduous trees should be used on the south-facing facades of public spaces and buildings (Coleman, 2009; Pressman, 2016).
- Reduce wind speed in open spaces by planting dense vegetation along the edges and against any blank walls to reduce wind acceleration (Figure 4) (Pressman, 2016).
- Use soft landscaping to filter and screen views into private dwelling units, while ensuring views to the street or open spaces are maintained for surveillance (Pressman, 2016).
- The use of evergreen trees (coniferous vegetation) and shrubs in pedestrian areas will serve as wind curtains and create a favourable environment by preventing wind and snow type (City of Minneapolis, 2011).
- It is necessary to use the trees in groups instead of lining the trees in cases that will be used as wind curtains. This will provide greater resistance to wind and reduce surface evaporation (Urban systems, 2000).
- Insulation should be provided in winter by using climbing plants or intense planting on the walls of the buildings (St. Clair, 2010).
- Banquets and plants should be used in order to prevent snow fall in the entrance of buildings (Cengiz et al., 2016).

- Form, colour, fruit, etc. that increase the attractiveness of the winter character of the area. Different plant species with interesting winter characteristics should be selected (Coleman, 2009; Cengiz et al., 2016).

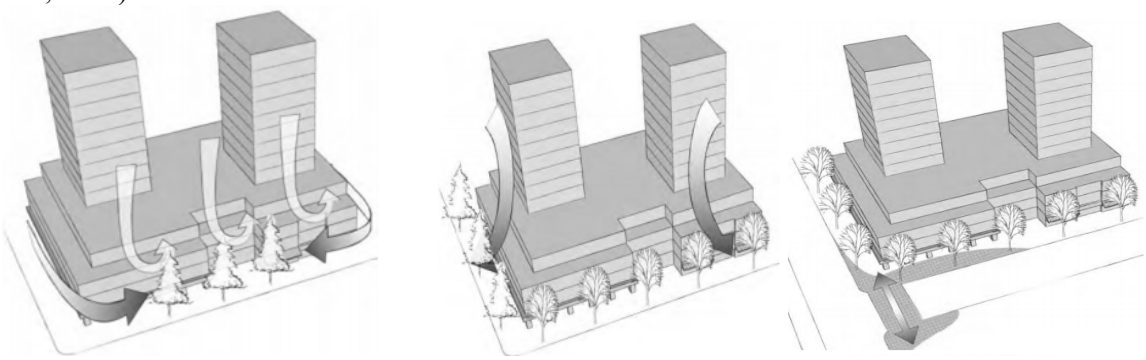

Figure 4. Use of trees to reduce the negative impact of wind (Pressman, 2016)

Plant Species That Can Be Used in Public Places in Winter Cities

In the public spaces discussed in the scope of the study; The types of plants that can be used in cities with severe winter, short summer and rainy season are given below, by taking advantage of the Alp , 2007, Tandoğan & Şişman 2018 and with another research in the table Table 1. and Table 2. Accordingly, it will be possible to make the area more interesting by creating different color and visual effects with plants in successive seasons throughout the year in public spaces, which are the visual pollution of winter cities. However, large and coniferous trees and shrubs are suitable plants for aesthetic and functional purposes in plant design studies for winter cities. Broad-leaved trees; *Acer campestre, Acer pseudoplatanus, Aesculus hippocastanum,* are resistant to salt and are suitable for use as wind and snow curtains. From coniferous trees, *Abies concolor* and *Picea pungens* are suitable for creating snow and wind curtains. *Fraxinus americana, Picea pungens, Symphoricarpus orbiculatus* and *Syringa vulgaris* are suitable for use in winter cities because of their salt-resistant plant species and their visual values.

Table 1: List of trees that can be used in plant design of winter cities

	Scientific name	Plant height (m)	Flowering time	Characteristics of plants
Trees	*Abies cilicica*	30	-	Light green body
	Abies concolor	25-30	-	Blue Green Conifer
	Acer campestre	10-15 m	-	Autumn yellow leaf color
	Acer negundo	More than 15 m	-	Autumn leaf color
	Acer platanoides	20-30	April	Red leaves
	Acer rubrum	25-40	-	Red leaves
	Aesculus carnea	20-25	April- May	Red Flowers
	Aesculus hippocastanum	20-25	April -May	White flowers
	Amygdalus communis	Up to 12 m	April -May	Light pink blossoms
	Betula alba	20-25	April	White body
	Catalpa bignonioides	7-15	June-July	Powder pink flowers
	Crataegus monogyna	3-7	-	Red berries (until winter)
	Cydonia japonica	1-1,5	April	Pink / Red flowered
	Cupressus arizonica	25	March -April	General view of bluish
	Elaeagnus angustifolia	5-7	June	General view of bluish and yellow flowers
	Fraxinus americana	More than 15 m	-	Green, bright gray
	Laburnum anagyroides	80-100 cm	May	Yellow flowers
	Ligustrum vulgare	5-7	June- July	Dark green leaves
	Malus floribunda	6-7	May	Pink flowers
	Picea ssp.	30-40cm	-	Bluish body
	Picea abies	More than 15 m	-	Decorative image

	Picea pungens 'Glauca'	20-25	-	Blue green color
	Pinus sylvestris	More than 15 m	-	Gray green color of tree and yellow color of trunk
	Prunus cerasifera Pissardii Nigra	5-8	April- May	Burgundy leaves
	*Prunus ceracifera '*Atropurpurea'	7-9	April - May	Red petals, white flowers
	*Prunus serrulata "*Kanzan"	7-10	May	Pink flowers
	Robinia pseudoacacia "Deca Isneana Hispida"	20-30	June	Pink flowers
	Salix caprea	12-15	April - May	Downy flowers
	Tamarix tetrandra	4-5	June	Tulum image
	Tilia tomentosa	20-25	June	Pink flowers

Table 2: List of Shrubs that can be used in Plant Design of Winter Cities

	Scientific name	Plant height (m)	Flowering time	Characteristics of plants
Shrubs	*Berberis thunbergii*-Atropurpurea	1.50- 3	May-June	Bouquet-red leaves
	Buddleja davidii	3	July- September	Lilac flowers
	Cotoneaster horizontalis	1.50	April	Red Berries
	Forsythia x intermedia	2-3	April-May	Yellow Flowers
	Laburnum anagyroides	5	May-June	Pink flowers
	Juniperus sabina	1-3	-	Dark green view
	Parthenocissus quenquefolia	1015	-	Red leaves in autumn
	Pyracantha coccinea	5	June- July	Orange-red berries
	Rosa hybrida	2-3	April-October	Different flower colors
	*Ribes aureum '*Prush'	1-2	April- May	Yellow Flowered Black Fruity
	Syringa vulgaris	5-6	May	Lilac flowers
	Sambucus nigra	More than 3 m	-	Black Berries
	Spiraea x vanhouttei	2-5	April-May	White flowers
	Symphoricarpos orbiculatus	1.5-2	-	White Berries
	Tamarix tetrandra	4-5	June	Tulum image
	*Thuja orientalis '*Aurea Nana'	1.5-2	-	Yellow color
	Weigela coraensis	2-3	May- June	Pink flowers
	Viburnum opulus	More than 3 m	May-early June	White flowers

Conclusions and Recommendations

The transformation of the spaces between buildings and structures in and around the city into habitable defined areas is only possible with the 'Planting Design' studies, which form an important part of the landscape architecture discipline. The compositions that emerge by arranging the visual characteristics of the plants and the functions they undertake in the design can be grasped through basic visual evaluation, which is one of the most important components of human perception. Plants, which provide climate control and aesthetical benefits in the regulation of public open spaces in cities, are one of the determining factors in revealing the living space and quality of life of the urban space with its ecological, socio-cultural, psychological, hygienic and functional benefits. However, unfavourable weather conditions in winter cities also physically and psychologically restrict human life and activities and thus the use of public open spaces. In this respect, suitable plantation should be realized in public areas and especially in areas where buildings are densely located. images of buildings with ornamental plants around them appears to be better quality than plant-free conditions, even in winter cities (Figure 5).

In the results of this study for Ardahan, Kars, Igdir, Agri, Van, Hakkari, Bitlis, Mus, Erzurum, Erzincan, Tunceli, Bingol, Elazig and Malatya provinces that located in Eastern Anatolia Region; created a list of ornamental plants for alternative use, which can provide visual improvement and create effective images in winter. In this context, it will be possible to make the area more interesting by creating different colour and visual effects with plants in successive seasons throughout the year in public spaces which are the visual pollution of winter cities. *Forsythia x intermedia* and *Syringa vulgaris,* which bloom early in the spring, will continue to colour the flowering plants such as *Buddleja davidii* and *Weigela coraensis* in summer. In autumn, the plants will be colored with fruits such as *Symphoricarpos orbiculatus* and *Pyracantha Coccinea* or red leaves such as *Acer platanoides* and *Parthenocissus quenquefolia*. Then in winter, the same area with conifers of different colours,

such as *Picea abies* and *Abies cilicica,* will have a better-quality image in terms of visual landscape. However, in parks and squares *Abies concolor, Picea pungens* and *Juniperus sabina* are coniferous plants that are suitable for forming snow and wind curtains. Broad-leaved and salt-resistant species *Fraxinus americana*, *Symphoricarpos orbiculatus* and *Syringa vulgaris* are suitable plants for creating snow and wind curtains in parks and squares.

Figure 5. Two different images of mass housing and their surrounding in winter (Url 4)

As a result, the public spaces in winter cities, which are arranged according to climatic conditions and arranged with the right planting design, will encourage the urbanite to spend more time in the outdoor space and enable the creation of more interesting urban spaces in terms of visual landscape. However, ecological improvement will also take place. Visual pollution that occurs in urban spaces includes the concern that urban objects and spaces are not aesthetic. The concept of aesthetics, on the other hand, addresses a wide audience from a single individual to a social level. Since the determinant of visual pollution is society, a social assessment seems necessary in the designs to be made. In this context, the relationships between aesthetic evaluation and user of the environment and evaluation methods should be investigated.

References

Alp Ş, (2007) Van Kenti ve Çevresindeki Geleneksel Konut Bahçelerinde Kullanılan Bitki Materyalinin Belirlenmesi. *Yüzüncü Yıl Üniversitesi Tarım Bilimleri Dergisi*, **17** (1), 1-6.

Austin R L, (1982) Designing *with Plants,* Van Nostrand Reinhold, New York. 5.

Ayaslıgil Y, (2004) *Bitkilendirme Tasarımı Ders Notları*, İ.Ü. Orman Fakültesi, Peyzaj Mimarlığı Bölümü, İstanbul.

Birisci T, Mansuroğlu S, Soğut Z, Kalaycı Onac A, (2017) "Evaluation of the Effects of Globalization On Change of Urban Landscapes Within the Scope of Tourism" *I^st^ International Conference on Tourism Dynamics and Trends,* (26-29 June 2017) Proceeding Book, Seville, Spain, pp:121-133.

Booth NK, (1996) Basic Elements of Landscape Architectural Design, Waveland Press, Inc. Illinois.

Candemir Z S, (2009) "İklime Duyarlı Yapılaşma İçin İmar Yönetmeliği Geliştirme Modeli", Basılmamış Doktora Tezi, Dokuz Eylül Üniversitesi Fen Bilimleri Enstitüsü, İzmir.

Cengiz C, Cengiz B, Mutlu BE, (2016) "Türkiye Kış Kentlerinde Dış Mekân Tasarımında Yaya Konforuna Yönelik Öneriler IWCS", *International Winter Cities Symposium 10-12 February*, Erzurum, Proceeding, p:333-349, ISBN No: 978-975-442- 811-7.

City of Minneapolis, (2011) A Guide to Winter City Design from The Minneapolis Plan for Sustainable Growth, http://www.minneapolismn.gov/www/groups/public/@cped/documents/webcontent/wcms1p-087554.pdf (connection on 23 September 2019)

Coleman PJ, (2009) Pedestrian Mobility in Winter. http://www.physicalactivitystrategy.ca/pdfs/BEAT/Pedestrian_ Mobility_Winter.pdf, (connection on 01 June 2019).

Dirik H, Ata C, (2005) *Kent Ormancılığının Kapsamı, Yararları, Planlanması ve Teknik Esasları*, İ.Ü. Orman Fakültesi Dergisi, 55(1): 1 - 14

Erbas E, (2003) Peyzaj Düzenlemelerinde Bitkisel Tasarım 'Bahçeşehir Doğa Parkı Örneği', MSc. Thesis, İ.T.Ü. Fen Bilimleri Enstitüsü, İstanbul.

Erdönmez E, Akı A, (2005) Açık Kamusal Kent Mekanlarının Toplum İlişkilerindeki Etkileri, *Megaron, YTÜ Mim. Fak*., **1**(1):67-87.

Erskine R, (1986) Livable Winter Cities. A Joint Venture by The American Institute of Architects And The Royal Architectural Institute of Canada, Edmonton, Alberta.

Gulgun B, Guney MA, Aktaş E, Yazici K, (2014) Role of The Landscape Architecture İn Interdisciplinary Planning of Sustainable Cities. *J. Environ. Protec. & Ecol*., 15(4), 1877-1880.

Henke M, (2006) "Urban Winter: Applying Winter City Planning Principles to Improve Livability At the University of Winnipeg", Degree of Master of City Planning, Department of City Planning, Faculty of Architecture, University of Manitoba.

Kelkit A, (2002) Çanakkale kenti açık-yeşil alanlarda kullanılan bitki materyali üzerinde bir araştırma. *Ekoloji Dergisi*, **10** (43), 17-21.

Konijnendijk C, Sayaka S, Randrup T B, Schıpperıjn J, (2004) "Urban and Peri - urban Forestry in a Development Contex - Strategy and ımplementation", Journal of Arboriculture, vol.30, no:5, pp. 269 – 276.

Köseoğlu B, (2012) Kentsel Kamusal Mekânların İklim Duyarlı Tasarlanması: Türkiye Örneklerinin Karşılaştırılması, Şehir Ve Bölge Planlama Anabilim Dalı, Gazi Üniversitesi, Fen Bilimleri Enstitüsü Yüksek Lisans Tezi, s. 122. Ankara.

Kottek M, Grieser J, Beck C, Rudolf B, & Rubel F, (2006) World map of the Köppen-Geiger climate classification updated. *Meteorologische Zeitschrift*, 15(3), 259-263.

Leszczynski N, (1999) Planting the Landscape-A Professional Approach to Garden Design, John Wiley&Sons, Inc., New York.

Olgyay O, (1962) "Design with Climate", Princeton. New Jersey: Princeton University Press.

Öztürk MZ, Çetinkaya G, Aydın S, (2017) Köppen-Geiger iklim sınıflandırmasına göre Türkiye'nin iklim tipleri. *Coğrafya Dergisi*, **35**, 17-27.

Pressman N, (2016) Winter Design Guidelines. p. 97, https://www.edmonton.ca/city_government/documents/PDF/WinterCityDesignGuidelines_draft.pdf

Robinson N, (2004) The Planting Design Handbook, Ashgate Publishing Company, Hampshire, England.

Scarfone S, (2007) *Professional Planting Design*, Hoboken, NJ. John Wiley & Sons.

St Clair P, (2010) *Guidelines for Climate Responsive Design in Cold Climates with Particular Reference to Beijing, China*, www.peterstclair.com (connection on 15 June 2019).

Tandoğan O, Şişman E E, (2018) Yaşanabilir Kış Kentleri İçin Kamusal Açık Mekan Tasarımı ve Bitkisel Tasarım. Megaron, 13(2).

Türkeş M, & Tatlı H, (2011) Use of the spectral clustering to determine coherent precipitation regions in Turkey for the period 1929–2007. *Int. J. Climato*., 31(14), 2055-2067.

Urban Systems, (2000) *Winter City Design Guidelines*, Fort St. John, The Energetic City. https://urbansystems.ca/category/about-us/

URL-1: http://blog.hanneketravels.net/2016/01/snow-in-oslo.html (retrieved on 15 September 2019).

URL-2: https://gezimanya.com/stockholm (retrieved on 15 September 2019).

URL-3: https://www.straitstimes.com/multimedia/photos/in-pictures snowfall-in-Moscow (retrieved on 15 September 2019).

URL-4: https://mapio.net/pic/p-9992638/, https://traveltriangle.com/blog/snowfall (retrieved on 15 September 2019).

Yazici K, Gulgun A B, (2017) Açık-Yeşil Alanlarda Dış Mekân Süs Bitkilerinin Önemi ve Yaşam Kalitesine Etkisi Tokat Kenti Örneği. *Ege Üniversitesi Ziraat Fakültesi Dergisi*, **54**(3), 275-284.

Yazici K, Kalaycı Önaç A, Gulgun A B, (2018) *Süs Bitkilerinin Kampüs Alanlarında İşlevsel Kullanımı Tokat Gaziosmanpağa Üniversitesi Örneği*. Uluslararası Marmara Fen ve Sosyal Bilimler Kongresi 2018, 1404-1415.

Yazici K., Gülgün Aslan, B. & Ankaya F, (2017). Examination of Landscape Scenery Areas and Activities: A Case Study in Van Province of Turkey Karabük Ünvi. Sosyal Bilimler enstitüsü Dergisi, özel sayı3 168-176.

Yildizci A C, (1988) *Bitkisel Tasarım*, İ.T.Ü. Mimarlık Fakültesi, Şehir ve Bölge Planlama Bölümü, Atlas Ofset, İstanbul.

Yildizci AC, (1986) *Kentsel Yeşil Alanlar*, Yüksek Lisans Ders Notları, İstanbul.

J. Int. Environmental Application & Science, Vol. 14(4): 160-171 (2019)

Rural Habitats and Land Surface Temperature: The Case of the Big Meander Delta and its Surroundings

Ebru Ersoy Tonyaloğlu*, Birsen Kesgin Atak

Aydın Adnan Menderes University, Faculty of Agriculture, Department of Landscape Architecture, Aydın, Turkey

Received September 18, 2019; Accepter December 3, 2019

Abstract: The aim of this study is to map the habitats in the Big Meander Delta National Park, Bafa Lake Natural Park and its vicinity, to analyse the spatial properties of mapped habitats and the relationship between defined habitats and land surface temperature. The main materials of this study are composed of Sentinel 2A (dated 11 August 2017) and Landsat 8 (dated 26 August 2017) satellite images, soil map and digital elevation model. To achieve the purpose of this study, we employed vegetation analysis, object-based habitat classification, determination of land surface temperature (LST) values, and analysis of the relationships between habitats and their LST values. In order to determine the relationships between habitats and LST values, the Spearman correlation analysis and the Zonal statistics of the whole study area were conducted. The results show that whilst the dominant habitat types are Market gardens and horticulture, High-stem orchards and Standing fresh water; Eastern Mediterranean *Tamarix tickets*, *Sarcopoterium phryganas*, and Mud flats and sand flats constituted the rare habitats. The highest spatial connectivity was provided by Standing Fresh Water, Running water and Eastern kermes oak garrigues. Water and wetland habitat types have lower mean LST values compared to habitats with little or no vegetation and salt marshes. Our results confirmed that the presence of vegetation and water features as well as their type, abundance and coverage are effective factors in the formation of lower mean LST values in rural areas, too. However, the size of and the distance between those habitat patches were not significantly correlated with their mean LST values in our study area. So, further empirical research with time intervals might be necessary to efficiently measure the relationships between the spatial characteristics of habitat patches and their mean LST values at different times in a year. In any case, we believe that this study is important for initiating a monitoring research on the changes in habitats and the associated land surface temperatures. Such a future work can help us to provide early step for adopting suitable policies for either overcome or minimise the local climate changes and other related problems.

Keywords: *Climate change, Habitat mapping, Land surface temperature, Landsat satellite image, Sentinel 2A satellite image.*

Introduction

Ecosystems are functional units which consist of dynamic and complex interactions between living communities such as plants, animals and microorganisms and abiotic environment, and there are many services provided by healthy ecosystems for human life. These may include supporting (primary production, soil production, etc.), provisioning (fresh water, food, fuel, etc.), regulating (climate, natural cycles, *etc*.), and cultural (aesthetic, recreational, *etc*.) (MEA, 2005). However, the increasing demand for limited resources and rapid urbanisation have led to decreases in animal and plant species diversity, degradation of ecosystems and deterioration in ecosystem services, and even confronted some species with extinction. Delta systems are among the most important ecosystems that include water and wetland habitats as well as other surrounding terrestrial habitats. With these characteristics, delta systems are threatened by intensive agricultural activities as well as problems such as disruption of the water regime, loss of natural/semi-natural habitats and the excessive use of pesticides. In parallel with these environmental problems, there has been an urgent need for the development of holistic planning and management approaches from international to local scale around the world in terms of conservation and sustainability of natural areas (Lacoeuilhe *et al.,* 2018).

Water and wetland systems are one of the most efficient ecosystems that enable the transition

* *Corresponding e-mail: ebru.ersoy@adu.edu.tr, , Tel: +90 5059738268, Fax: 0256 772 72 33*

between terrestrial and aquatic ecosystems. They are also important areas for the survival, sustainability and development of all living organisms. Historically concentrated around deltas, flood plains, rivers, sea and lake shores with the first settlements, the human life still depends on water and wetlands (Mitsch & Gosselink, 2000; Atalay, 2008). Evidence suggests that deltas and its surroundings are among the most important systems for biodiversity and have crucial functions in improving water quality of the region, reducing the risk of flood and drought and mitigating the negative effects of climate change (Song, 2003; MEA, 2005; Atalay, 2008; Yang & Tong, 2011). However, accurate and detailed data on the location, spatial characteristics and potential benefits of deltas and its surroundings are often scarce or difficult to access. Hence, the lack of enough data on the current status of these systems is one of the main challenges in land use planning and management. The Land Surface Temperature (LST) is an important indicator of the current status of surface energy and water balance in terrestrial and aquatic habitats at local and regional scales (Mannstein, 1987). The past thirty years have seen increasingly rapid advances in LST analysis, particularly for measuring the adverse effects of urban heat islands and local climate change in densely built-up urban areas (Saaroni and Ziv, 2003; Jin *et al.,* 2011; Klein and Coffman, 2015). On top of anthropogenic heat mainly stemming from artificial surfaces, there are also other factors affecting the formation of heat islands such as atmospheric pollution, loss of vegetation cover and water surfaces (Santamouris, 2014).

Studies on LST and urban heat islands emphasise that the presence of vegetation and water, especially their abundance and density, are one of the most important factors in reducing/eliminating the negative effects of urban heat islands (Chen *et al.,* 2006; Hathway and Sharples, 2012). The methods used for the modelling of heat islands and determining their characteristics are mainly divided into two groups. Whilst the first group studies are based on air temperature measurements, the second group studies are based on land surface temperature (LST) (Streutker, 2003). The estimations of the LST based on thermal remote sensing data (Streutker, 2002; Mathew *et al*., 2017), is one of the important applications for addressing issues on land and water management in terrestrial and aquatic habitats. Despite that there has been little quantitative analysis of LST in rural areas, particularly the ones with important terrestrial and aquatic habitats. The aim of this study is, therefore, to identify the habitats in the delta system of the Big Menderes Delta National Park, the Bafa Lake Nature Park and its vicinity, and to analyse the relationship between spatial structural characteristics of these habitats and land surface temperature.

Material and Method

Material

This study was conducted within the Big Menderes Delta National Park, Bafa Lake Nature Park, Azap Lake and flood area, Sarıkemer flood area and their immediate vicinity. The study area, covering an area of 55165 ha, is in the province of Aydın, the Aegean Sea Region (Figure 1). The study area is in a natural basin which is shaped by the Big Meander River through time and includes two important protection areas namely, the Big Menderes Delta National Park, Bafa Lake Nature Park. There are many lagoons and swamps in the area where the Big Meander Delta flows into the sea, which has the international importance of 'Class A Wetland' (Anonymous, 2017).

Also, Bafa Lake and its surroundings, as a flood plain, share similar ecological characteristics with the Big Menderes Delta. Ecologically, including a wide variety of habitats, study area is rich in biological diversity (Figure 2). Despite having a variety of habitats and ecosystems, the study area suffers a range of issues which also changes the structure and functioning of the area (Eşbah et al., 2009). These issues are mainly composed of burning the natural vegetation around wetlands, pollution and heavy grazing activities (Figure 3).

The habitat map used for analysing the spatial characteristics of the study area was obtained from 7 layers of 10 m spatial resolution including; Sentinel-2A satellite image (dated 11 August 2017) true colour bands (B02-blue, B03-green and B04-red), digital elevation model (DEM) and three main features of soil map (major soil groups, land use capability and other soil properties). In order to estimate the land surface temperature in the research area, cloud-free Landsat 8 satellite image of 26 August 2017 were used, considering the periods during which vegetation was active.

ArcGIS 10.5.1 and e-Cognition Developer64 software were used for identification, classification and mapping of habitats. For the analysis of landscape structural properties, we have used patch and class level landscape metrics in FRAGSTATS v4.2.1. Finally, statistical analyses were performed in

ArcGIS 10.5.1, and MatlabTM.

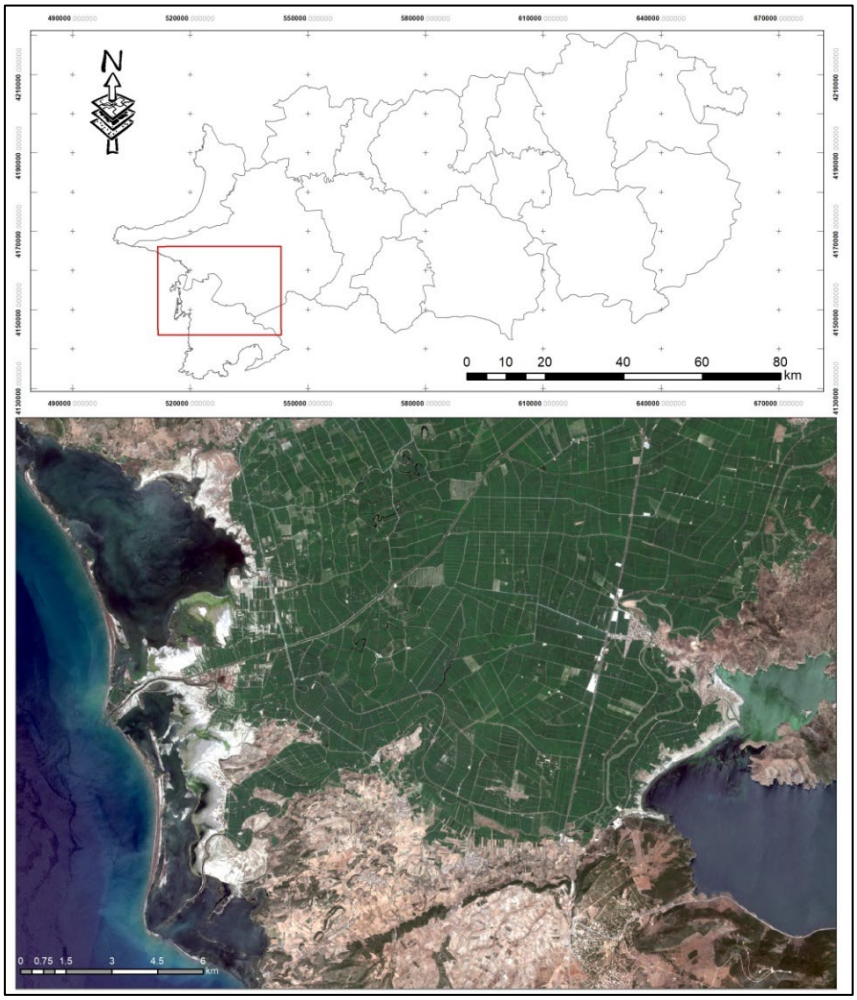

Figure 1. Study Area

Figure 2. Different habitat types in the study area

Figure 3. Main issues in the study area4

Methods

Vegetation analysis

For the vegetation analyses, six-day field survey was carried out on 11.05.2017, 08.06.2017, 18.10.2017, 23.11.2017, 24.11.2017 and 14.12.2017. During field surveys, plant-species composition was recorded, and the characteristics of the recorded plant taxa were determined in terms of their community formation (values of presence, abundance-coverage, frequency and constancy). Identification of plant communities based on vegetation analysis was the baseline data for the classification of habitats in the study area. According to the findings obtained from the vegetation analysis records, the main habitat types and the associated plant communities were defined in the study area (Table 1).

Table 1. Main Habitat types in the study area

CORINE Habitat Codes	CORINE Habitat Types
11.12	Shelf and slope waters
14	Mud flats and sand flats
15.11	Glasswort swards
15.51	Mediterranean tall rush saltmarshes
15.61	Mediterranean salt scrubs
22	Standing fresh water
24	Running water
32.144	Aegean pine arborescent matorrals
32.5D	Arbutus andrachne garrigues
32.51	Eastern kermes oak garrigues
33.31	*Sarcopoterium phryganas*
42.85	Aegean pine forests
44.89133	Eastern Mediterranean *Tamarix tickets*
82.12	Market gardens and horticulture
83.1	High-stem orchards
84	Tree lines, hedges, small woods, bocage, parkland dehesa
86	Towns, villages, industrial sites

Habitat mapping

In this study, an object-based classification approach was applied by using e-Cognition Developer64 software in order to identify different habitat types. In the object-based classification method, images are segmented according to characteristics such as criteria, colour and shape (Pillai et al. 2005; Mathieu et al. 2007). After the pre-processing of 7 selected layers in ArcGIS 10.5.1, the habitat map

was created by utilising an object-based classification using the nearest neighbour supervised classification method. The application of object-based supervised classification used in the study consists of three steps: a) the segmentation stage (multi-resolution segmentation algorithm), (b) selection of sample areas that represents different habitat types and, (c) performing supervised classification by the nearest neighbour classification method. Images are segmented according to their main characteristics like colour and shape, so the segmentation step is one of the most important stages of object-based classification. Since the size of objects defined in a satellite image varies according to the parameters used in the analysis, the parameters of segmentation is quite important to obtain an object structure that would provide the most suitable homogeneity in the satellite image. For this study, we applied the multi-resolution segmentation algorithm which works based on the parameters of scale and composition of heterogeneity criterion. In this algorithm, the larger the scale parameter, we get the larger sized objects. Whereas, the homogeneity parameters relate to the grouping of pixels, in other words the shape and density of defined objects (Pillai *et al.,* 2005; Mathieu *et al.,* 2007). In the segmentation step, each layer was equally weighted (1 value) with the value of 15 for the shape and the value of 0.3 for the compactness parameters (Figure 2).
After segmentation step, based on field surveys and GPS points, we have determined the sample areas that represent different habitat types. Next, we performed a supervised classification by the nearest neighbour classification method and the accuracy of the result map was increased by manual editing of the defined habitat classes. We also overlapped the vector data of roads and channels, which have a significant impact on habitat fragmentation, with the final habitat map. Finally, based on the Sentinel-2A satellite image, we calculated the average width of the vegetation corridors along the field boundaries and roadsides and creating a buffer of 5 m surrounding roads, channels and field boundaries, we obtained vegetation corridors along the roadsides and the borders of agricultural areas. The accuracy assessment of the habitat map was carried out by using the sample based error matrix method with the help of ArcGIS 10.5.1 software. Each habitat defined in the study area is coded using CORINE biotopes habitat codes (Devillers *et al.,* 1991).

Analysis of spatial characteristics of habitat types

The spatial and structural characteristics of habitats were analysed using patch and class level landscape metrics in FRAGSTATS v4.2.1. The selected landscape metrics are composed of 3 metrics at class level and 2 metrics at patch level (Table 2). Before running FRAGSTATS landscape metric analysis, we resampled the habitat to 30 m resolution in order to obtain spatial consistency between data layers.

Table 2. Landscape metrics that are used in this study

Landscape Metric	Abbreviation	Reason for Selection
Total class area, ha *	CA	Dominancy in the landscape
Number of patches*	NP	Together with CA and AREA_MN, fragmentation
Mean area, ha*	AREA_MN	Together with CA and NP, fragmentation
Effective MESH size, ha*	MESH	Connectivity / fragmentation
Patch area, ha**	AREA	Size of each habitat patch
Euclidean nearest neighbour distance**	ENN	The shortest edge to edge distance between each habitat

**class level metrics, **patch level metrics*

Determination of Land Surface Temperature (LST)

The retrieval of LST in an area is provided by thermal remote sensing data using satellite images (Chudnovsky et al., 2004; Jin et al., 2011). We applied the LST retrieval process conducted in the literature using the metadata file of Landsat 8 satellite image (see USGS, 2018a; Oğuz and Zengin, 2011; Chen *et al.,* 2014; Du *et al.,* 2016).LST data, based on thermal remote sensing, provides synchronous and continuous data set on the radiative temperature obtained from a terrain surface for larger areas (Du *et al.,* 2016). We have used thermal bands (Band 10 and 11) as well as near infrared and red bands (Band 4 and 5) of Landsat 8 satellite image for the hottest period of summertime in Aydın (dated 26 August 2017). Whilst thermal bands were mainly used for the conversion of

brightness values to spectral radiance values, spectral radiance values to reflectance values and radiance values to brightness temperature values; near infrared and red bands were used for the calculation of ground surface emissivity value (USGS, 2018b, c). For the determination of LST values and performing spatial analysis at the same spatial resolution, thermal bands of Landsat 8 satellite images were resampled to 30 m with the nearest neighbour algorithm. After that, we retrieved the LST of the study area.

The relationship between habitats and LST values

The relationship between habitats and LST values were evaluated using two approaches. The Zonal statistics tool of ArcGIS 10.5.1 was used to define minimum, mean, maximum LST values of each habitat type. On the other hand, the Spearman correlation analysis was used to quantify the effect of the habitat patch pattern on the mean LST values. The Spearman correlation analysis was performed in the MatlabTM by calculating the cross-correlation coefficients (e.g. patch area value versus mean LST value, ENN value versus mean LST value, etc.) (Matlab and Statistics Toolbox Release, 2012). Spearman's correlation coefficient (r_s) is a statistical measure of the strength of a monotonic relationship between paired data where the closer rs is to ±1 the stronger the monotonic relationship. The relationship between habitats and LST values were evaluated according to the Cohen standards (Cohen, 2013). According to Cohen standards, correlation coefficients between 0.10 and 0.29 are weak, correlation coefficients between 0.30 and 0.49 are moderate and correlation coefficients higher than 0.50 represent strong correlation.

RESULTS

Habitat Map and the Spatial Characteristics of Habitat Types

The resulting habitat map includes 17 habitat types with the total accuracy of 83.33% (kappa = 0.82) (Figure 4). However, because the boundary of Shelf and slope waters habitat type depends on the selection of case study area and it is restricted to the area that we defined within our study, it was excluded from further analysis.

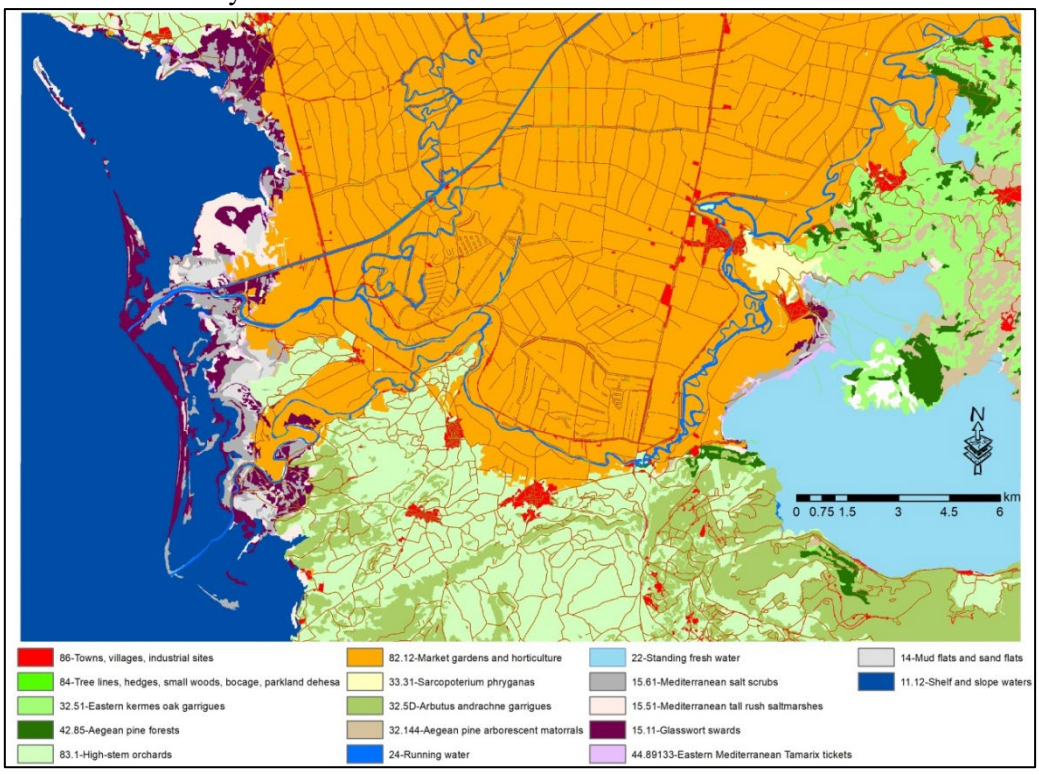

Figure 4. Habitat Map

Table 3 represents the results of landscape metrics at class level. Whilst the dominant habitat types in the study area are composed of Market gardens and horticulture (41.21%), High-stem orchards (13.29%) and Standing fresh water (10.54%), the rare habitat types are Eastern Mediterranean

Tamarix tickets (0.27%), *Sarcopoterium phryganas* (0.46%) and Mud flats and sand flats (0.80%).

Table 3. Result of the landscape metrics

Habitat Type	CA	NP	AREA_MN	MESH
14- Mud flats and sand flats	355.12	34	**10.44**	0.27
15.11- Glasswort swards	1225.67	284	4.32	2.36
15.51-Mediterranean tall rush saltmarshes	629.03	181	3.48	1.14
15.61-Mediterranean salt scrubs	954.82	303	3.15	0.69
22- Standing fresh water	**4701.38**	79	**59.51**	**376.59**
24-Running water	816.12	121	6.74	7.94
32.144 - Aegean pine arborescent matorrals	1104.24	280	3.94	1.32
32.5D- Arbutus andrachne garrigues	3686.32	645	5.72	12.6
32.51- Eastern kermes oak garrigues	2100.32	214	**9.81**	**9.42**
33.31- Sarcopoterium phryganas	205.85	31	6.64	0.48
42.85- Aegean pine forests	662.80	117	5.67	0.72
44.89133- Eastern Mediterranean *Tamarix tickets*	118.42	80	1.48	0.03
82.12- Market gardens and horticulture	**18376.28**	**1267**	**14.50**	**37.38**
83.1- High-stem orchards	**5924.76**	**1080**	5.49	6.21
84- Tree lines, hedges, small woods, bocage, parkland dehesa	1253.10	**1166**	1.07	0.18
86- Towns, villages, industrial sites	2472.29	811	3.05	**23.16**

Even though the habitat types of Market gardens and horticulture and High-stem orchards dominate the study area, they demonstrate a patchier pattern in the landscape with lower mean patch area and the high number of patches. Standing fresh water represents the highest physical connectivity with the largest mean area and MESH value, and the lowest patch number. This followed by Running water, Eastern kermes oak garrigues, *Sarcopoterium phryganas*, Arbutus andrachne garrigues, and Tree lines, hedges, small woods, bocage, parkland dehesa. Towns, villages, industrial sites, constituting an important component of cultural habitats, cover only 5.54% of the total area with a patchier but closely positioned pattern.

The Relationships between Habitats and LST

Figure 3 represents the distribution of LST values in the study area. Whilst the areas in bright red reported the highest LST values with 42.65°C, the areas in dark blue had the lowest LSt values with 24.10°C. From Figure 5, we can clearly see that the lakes on the eastern part of the study area and the patches of Market gardens and horticulture show lower temperatures in the study area. Table 4 shows the relationship between habitat types and their min, max and mean LST values in degrees.

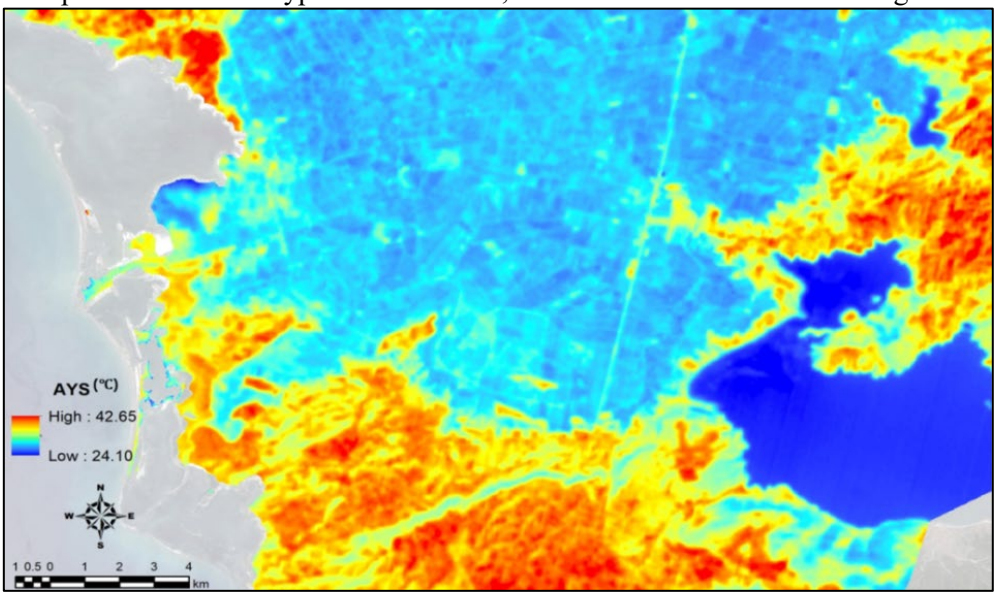

Figure 5. LST Map

Table 4. Relationship between habitat types and LST

CORINE Habitat Codes and Types	Min LST(°C)	Max LST(°C)	Mean LST(°C)
14- Mud flats and sand flats	28.86	38.24	34.72
15.11- Glasswort swards	26.71	42.65	35.15
15.51-Mediterranean tall rush saltmarshes	24.91	39.93	30.41
15.61-Mediterranean salt scrubs	26.45	40.63	35.13
22- Standing fresh water	24.10	35.20	**25.57**
24-Running water	27.09	37.77	**29.26**
32.144 - Aegean pine arborescent matorrals	25.27	41.92	35.83
32.5D- Arbutus andrachne garrigues	27.11	39.93	33.38
32.51- Eastern kermes oak garrigues	25.14	42.12	35.44
33.31- *Sarcopoterium phryganas*	29.84	39.46	35.17
42.85- Aegean pine forests	26.23	38.67	32.22
44.89133- Eastern Mediterranean Tamarix tickets	25.05	37.12	31.19
82.12- Market gardens and horticulture	26.53	38.16	**28.98**
83.1- High-stem orchards	27.87	41.89	36.62
84- Tree lines, hedges, small woods, bocage, parkland dehesa	24.23	40.99	31.70
86- Towns, villages, industrial sites	26.51	41.40	32.16

As expected, standing fresh water have the lowest mean LST value because of the cooling effect of water surfaces through evaporation (Hathway & Sharples, 2012; Sun *et al.,* 2012). Running water reported a higher LST value, and that result was attributed to the neighbouring patches of other habitat types (such as Mediterranean salt scrubs and Mediterranean tall rush saltmarshes towards to the coastal parts of the study area) with higher LST values. Surprisingly, Market gardens and horticulture has the third lowest LST value whilst High-stem orchards reported the highest LST value. However, this was a natural result of vegetation coverage on the soil surface at the time of the satellite image was taken. Since the density and coverage of healthy vegetation is an important factor in decreasing the LST, areas of low-density vegetation report higher LST values compared to (Gill *et al.,* 2007).
Glasswort swards, Mediterranean salt scrubs and Mud flats and sand flats reported higher LST because of their high content of salt (Orhan *et al.,* 2014; Gorji *et al.,* 2015). On the other hand, Mediterranean tall rush saltmarshes reported a lower LST value compared to abovementioned salty habitat types because of the height and density of vegetation on it at the time of LST retrieval. A similar surprising result was obtained for Aegean pine arborescent matorrals, Eastern kermes oak garrigues, *Sarcopoterium phryganas* and *Arbutus andrachne* garrigues, where they reported higher values of LST. But this was again a natural result of the scarcity and cover of vegetation on those habitats. Contrary to urban areas, the habitat type of Towns, villages, industrial sites reported moderate LST values because of the abundance and cover of vegetation patches within them (Figure 6). This result can also be explained with the fact that rural areas generally have low density of population, buildings and grey infrastructure over large areas of land compared to the urban areas (Houghton *et al.,* 2017).

Figure 6. An example of Towns, villages, industrial sites habitat type in the study area

Table 5 shows the correlation between habitat types and the area of, and distance between their patches and the mean LST values. Contrary to our expectations, the size of and the distance between different habitat patches were not significantly correlated with the mean LST values in our case study area. In general, the size and habitat patches and the mean LST were inversely correlated. In other words, the increasing size of habitat patches with fresh water, trees, shrubs and ground cover vegetation resulted in lower mean LST values.

Table 5. Relationships between landscape metrics and mean LST values

CORINE Habitat Codes and Types	Area (ha)	ENN (m)
14- Mud flats and sand flats	-0.0027	-0.359
15.11- Glasswort swards	0.1136	-0.1706
15.51-Mediterranean tall rush saltmarshes	0.1199	-0.0167
15.61-Mediterranean salt scrubs	0.1733	-0.1754
22- Standing fresh water	-0.6681	0.5387
24-Running water	-0.0701	0.0992
32.144 - Aegean pine arborescent matorrals	0.0688	0.0141
32.5D- Arbutus andrachne garrigues	-0.1571	-0.3313
32.51- Eastern kermes oak garrigues	0.0594	-0.1625
33.31- *Sarcopoterium phryganas*	-0.0183	-0.2041
42.85- Aegean pine forests	-0.217	0.302
44.89133- Eastern Mediterranean Tamarix tickets	-0.2047	0.1183
82.12- Market gardens and horticulture	-0.1689	0.1503
83.1- High-stem orchards	0.1613	-0.2882
84- Tree lines, hedges, small woods, bocage, parkland dehesa	0.0386	0.1595
86- Towns, villages, industrial sites	0.1324	-0.4827

However, if the coverage of vegetation was low or the salt content of soil and wetlands was high, the size and habitat patches and the mean LST were positively correlated. Towns, villages, industrial sites, Mud flats and sand flats, Arbutus andrachne garrigues, High-stem orchards and *Sarcopoterium phryganas* positively correlated with the distance between their patches. That means when the patches of those habitats become distant from each other, they get lower mean LST values. On the other hand, when the distance between the patches of Standing fresh water and Aegean pine forests habitats increase, they get higher mean LST vales, and vice versa.

Discussion and Conclusions

The aim of this study was the identification and spatial analysis of habitats in the delta system of the Big Menderes Delta National Park, the Bafa Lake Nature Park and its vicinity as well as the analysis of the correlations between spatial structural characteristics of these habitats and land surface temperature. This study is important in terms of defining the natural and semi-natural habitats, determining their spatial characteristics and the relationship between habitats and LST in the case of an area that includes two important protection areas within its boundaries. As a result of the analysis of spatial characteristics of habitat types in the study area, we found that the dominant habitat types were Market gardens and horticulture, and High-stem orchards as expected, because of the presence of fertile soils in the delta systems. In general, these areas thought to create barrier effects between natural and semi-natural areas (Benton *et al.,* 2003; Kerbiriou *et al.,* 2018), however, in our case study area natural and semi-natural habitats exhibit fragmented and isolated pattern with the connecting landscape components of the habitat type of Tree lines, hedges, small woods, bocage, parkland dehesa in between agricultural areas and other natural semi-natural habitats. So, whilst the habitat type of Tree lines, hedges, small woods, bocage, parkland dehesa reduce the barrier effect of agricultural areas in our case study area, it also provide strong physical connections between the most connected habitat types of Standing fresh water and Running water as well as representing high potential of supporting,

enhancing and conserving biodiversity (Lookingbill *et al.,* 2010; Zahn *et al.,* 2010; Lacoeuilhe *et al.,* 2018). In this context, water and vegetation corridors of the habitat types of Tree lines, hedges, small woods, bocage, parkland dehesa and running between Big Meander Delta National Park and Bafa Lake Nature Park form a network in the Big Meander Delta plain and play an important ecological role in supporting biodiversity.

This study represents the results of the hottest period of summertime in Aydın (dated 26 August 2017). The estimations of the LST based on thermal remote sensing data have been widely used for monitoring water and wetland systems as well as other natural areas to obtain spatially and temporally frequent and consistent information on their environmental conditions (Guo *et al.,* 2017).The formation of high LST values, which is regarded as a reflection of the local climate change in the local environment, is a serious problem in urban areas. However, there is only scarce literature on the relationships between rural habitats and LST. The LST is an important indicator for the determination of shifts in surface temperature, presence of water and humidity, soil moisture, evaporation and salinity, for detecting the changes in the territories of ecologically important animal and plant species, and also for detecting the changes in the populations of species. Hence, retrieval of temporal LST values and its periodical evaluation through time can provide landscape planners and managers invaluable information on the changes in habitats, hydrological system and biodiversity. Local and global climate change is one of the most threating factors for biodiversity and nature conservation since every individual reacts in a different way against to climatic factors. Our findings show that the habitat types of Standing fresh water, Market gardens and horticulture and Running water had the lowest LST values, however, the size of and the distance between those habitat patches were not significantly correlated with their mean LST values in our study area. So, further empirical research with time intervals might be necessary to efficiently measure the relationships between the spatial characteristics of habitat patches and their mean LST values at different times in a year.

It is also important to note that water and wetland systems generally accommodate a very high biodiversity and provide a series of ecosystem services, including supply, regulation, support and cultural services at regional and local scales (MEA, 2005). Besides, whilst they help to mitigate the adverse effects of global and regional climate change by regulating carbon cycle and capacity of carbon storage at global/regional scales (Song, 2003; Yang & Tong, 2011), they also play a key role in determining local climates at local scales through their cold-humid effects and energy exchange properties (Gao *et al.,* 2003; Nie & Wang, 2010). In this context, according to the principles of the United Nations Framework Convention on Climate Change (21 March 1994), measures to be taken to prevent climate change on a large scale and at minimum cost. With the development of thermal remote sensing technologies, LST retrieval using satellite images is now one of the practical ways of detecting the thermal environment of different habitats. Rapid observations of the LST values of different habitats are, therefore, important for understanding wetland systems and their surroundings.

Accordingly, this study is important for initiating a monitoring research on the changes in habitats and the associated land surface temperatures. Finally, as mentioned earlier under material section, the water and wetland system in the study area suffers from various environmental problems pollution, burning the natural vegetation around wetlands as well as heavy grazing activities (Eşbah *et al.,* 2009). Therefore, this study constitutes the base information for future monitoring work in the study area. Such a future work can help us to provide early step for adopting suitable policies for either overcome or minimise the local climate changes and other related problems (Pal & Ziaul, 2017).

Acknowledgment: *This study is supported by Adnan Menderes University Scientific Research Projects Coordination Unit (Project No: ZRF-17044).*

References

Anonymous, (2017) Doğa Koruma ve Milli Parklar Genel Müdürlüğü, Dilek Yarımadası. Retrieved September 28, 2019, from http://www.dilekyarimadasi.gov.tr/hakkimizda.asp?id=1

Atalay İ, (2008) *Ekosistem Ekolojisi ve Coğrafyası*, Cilt II. İzmir: META Basım Matbaacılık Hizmetleri.

Benton TG, Vickery JA & Wilson JD, (2003) Farmland biodiversity: is habitat heterogeneity the key? *Trends in ecology & evolution*, 18(4), 182-188.

Chen A, Yao XA, Sun R, Chen L, (2014) Effect of urban green patterns on surface urban cool islands and its seasonal variations. *Urban forestry & urban greening*, **13**(4), 646-654.

Chen XL, Zhao HM, Li PX, Yin ZY, (2006) Remote sensing image-based analysis of the relationship between urban heat island and land use/cover changes. *Remote sensing of environment*, *104*(2), 133-146.

Chuan Y & Tong P, (2011) Effects of LUCC on Carbon Stocks and Emission in Wetland [J]. *Wetland Science & Management*, **7(3)**, 56-59.

Chudnovsky A, Ben-Dor E, Saaroni H, (2004) Diurnal thermal behavior of selected urban objects using remote sensing measurements. *Energy and Buildings*, **36**(11), 1063-1074.

Cohen J, (2013) *Statistical power analysis for the behavioral sciences*. Routledge.

Devillers P, Devillers-Terschuren J, Ledant JP, (1991) CORINE Biotopes manual: habitats of the European Community. *Publication EUR*, *12587*(3).

Du H, Wang D, Wang Y, Zhao X, Qin F, Jiang H, Cai Y, (2016) Influences of land cover types, meteorological conditions, anthropogenic heat and urban area on surface urban heat island in the Yangtze River Delta Urban Agglomeration. *Sci.Total Environ.*, **571**, 461-470.

Eşbah Tunçay H, Kelkit A, Deniz B, Kara B & Bolca M, (2009) Peyzaj sütrüktür indeksleri ile koruma alanları ve çevresindeki peyzajın geçirdiği değişimin tespiti ve alan kullanım planlaması önerilerinin geliştirilmesi: Dilek Yarımadası-Menderes Deltası Milli Parkı ve Bafa Gölü Koruma Alanı örneği. *TÜBİTAK, Çevre, Atmosfer, Yer ve Deniz Bilimleri Araştırma Grubu, Proje Sonuç Raporu,* Ankara.

Gao J, Lu X, Liu H, (2003) Cold-humid effect of wetlands. *Rural Eco-environment*, **19**(1), 18-21.

Gill SE, Handley JF, Ennos AR & Pauleit S, (2007) Adapting cities for climate change: the role of the green infrastructure. *Built Environ.*, **33**(1), 115-133.

Gorji T, Tanik A, Sertel E, (2015) Soil salinity prediction, monitoring and mapping using modern technologies. *Procedia Earth & Planetary Sci.*, **15**, 507-512.

Guo M, Li J, Sheng C, Xu J & Wu L, (2017). A review of wetland remote sensing. *Sensors*, **17**(4), 777.

Hathway EA, Sharples S, (2012) The interaction of rivers and urban form in mitigating the Urban Heat Island effect: A UK case study. *Building & Environ.*, **58**, 14-22.

Houghton A, Austin J, Beerman A, Horton C, (2017) An approach to developing local climate change environmental public health indicators in a rural district. *J. Environ. & Public Health*, **2017**, 1-16.

Jin MS, Kessomkiat W, Pereira G, (2011) Satellite-observed urbanization characters in Shanghai, China: Aerosols, urban heat island effect, and land–atmosphere interactions. *Remote Sensing*, **3**(1), 83-99.

Kerbiriou C, Azam C, Touroult J, Marmet J, Julien JF, Pellissier V, (2018) Common bats are more abundant within Natura 2000 areas. *Bio. Conser.*, **217**, 66-74.

Klein PM, Coffman R, (2015) Establishment and performance of an experimental green roof under extreme climatic conditions. *Sci. Total Environ.*, **512**, 82-93.

Lacoeuilhe A, Machon N, Julien JF & Kerbiriou C, (2018) The relative effects of local and landscape characteristics of hedgerows on bats. *Diversity*, **10**(3), 72.

Lookingbill TR, Elmore AJ, Engelhardt KA, Churchill JB, Gates JE & Johnson JB, (2010), Influence of wetland networks on bat activity in mixed-use landscapes. *Bio. Conser.*, **143**(4), 974-983.

Mannstein H, (1987) Surface energy budget, surface temperature and thermal inertia. In *Remote sensing applications in meteorology and climatology* (pp. 391-410). Springer, Dordrecht.

Mathew A, Khandelwal S, Kaul N, (2018) Analysis of diurnal surface temperature variations for the assessment of surface urban heat island effect over Indian cities. *Energy & Build.*, **159**, 271-295.

Mathieu R, Aryal J, Chong A (2007) Object-based classification of Ikonos imagery for mapping large-scale vegetation communities in urban areas. *Sensors*, *7*(11), 2860-2880.

MATLAB, Release ST, (2012) Natick. *Massachusetts, United States: The MathWorks Inc*.

MEA, (2005) Millennium ecosystem assessment. *Ecosystems and human well-being: current state and trends. World Resources Institute, Washington, DC, États-Unis*.

Mitsch WJ, Gosselink JG, (2000) The value of wetlands: importance of scale and landscape setting. *Ecological Economics*, **35**(1), 25-33.

Nie X, Wang Y, (2010) "Cold-humidity island" effect of marsh wetlands on localized micro-climate. *J. Ecology & Rural Environ.*, **26**(2), 189-192.

Oguz H, Zengin M, (2011) Analyzing land use/land cover change using remote sensing data and landscape structure metrics: a case study of Erzurum, Turkey. *Fresenius Environmental Bulletin*, **20**(12), 3258-3269.

Orhan O, Ekercin S, Dadaser-Celik F, (2014) Use of landsat land surface temperature and vegetation indices for monitoring drought in the Salt Lake Basin Area, Turkey. *The Scientific World Journal*, *2014*.

Pal S, Ziaul SK, (2017) Detection of land use and land cover change and land surface temperature in English Bazar urban centre. *The Egyptian Journal of Remote Sensing and Space Science*, *20*(1), 125-145.

Pillai RB, Weisberg PJ, Lingua E, (2005) Object-oriented classification of repeat aerial photography for quantifying woodland expansion in central Nevada. In *20th Biennial Workshop on Aerial Photography, Videography, and High Resolution Digital Imagery for Resource Assessment, Waslaco, TX, October* (pp. 2-6).

Saaroni H, Ziv B, (2003) The impact of a small lake on heat stress in a Mediterranean urban park: the case of Tel Aviv, Israel. *International journal of Biometeorology*, **47**(3), 156-165.

Santamouris M, (2014) Cooling the cities–a review of reflective and green roof mitigation technologies to fight heat island and improve comfort in urban environments. *Solar energy*, *103*, 682-703.

Song CC, (2003) Advance in research on carbon cycling in wetlands. *Scientia Geographica Sinica/Dili Kexue*, *23*(5), 622-628.

Streutker DR, (2002) A remote sensing study of the urban heat island of Houston, Texas. *International Journal of Remote Sensing*, *23*(13), 2595-2608.

Streutker DR, (2003) Satellite-measured growth of the urban heat island of Houston, Texas. *Remote Sensing of Environment*, *85*(3), 282-289.

USGS, (2018a) The United States Geological Survey. EarthExplorer-Home. Retrieved August 20, 2019, from https://earthexplorer.usgs.gov/

USGS, (2018b) The United States Geological Survey. Landsat 8 Data Users Handbook - Section 5. Retrieved August 20, 2019, from https://landsat.usgs.gov/landsat-8-l8-data-users-handbook-section-5

USGS, (2018c) The United States Geological Survey. What are the band designations for the Landsat satellites? Retrieved August 20, 2019, from https://landsat.usgs.gov/what-are-banddesignations-landsat-satellites

Zahn A, Rottenwallner A, Güttinger R, (2006) Population density of the greater mouse-eared bat (Myotis myotis), local diet composition and availability of foraging habitats. *J. Zoology*, **269**(4), 486-493.

J. Int. Environmental Application & Science, Vol. 14(4): 172-176 (2019)

Measurements of Heavy Metal Concentrations in Tap Water

Mirela Alushllari*

Institute of Applied Nuclear Physics, University of Tirana, Tirana, Albania

Received October 05, 2018; Accepted November 14, 2019

Abstract: The presence of heavy metals pollution in water can move and reach to another environmental media that surrounds or contacts water, soil, aerosols, vegetation or the organisms under the influence of atmospheric conditions. The presences of heavy metals pollution and their exposure time in water have negative impacts to environment media and represent problems for human health. Metal pollution in water media affect in the quality of water in depend the use. The object of this study were the tap water samples are collected in the network of public water supply system, in Tirana city and the goal of this study was the analysis and identification of heavy metals in representative water samples from sources of water to consumers. During this survey we were collected samples at different points of the public water supply system, from sources of water, storage of water and finally in the consumer from different locations in Tirana city. The analyses of heavy metals in representatives sampling of tap water were performed at the Institute of Applied Nuclear Physics, University of Tirana. Water samples were analysed using graphite furnace atomic absorption spectrometry to determine the concentration of total heavy metals. The current study reports the presence of heavy metals in the analysed tap water samples, although it should be mentioned that their concentrations are quite low, compared with the Maximum Contaminant Levels recommended by the Environmental Protection Agency and World Health Organization.

Keywords: *Heavy Metals, Tap Water, Graphite Furnace, Atomic Absorption Spectrometry*

Introduction

The water is an important natural resource for development of life (Vanloon, & Duffy, 2005). Water quality depends on the purpose of its use. Industrial and agricultural development, influence in the natural processes and aquatic environments (Alushllari & Civici, 2014). The presence of heavy metals in water is hazardous because they have high toxicity at low concentrations (Censi *et al.*, 2006). In natural environment their concentration is low (Alushllari, 2013).

There are different types of sources of pollutants, where among the main we can mention: point sources where pollutants come from single (localized pollution) and no point sources, where pollutants come from dispersed (and often difficult to identify) sources. Pollutants and metals can exist in water in different states; they can be dissolved or can be in suspension (Alushllari *et al.,* 2012)

They can reach the food chain through the drinking water supply, respiration system and food consumption (Gazso, 2001). The exposure to lead in the environment results in a wide range of negative effects, depending from the level of lead and time of extended (Alushllari & Civici, 2014). The main sources of drinking water in Tirana are the source of Selita Shën-Mëri, groundwater and surface water of the Bovilla Lake (Italian-Albanian cooperation). Road of network distribution of drinking water is: 1. the source of water; 2. the storage of water; 3. the customers. Two main sources of water are mixed. Distribution of water in the public water system is not divided on the basis of water resources, because the different parts of network can communicate among themselves, said an expert. The presence of the contaminants in drinking water in the different parts of network from the source to the consumer has various reasons. Some of them are: There is no balance between the amount of water resources, the amount of water storage and the amount of water that the customers spend. Often water storage is emptied, their level is not sustainable over time; Supply of drinking water of consumer is part time, usually 2-3 times during the day. The passage of water from their storage of water to the consumers causes pressure changes; a part of the distribution network of drinking water is amortized. The pipeline material of network water supply is made of metal alloys. Network communication with

**Corresponding: E-Mail: m.alushllari@gmail.com; Tel: +355698140573; Fax: +35543451371*

the external environment and the absence of continues water along the network creates conditions for pollution problems; Damage and cracks in pipelines of drinking water network, crossing the tap water with sewage pipelines in some points, the residence time of water in the storage, etc., have created a risk to use tap water from consumers in some areas; New constructions especially in rural area, have made possible that often unauthorized people (not the water supply specialist) have intervened and damaging the parts of the distribution network of drinking water to the city of Tirana from the source-storage-consumers.

Environmental international Organizations, especially World Health Organization and Environmental Protection Agency have recommended specified maximum levels for the presence of heavy metals in water. The purpose of this study was: The evaluation of the distribution of heavy metals from the source of water to the consumer, through the public water supply system in the city of Tirana. The concentrations of heavy metals Cd, Cr, Cu and Pb that are found in tap water samples, their concentrations are compared with Maximal Concentration Level recommended by EPA and WHO for drinking water standard (EPA) and (WHO, 1993). The object of study: the water in source, storage water and consumers (from the public water supply system of Tirana). One of the most important techniques is used to determine the elements in the environment and especially in water is classified method of Atomic Absorption Spectrometry. Drinking water samples were analysed using Graphite Furnace Atomic Absorption Spectrometry for their Cd, Cr, Cu and Pb content.

Materials and Methods

The current study reports the analysis of heavy metals Cd, Cu, Cr and Pb in the drinking water supply system, through its distribution path in the Tirana City. We have chosen six sampling stations in the sources, six sampling stations in the storage water, seventeen samples station in consumers (when sixteen water samples were from tap water and one sampling station was filtered water. We have collected a total of 30 drinking water samples from public system. Sampling stations are presented in Table 1, where source water samples are 1- 6, storage water samples are 7-12 and consumers are 13-30. For each representative samples of drinking water supply were taken two parallel samples. Drinking water samples were analysed using Atomic Absorption Spectrometer, Aanalyst 800 Perkin Elmer, with Atomic Absorption Spectrometry Graphite Furnace method (Perkin Elmer, 1996), autosampler AS-800 and graphite tube THGA Perkin Elmer with number BO504-033 and end caps. Hollow cathode lamps is used as radiation source for the determination of Cr and Cu, while Electrodeless Discharge Lamps used for the determination of Cd and Pb according recommended conditions. Acids used for the treatment of samples, preparation of standard solutions have high grade purity; they were Merck, Darmstadt, Germany. Reagents are used for treatment, measured and control interference in Atomic Absorption Spectrometry for water samples are: nitric acid concentration 65%, hydrochloric acid concentration 33%, standard of cadmium 1000 ppm, standard of Chrome 1000 ppm, standard of cupper 1000 ppm, standard of lead 1000 ppm, bi distil water, Mg (NO) $_3$ and Palladium. Glass and Teflon vessels used were treated with solution 10% v/v nitric acid, for 24 hours and then washed with water bi distilled. Drinking water samples were collected in polyethylene bottles of 1L. All drinking water samples are filtered. PH was measured in 6.8-7.2 ranges. The samples were acidified with nitric acid until pH 2, after was added Methyl isobutyl ketone. 200 ml of water sample transferred in a glass of 400 ml, added 4ml HNO_3cc and digested in a hot plate for about 2 hours, until 1-3 ml. After, samples were cold in room temperature, add 1 ml HCl cc, transferred in a balloon of 25 ml and filled with bi-distil water. All samples are measured in the Atomic Absorption Spectrometer used graphite furnace method for determination concentration of metals. Three applications were carried out for the measurement of blank, calibration standards and samples. A calibration curve defined using this equation is forced to go through zero absorbance and zero concentration. Instrumental parameters, calculation of detection limit and sensitivity control is based on Analytical Methods of Atomic Absorption Spectrometry, from Perkin Elmer (1996). The correlation coefficient of the calibration curves, for the analyzed elements Cd, Cu, Cr and Pb were respectively: 0.99854; 0.99644; 0.99512; 0.99589. Reference standard solution "AA Test Mix by Perkin Elmer" was used for the analytical quality control of the analysis. For control of interference is used modifier matrix according standard conditions by Atomic Absorption Spectrometry Graphite Furnace. Matrix modifier 0.05 mg $NH_4H_2PO_4$ + $Mg(NO_3)_2$ used for determined Pb and Cd, for determination Cr used 0.015 mg $Mg(NO_3)_2$ matrix modifier and for determination of Cu used 0.005 mg Pd + 0.003 mg $Mg(NO_3)_2$ matrix modifier.

During the analyses were taken 20 micro litter solutions (blank, standard or sample) plus the volume of the specified chemical modifier. When used the method GFAAS for the correction of the background used Zeeman-Effect Background correction**.**

In the table 1 are presented concentration of elements Cd, Cr, Cu and Pb in representative drinking water samples and standard deviation. The concentration of heavy metals in tap water samples is compared with EPA and WHO specified maximum contaminant level recommended by Environmental Protection Agency and World Health Organization (EPA) and (WHO 1993).

Table 1. Concentration of heavy metals Cd, Cr, Cu and Pb in public water system

Nr	**Sampling points**	**Code**	**Pb (µg/L) ±SD**	**Cd(µg/L) ±SD**	**Cr(µg/L) ±SD**	**Cu(µg/L) ±SD**
1	Shën Mëri 1	m1_B 1	0.22±0.03	0	0	2.3±1.21
2	Shën Mëri 2	m2_B 2	0.43±0.11	0.17±0.04	0.1±0.01	4.2±0.08
3	Tirana 1	m3_D1	0.51±0.25	0.42±0.01	0.8±0.02	0
4	Tirana 2	m4_D2	0.43±0.01	0	2.9±0.01	1.8±0.01
5	Bovilla 1	m5_B1	0.31±0.13	0.15±0.01	0.11±0.14	3.5±0.01
6	Bovilla 2	m6_B2	0.18±0.01	0.19±0.02	0.16±0.01	4.8±1.08
7	Tirana e Re	m7_SW1	1.35±1.11	0.063±0.02	6.6±1.98	1.9±0.03
8	Bërxull_B	m8_SW2	0.78±0.05	0.061±0.01	0.3±0.03	0.8±0.03
9	Globe-21 Dhjetori	m9_SW3	0.23±0.02	0.022±0.01	1.8±0.02	0.2±0.01
10	Laknas	m10_SW4	0.46±0.02	0	1.9±0.01	0
11	Laknas_w	m11_SW5	0.8±0.01	0.041±0.01	0.1±0.01	3.4±0.01
12	Kroi	m12_SW6	0.65±0.06	0.037±2.14	5.4±0.01	2.5±0.09
13	Libri Universitar	m13_C1	0.24±0.23	0	0.2±0.01	2.3±0.01
14	Pallati me shigjeta	m14_C2	0.56±0.32	0.013±0.04	1.4±0.03	1.2±0.01
15	Grand-M.Grameno	m15_C3	0.67±0.01	0	0.9±0.02	1.4±0.01
16	Pallati Kongreseve	m16_C5	1.9±0.01	0.032±0.01	3.1±0.02	0.7±0.03
17	Fakulteti Ekonomik	m17_C6	0.85±0.03	0	0.7±0.01	0
18	Pazari i Ri	m18_C7	0.6±0.01	0.015±0.01	1.1±0.01	0.1±0.01
19	Frigoriferi	m19_C8	2.8±2.34	0.064±0.02	1.5±0.01	0.30.01
20	Don_Bosko_Pipelines	m20_C9	11.8±1.76	0.082±0.01	3.8±0.07	10.1±2.35
21	Don_Bosko_Depo	m21_C10	3.7±0.01	0.032±0.01	0	2.5±0.01
22	Kombinat	m22_C11	0.88±0.01	0.027±0.01	1.9±0.03	3.8±0.08
23	Laprakë	m23_C12	0.6±0.07	0	2.4±0.01	1.1±0.05
24	Uje rrjeti Tirana e Re	m24_C13	0.62±0.01	0.018±0.09	0.1±0.01	0.3±0.02
25	Uje i filtruar (24)	m25_C13	0	0	0	0
26	IFBZ	m26_C14	0.5±0.01	0.023±0.04	1.8±0.01	0.9±0.02
27	Rr. Elbasanit_uje rrjeti	m27_C15	0.34±0.02	0.032±0.12	2.5±0.05	2.1±0.01
28	Rr. Elbasanit_depo	m28_C17	0.27±0.01	0.013±0.01	3.1±1.67	4.7±0.01
29	Sheshi Willsom	m29_C18	0.45±0.01	0.043±0.01	0.9±1.48	2.9±0.08
30	Rr. Vasil Shanto	m30_C19	0.87±0.01	0.011±0.87	1.3±0.05	3.5±1.39
31	MCL specified by WHO		10	50	50	2000
32	MCL specified by EPA		15	5	100	1300

Results and Discussion

The data of table 1 are presented in graphical forms. The graph in figure 1 is presented the dependence of the metals concentration Cd, Cr, Cu and Pb in public water system, while the graph in figure 2 is presented the dependence of the metals average concentration Cd, Cr, Cu and Pb, in public water system.

From results obtained after we analysed representative of tap water samples, is observed presence of Cd, Cr, Cu and Pb in most of the samples. The average concentration of Cd, Cr, Cu and Pb in public water supply system was found in the order respectively 0.05 µg/L; 1.56 µg/L; 2.11 µg/L; 1.13 µg/L. During the sampling we had taken at the same family two samples, where S_24 was tap water sample from public water supply system and S_25 was filtered water sample. While the graph in figure 3 is presented the plot for distribution of metals in tap water and the graph 4 is presented the tree diagram of Cd, Cr, Cu and Pb in tap water.

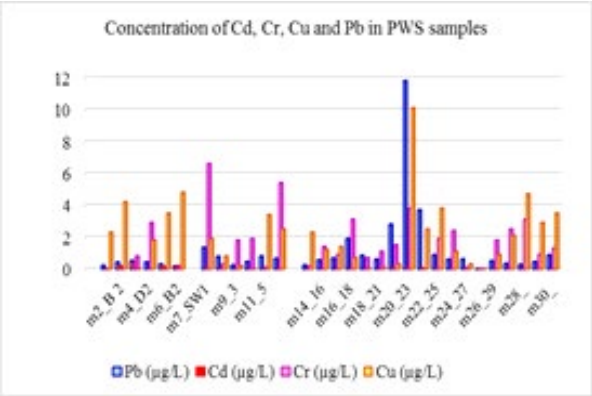

Figure 1. Variation of metals content in samples.

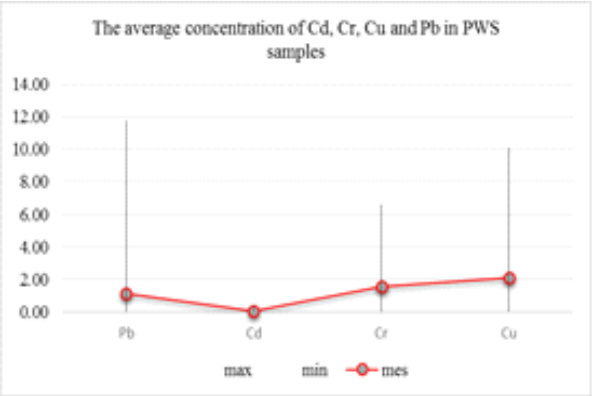

Figure 2. Variation of average content in samples.

From analysis of these samples in this family is observed that the concentration of metals was under detection limit. The mean concentrations level of lead in Cd, Cr, Cu and Pb in tap water samples that are collected at different points from source to consumers in public water supply system of Tirana, are compared with (MCL) specified by WHO and EPA (table1). None of the analysed samples contained metals above MCL for drinking water standard.

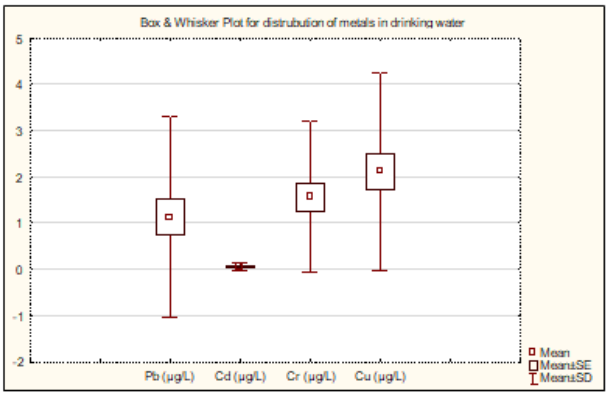

Figure 3. Plot for distribution of metals in water.

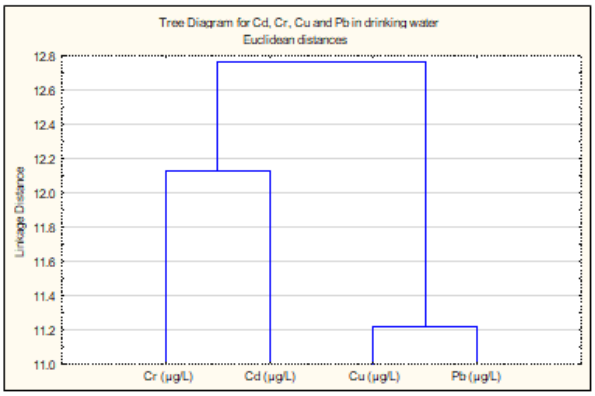

Figure 4. Tree diagram of Cd, Cr, Cu and Pb.

Conclusion

From the obtained results after we analysed representative of public water system samples, we observed the presence of Cd, Cr, Cu and Pb in most of the samples. The average concentration of Cd, Cr, Cu and Pb in public water system was found in the order respectively 0.05 µg/L; 1.56 µg/L; 2.11 µg/L; 1.13 µg/L. During the sampling we had taken at the same family tow samples, where S_24 was tap water sample from public water system and S_25 was filtered water sample. From analysis of these samples in this family is observed the concentration of metals were under detection limit. The mean concentrations level of lead in Cd, Cr, Cu and Pb in tap water samples that are collected at different points from source to consumers in public water supply system of Tirana, are compared with maximum concentration level specified by WHO and EPA (table1). No of the analysed samples contained metals above maximum concentration level for drinking water standard. This work presented an assessment for a few metals, but the concentration of heavy metals in drinking water should be monitored continuously.

Acknowledgements: *This is a part of my work regarding the assessment of metals in the environmental media (soil, water, aerosols, vegetable, etc). My appreciation is sent to Institute of Applied Nuclear Physics, University of Tirana; to Faculty of Natural Sciences and to my Family.*

References

Alushllari M, Civici N, (2014) *Analyses of Lead in Water Depend the Weather, near the Ex-Factory Production of Batteries Region*, Berat, Albania. *Appl. Sci. Reports*, pp.122-125,

Alushllari M, Civici N, (2014). Determination of Lead Accumulation by Leaves of Different Vegetation, Grow in Soil Pollution. *Europ. Sci. J.* **10**(12), 273-280.

Alushllari M, Civici N, Malollari I, (2012) Study and Verification of the Content of Arsenic (As), Cobalt (Co) and Copper (Cu) in Surface Water in the Region of Tirana City, Albania. *JIEAS*, **7**(2). 205-209. 2012.

Alushllari M, (2013) http://www.doktoratura.unitir.edu.al/wp-content/uploads/2013/10/Doktoratura-Mirela-Alushllari-Fakulteti-i-Shkencave-i Natyrore-Departamenti-i-Kimise-Industriale.pdf, pg 2

Anonymous (1993) *WHO, s drinking Water standard 1993*. http://WWW.lenntech.com/applications /drinking/standards/Who-s-drinking-Water-standards.htm

Anonymous, *EPA drinking Water standard*. http://Water.epa.gov/drink/contaminants/index. cfm#Inorganic.

Censi P, Spoto SE, Saiano F, Sprovieri M, Mazzola S, Nardone G, Di Geronimo SI, Punturo R, Ottonello D, (2006) Heavy metals in coastal Water system. *Chemosphere* **64**, 1167-1176.

Gazso LG (2001). The Key Microbial Processes in the Removal of Toxic Metals and Radionuclides from the Environment. A review. Cent. Eur. *J. Occup. Environ. Med*., **7**(3), 178–185.

Perkin Elmer (1996) *Analytical Methods for Atomic Absorption Spectroscopy and Recommended conditions for THGA furnaces and recommended conditions for THGA furnaces* (Perkin – Elmer),

Vanloon, GW. Duffy SJ, (2005). *The Hydrosphere. In: Environmental Chemistry: A Global Perspective*. 2nd Ed. New York: Oxford University Press, pp: 197-211.

J. Int. Environmental Application & Science, Vol. 14(4): 177-182 (2019)

Research Paper

Batch Adsorption of Methylene Blue Dyestuff Using Van Sour Cherry Pulp and Statistical Comparison

Halime Yıldız[1], Canan Demir[1,*], Ali Rıza Kul[1]

[1]*Yuzuncu Yıl University, Vocational School of Health Care, Van, Turkey*

Received September 05, 2018; Accepted December 01, 2019

Abstract: Water contamination which is defined as change by physical, chemical and biological reasons causes environmental pollution. This pollution can be caused by both human wastes and industrial processes. Since dyestuffs are difficult to separate chemically and biologically, wastewater with dyestuffs damages the ecosystem and causes toxic affect to human life. Adsorption process is one of the alternative methods in the treatment of wastewater dyestuff. In this study, the use of Van sour cherry pulp without any chemical process, which is abundantly available in the city of Van, low-cost and plant waste, has been investigated as a bio adsorbent in treatment of methylene blue dyestuff. In order to obtain sour cherry pulp, the Van sour cherry was removed from stems, boiled in pure water with seeds and then strained to get the pulp. 1 gr of methylene blue dyestuff was dissolved in 1L distilled water and 1000 ppm solution stocks were prepared for the whole experimental study. One-way variance analysis (ANOVA) was utilized to determine whether there was a difference between both time and temperature levels for all concentrations. Tukey multiple comparison test was utilized to determine from which group (s) the difference was caused by variance analysis.

Keywords*: Bio adsorbent, Methylene Blue, Sour Cherry,*

Introduction

Water contamination which is defined as change by physical, chemical and biological reasons causes environmental pollution. This pollution can be caused by both human wastes and industrial processes (Gerçel & Seyidoğlu, 2015). The coloring substances (Uçar, 2009) which needed to color products used in textile, leather, cosmetics, printing, plastic, construction, pharmaceutical, food and other industries are synthetic and organic chemicals (Çay & Uyanık, 2002). Since dyestuffs are difficult to separate chemically and biologically, (Uslu *et al*., 2015) wastewater with dyestuffs damages the ecosystem and causes toxic affect to human life. One of these dyes being methylene blue, is widely used in the textile industry, belongs to the class of cationic dyes found in wastewater and has the general formula as $C_{16}H_{18}ClN_3S$ (Yaşar & Özcan, 2004). In dyestuff treatment of wastewater, highly efficient treatment methods such as; coagulation, flocculation, chemical oxidation, filtration, reverse osmosis etc., are used. However, the treatment efficiencies of these methods are limited (Angın *et al*, 2016, Gerçel & Seyidoğlu, 2015). Another method is adsorption process. Adsorption is the accumulation of dissolved substances in the solution on a boundary (liquid-gas liquid-solid or liquid-liquid). Adsorption method is easy, convenient to regeneration, inexpensive and effective, so it became a preferred method in recent years (Uslu *et al.,* 2015). In adsorption duration, among the parameters that can affect the treatment efficiency are adsorbed substance and properties of solvent, amount, surface area, pH and contact time, and temperature. In this process, usually active carbon is used as the adsorbent. However, production of active carbon is highly expensive, so other remedies are being sought (Gerçel & Seyidoğlu, 2015). In order to reduce the cost in wastewater treatment, industrial and plant wastes which are abundant and inexpensive, have been tested and are still being tested (Çay & Uyanık, 2002). In the literature, in dye adsorption, various wastes such as apple pulp, wheat husk, olive waste, almond shell, garlic husk, pomegranate peel, cherry stems and seeds are used as adsorbent (Savcı *et al,* 2017, Gerçel & Seyidoğlu, 2015). In this study, the use of Van sour cherry pulp without any chemical process, which is abundantly available in the city of Van, low-cost and plant waste, has been investigated as a bio adsorbent in treatment of methylene blue dyestuff.

**Corresponding: E-Mail: canandemir@yyu.edu.tr; Tel: +9 05055213510 Fax: +904322251303*

Materials and Method

In order to obtain sour cherry pulp, the Van sour cherry was removed from stems, boiled in pure water with seeds and then strained to get the pulp. The sour cherry pulp remaining on the strainer was dried on the blotting paper. It was then milled in a mill and passed through a 230 mesh sieve. After 5 days in the oven at 100 ^{O}C, it was placed in the desiccator for use in the experiment. 1 gr of methylene blue dyestuff was dissolved in 1L distilled water and 1000 ppm solution stocks were prepared for the whole experimental study. Adsorption operations were performed in intermittent processes. Water baths with temperature controls were used. Using magnetic stirrers, the system was expected to reach equilibrium concentration. Samples were taken at predetermined times during the experiments and centrifugation was performed. In adsorption equilibrium studies, 1 gram of sour cherry pulp was treated with 1000 ml methylene blue solution. Prepared methylene blue solution in the concentration of 15 ppm, 25 ppm, 35 ppm, 45 ppm, 55 ppm, 65 ppm, 75 ppm, 85 ppm and at pH = 5 and temperatures of 25 ^{o}C, 35^{O}C, 45^{o}C, was shaken with sour cherry pulp at different times (5, 10, 15, 20, 30, 40, 50, 60, 70, 80, 90, 100, 110, 120, 130, 140, 150, 160, 180, 200 and 240 minutes). The adsorption of methylene blue in the sour cherry pulp sample at constant pH = 5, the concentration was examined with respect to temperature and time. All adsorption measurements were made by Termo Scientific brand ICE 300 Series AA model spectrometer (Benek, 2015).

Statistical Analysis

Descriptive statistics for the feature emphasized;

The mean; $\bar{x} = \frac{1}{n}\sum_{i=1}^{n} x_i$, standard deviation; $s = \sqrt{\frac{\sum_{i=1}^{n}(x_i-\bar{x})^2}{n-1}}$ values were calculated and the minimum (x_{min}) and maximum (x_{max}) values were determined. One-way variance analysis (ANOVA) was utilized to determine whether there was a difference between both time and temperature levels for all concentrations. Tukey multiple comparison tests were utilized to determine from which group (s) the difference was caused by variance analysis. Statistical significance level was taken as 5% in the calculations and SPSS statistical package program was used for analyses.

Findings

Descriptive statistics and comparison results of adsorption of methylene blue dye on Van sour cherry pulp; concentration (15 ppm, 25 ppm, 35 ppm, 45 ppm, 55 ppm, 65 ppm, 75 ppm and 85 ppm) and values with respect to time are presented in Table 1. As shown in Table 1; the difference between the times for each concentration was statistically significant ($p < 0.001$). With reference to this, while 15 ppm concentration of methylene blue, when shaken for 5 minutes, adsorbed an average of 3.92 units of substance, at the same concentration, when shaken for 240 minutes, an average of 12.99 units of substance were adsorbed (Figure 1). Similarly, at a concentration of 25 ppm; while an average of 7.93 units were adsorbed when shaken for 5 minutes, an average of 21.62 units were adsorbed when shaken for 240 minutes at the same concentration (Figure 2). Similarly, when it was increased to 35 ppm, it was adsorbed for an average of 15.24 units when shaken for 5 minutes and 28.94 units of material was adsorbed when shaken for 240 minutes (Figure 3). When it was increased to 45 ppm, the average of 20.56 units of substance was adsorbed when shaken for 5 minutes while it was shaken for 240 minutes and 37.93 units of material were adsorbed (Figure 4). When it was increased to 55 ppm, it was adsorbed on average of 26.56 units for 5 minutes and 45.22 units on average when shaken for 240 minutes (Figure 5). When it reached 65 ppm, it was adsorbed on average of 32.69 units when shaken for 5 minutes and 53.64 units when shaken for 240 minutes (Figure 6). Similarly, when it was increased to 75 ppm, it was adsorbed on average of 37.72 units when shaken for 5 minutes and 62.59 units of substance when shaken for 240 minutes (Figure 7). When methylene blue concentration increased to 85 ppm, 40.85 units of material were adsorbed for 5 minutes on shaking and 70.1 units of material were adsorbed on shaking for 240 minutes (Figure 8).

Descriptive statistics and comparison results of adsorption of methylene blue solution on Van sour cherry pulp; concentration (15 ppm, 25 ppm, 35 ppm, 45 ppm, 55 ppm, 65 ppm, 75 ppm and 85 ppm) values with respect to temperature are given in Table 2. When Table 2 is examined; it can be seen that adsorption of methylene blue solution at different concentrations on Van sour cherry pulp does not change with temperature (25^{o}C, 35^{o}C, 45^{o}C).

Figures 1-8. Adsorption of methylene blue dye on Van sour cherry pulp; concentration (15 ppm, 25 ppm, 35 ppm, 45 ppm, 55 ppm, 65 ppm, 75 ppm and 85 ppm)

Figure 1. 15 ppm

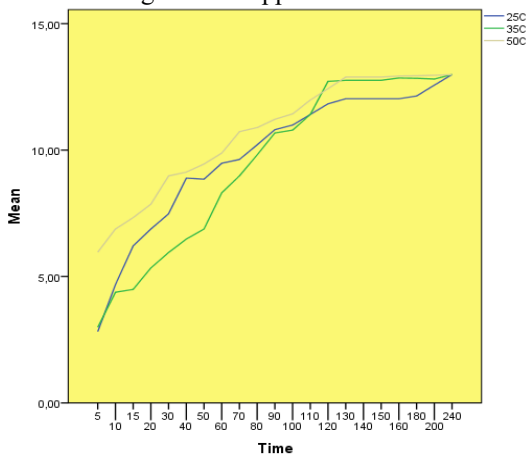

Figure 2: 25 ppm

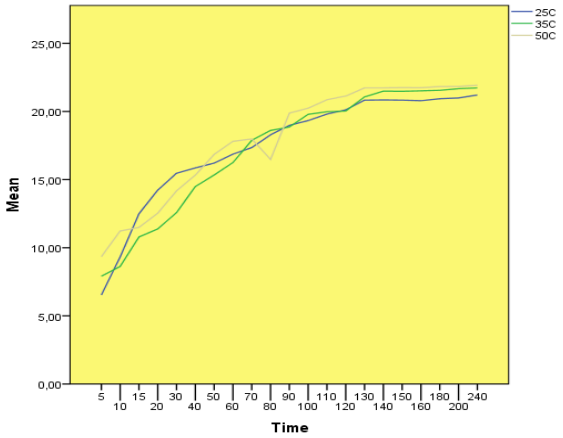

Figure 3. 35 ppm

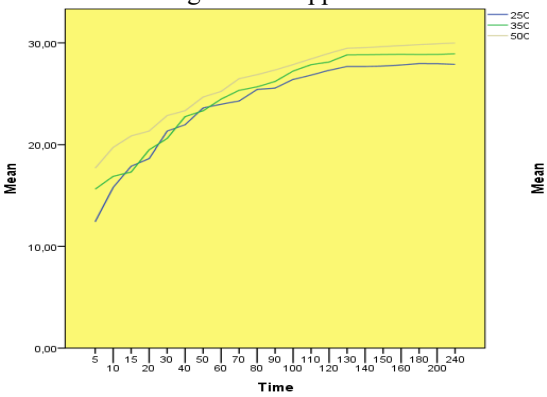

Figure 4. 45 ppm

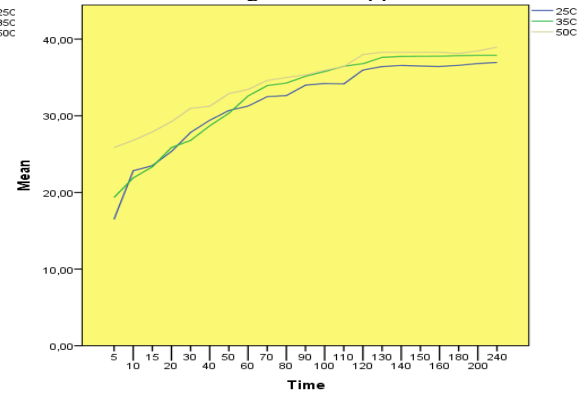

Figure 5. 55 ppm

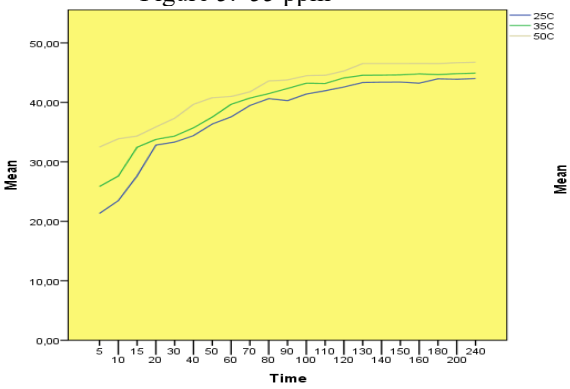

Figure 6. 65 ppm

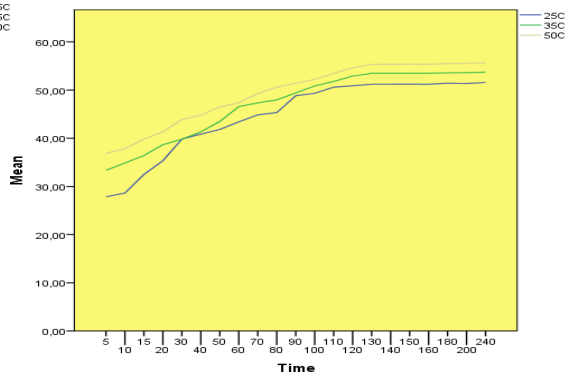

Figure 7. 75 ppm

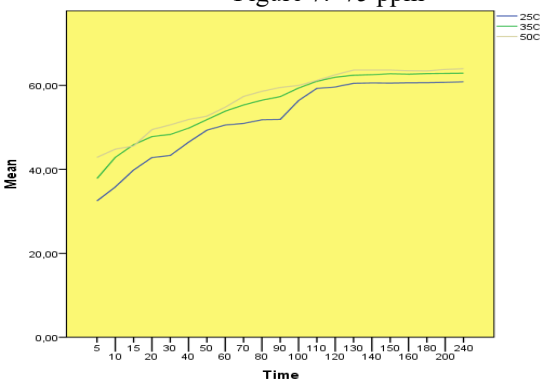

Figure 8: 85 ppm

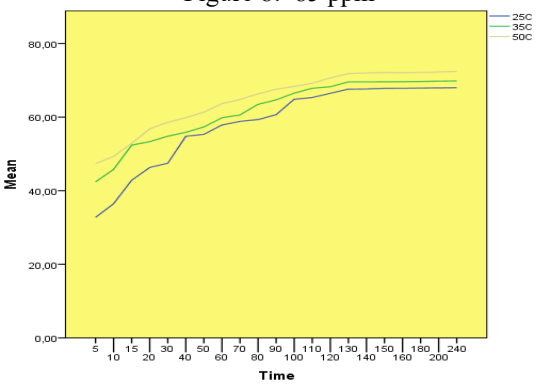

Table 1. Descriptive statistics and comparison results of absorbance values for various time intervals

		n	Mean	Std. Deviation	Min	Max	*p*			n	Mean	Std. Deviation	Min	Max	*p*
Ppm 15	5	3	3.923	1.766	2.82	5.96	0.001	Ppm 55	5	3	26.56	5.613	21.33	32.49	0.001
	10	3	5.313	1.365	4.38	6.88			10	3	28.32	5.241	23.47	33.88	
	15	3	6.01	1.431	4.49	7.33			15	3	31.48	3.456	27.64	34.34	
	20	3	6.693	1.27	5.34	7.86			20	3	34.16	1.565	32.82	35.88	
	30	3	7.47	1.515	5.95	8.98			30	3	35	2.086	33.33	37.34	
	40	3	8.167	1.466	6.48	9.13			40	3	36.61	2.742	34.41	39.68	
	50	3	8.393	1.344	6.88	9.45			50	3	38.23	2.29	36.37	40.79	
	60	3	9.223	0.816	8.31	9.88			60	3	39.41	1.731	37.56	40.99	
	70	3	9.78	0.885	8.98	10.73			70	3	40.67	1.146	39.49	41.78	
	80	3	10.3	0.546	9.81	10.89			80	3	41.91	1.535	40.63	43.61	
	90	3	10.9	0.282	10.68	11.22			90	3	42.14	1.754	40.29	43.78	
	100	3	11.07	0.327	10.79	11.43			100	3	43.04	1.548	41.41	44.49	
	110	3	11.6	0.329	11.41	11.98			110	3	43.23	1.301	41.96	44.56	
	120	3	12.33	0.454	11.83	12.72			120	3	44	1.349	42.59	45.28	
	130	3	12.56	0.464	12.03	12.89			130	3	44.81	1.61	43.34	46.53	
	140	3	12.56	0.464	12.03	12.89			140	3	44.83	1.585	43.39	46.53	
	150	3	12.56	0.464	12.03	12.89			150	3	44.86	1.572	43.41	46.53	
	160	3	12.6	0.498	12.03	12.93			160	3	44.85	1.656	43.23	46.54	
	180	3	12.64	0.436	12.14	12.94			180	3	45.05	1.32	43.96	46.52	
	200	3	12.78	0.197	12.57	12.96			200	3	45.13	1.42	43.89	46.68	
	240	3	12.99	0.006	12.98	12.99			240	3	45.22	1.4	44	46.75	
Ppm 25	5	3	7.927	1.405	6.53	9.34	0.001	Ppm 65	5	3	32.69	4.535	27.86	36.86	0.001
	10	3	9.73	1.345	8.63	11.23			10	3	33.79	4.715	28.63	37.87	
	15	3	11.59	0.854	10.79	12.49			15	3	36.24	3.668	32.49	39.82	
	20	3	12.71	1.434	11.38	14.23			20	3	38.45	3.006	35.34	41.34	
	30	3	14.08	1.448	12.58	15.47			30	3	41.17	2.344	39.82	43.88	
	40	3	15.23	0.691	14.49	15.86			40	3	42.34	2.163	40.86	44.82	
	50	3	16.13	0.758	15.34	16.85			50	3	43.94	2.362	41.83	46.49	
	60	3	16.98	0.785	16.25	17.81			60	3	45.78	2.092	43.41	47.36	
	70	3	17.74	0.339	17.35	17.98			70	3	47.16	2.22	44.86	49.29	
	80	3	17.79	1.149	16.48	18.61			80	3	47.97	2.63	45.33	50.59	
	90	3	19.24	0.557	18.86	19.88			90	3	49.88	1.357	48.82	51.41	
	100	3	19.79	0.455	19.33	20.24			100	3	50.81	1.446	49.34	52.23	
	110	3	20.22	0.564	19.81	20.86			110	3	51.96	1.448	50.61	53.49	
	120	3	20.43	0.611	20.03	21.13			120	3	52.8	1.867	50.88	54.61	
	130	3	21.21	0.466	20.83	21.73			130	3	53.34	2.053	51.23	55.33	
	140	3	21.35	0.46	20.84	21.73			140	3	53.35	2.058	51.23	55.34	
	150	3	21.35	0.473	20.83	21.75			150	3	53.35	2.057	51.24	55.35	
	160	3	21.35	0.496	20.79	21.74			160	3	53.35	2.073	51.22	55.36	
	180	3	21.44	0.461	20.93	21.83			180	3	53.48	2.036	51.41	55.48	
	200	3	21.5	0.45	20.99	21.84			200	3	53.51	2.102	51.36	55.56	
	240	3	21.62	0.372	21.21	21.93			240	3	53.64	2.036	51.56	55.63	
Ppm 35	5	3	15.24	2.661	12.41	17.69	0.001	Ppm 75	5	3	37.72	5.191	32.48	42.86	0.001
	10	3	17.47	2.034	15.79	19.73			10	3	41.17	4.733	35.82	44.82	
	15	3	18.68	1.906	17.31	20.86			15	3	43.78	3.398	39.86	45.89	
	20	3	19.82	1.385	18.63	21.34			20	3	46.71	3.461	42.83	49.48	
	30	3	21.6	1.149	20.61	22.86			30	3	47.42	3.735	43.31	50.61	
	40	3	22.69	0.693	21.96	23.34			40	3	49.4	2.724	46.49	51.89	
	50	3	23.87	0.712	23.33	24.68			50	3	51.3	1.729	49.36	52.68	
	60	3	24.56	0.634	23.97	25.23			60	3	53.09	2.232	50.57	54.82	
	70	3	25.37	1.1	24.29	26.49			70	3	54.56	3.285	50.96	57.39	
	80	3	26	0.775	25.43	26.88			80	3	55.64	3.474	51.82	58.61	
	90	3	26.37	0.901	25.56	27.34			90	3	56.25	3.934	51.89	59.53	
	100	3	27.17	0.732	26.41	27.87			100	3	58.6	1.917	56.41	59.99	
	110	3	27.71	0.811	26.83	28.43			110	3	60.5	1.039	59.31	61.21	
	120	3	28.14	0.835	27.31	28.98			120	3	61.37	1.536	59.63	62.53	
	130	3	28.66	0.911	27.68	29.48			130	3	62.21	1.597	60.51	63.68	
	140	3	28.68	0.934	27.68	29.53			140	3	62.28	1.564	60.59	63.68	
	150	3	28.74	0.96	27.73	29.64			150	3	62.34	1.613	60.55	63.68	
	160	3	28.82	0.957	27.83	29.74			160	3	62.28	1.492	60.63	63.53	
	180	3	28.88	0.935	27.96	29.83			180	3	62.31	1.486	60.64	63.48	
	200	3	28.91	0.981	27.95	29.91			200	3	62.47	1.581	60.73	63.82	
	240	3	28.94	1.05	27.89	29.99			240	3	62.59	1.59	60.86	63.99	

Ppm 45	5	3	20.56	4.808	16.48	25.86	0.001	Ppm 85	5	3	40.85	7.438	32.76	47.39	0.001
	10	3	23.83	2.6	21.88	26.78			10	3	43.88	6.635	36.49	49.33	
	15	3	24.91	2.585	23.34	27.89			15	3	49.38	5.654	42.86	52.88	
	20	3	26.81	2.112	25.34	29.23			20	3	52.16	5.343	46.33	56.82	
	30	3	28.53	2.186	26.78	30.98			30	3	53.64	5.659	47.48	58.61	
	40	3	29.78	1.315	28.69	31.24			40	3	56.85	2.663	54.81	59.86	
	50	3	31.3	1.386	30.33	32.89			50	3	58	3.059	55.33	61.34	
	60	3	32.42	1.093	31.26	33.43			60	3	60.46	2.951	57.88	63.68	
	70	3	33.68	1.082	32.49	34.61			70	3	61.43	3.058	58.86	64.81	
	80	3	33.96	1.21	32.63	34.99			80	3	63.06	3.52	59.34	66.34	
	90	3	34.82	0.725	33.99	35.33			90	3	64.32	3.47	60.68	67.59	
	100	3	35.3	0.948	34.21	35.93			100	3	66.58	1.74	64.86	68.34	
	110	3	35.67	1.317	34.15	36.45			110	3	67.48	1.973	65.34	69.23	
	120	3	36.91	1.021	35.96	37.99			120	3	68.47	2.103	66.48	70.67	
	130	3	37.43	0.938	36.42	38.27			130	3	69.67	2.106	67.61	71.82	
	140	3	37.52	0.874	36.56	38.27			140	3	69.74	2.174	67.65	71.99	
	150	3	37.5	0.915	36.49	38.27			150	3	69.85	2.142	67.85	72.11	
	160	3	37.49	0.95	36.43	38.27			160	3	69.85	2.109	67.86	72.06	
	180	3	37.51	0.824	36.57	38.12			180	3	69.91	2.112	67.91	72.12	
	200	3	37.72	0.838	36.81	38.46			200	3	70.01	2.178	67.95	72.29	
	240	3	37.93	0.996	36.96	38.95			240	3	70.1	2.242	68	72.46	

Table 2. Descriptive statistics and comparison results of absorbance values for various temperatures

	°C	n	Mean±Std. Deviation	Minimum	Maximum	p
Ppm 15	25	21	9.8090±2.79397	2.82	12.99	0.370
	35	21	9.4752±3.43386	2.99	12.99	
	45	21	10.6967±2.28360	5.96	12.98	
Ppm 25	25	21	17.4900±4.07434	6.53	21.21	0.860
	35	21	17.2867±4.60952	7.91	21.73	
	45	21	17.9943±4.15802	9.34	21.93	
Ppm 35	25	21	24.1014±4.53139	12.41	27.96	0.292
	35	21	24.9038±4.47129	15.63	28.93	
	45	21	26.1829±3.83308	17.69	29.99	
Ppm 45	25	21	31.7614±5.68158	16.48	36.96	0.278
	35	21	32.6476±5.98935	19.34	37.89	
	45	21	34.3890±4.22175	25.86	38.95	
Ppm 55	25	21	38.0248±6.86974	21.33	44.00	0.086
	35	21	39.7652±5.93955	25.86	44.92	
	45	21	42.1414±4.78569	32.49	46.75	
Ppm 65	25	21	44.7300±7.89309	27.86	51.56	0.111
	35	21	47.1238±7.03597	33.34	53.73	
	45	21	49.4338±6.41651	36.86	55.63	
Ppm 75	25	21	52.1548±9.06658	32.48	60.86	0.133
	35	21	55.6595±7.67939	37.82	62.91	
	45	21	57.0414±7.09089	42.86	63.99	
Ppm 85	25	21	58.3014±11.06959	32.76	68.00	
	35	21	61.9519±8.50299	42.41	69.83	0.081
	45	21	64.8448±7.98858	47.39	72.46	

Results and Recommendation

In this study, adsorption of methylene blue dye solution onto Van sour cherry pulp was investigated at temperatures (25ºC, 35ºC, 45ºC), times (5, 10, 15, 20, 30, 40, …. 240 min) and concentrations (15, 25, 35, .. 85 ppm). In Table 1, the results of the comparison of the adsorption of methylene blue dye solution on Van sour cherry pulp with respect to time are given. The differences between the times for each concentration were found to be statistically significant (p <0.001). It is observed that the amount of adsorbed methylene blue increases after a certain period of time, depending on the ambient conditions and the amount of adsorbent surface, it reached saturation by the dyeing anions then the amount taken was approximately fixed. In Table 2, the results of the comparison of the adsorption of methylene blue dyestuff solution on Van sour cherry pulp with

respect to temperature are given; it was observed that the adsorption efficiency did not change with temperature. Similar results were obtained in a study using banana peel as an adsorbent against Acid Blue 121 dyestuff (Uslu *et al*, 2015). There are many studies in the literature regarding the adsorption removal of dyes from aqueous solutions. In a study, the adsorption of methylene blue on bamboo-based activated carbon was investigated and it was stated that bamboos could be used as a raw material in the preparation of activated carbon (Hameed & Din, 2007). In a similar study, it was stated that coconut cored carbon may be preferred as an effective adsorbent for removing methylene blue from waste waters (Kavitha & Namasivayam, 2007). In a study by Dural et al., It was proved that *Posidonia oceanica* (L.) dead leaves could be used in the preparation of activated carbon for methylene blue adsorption. In another study, adsorbent material was produced from cotton stalk for adsorption of methylene blue and it has proved to have significant potential for removal of methylene blue dye from aqueous solutions (Deng *et al*., 2011).

This study shows that sour cherry pulp, which is abundant in the city of Van, is inexpensive agricultural waste and can be used as an effective bio adsorbent for the treatment of waste water containing dye.

References

Angın D, Akçay FD, Güneş S, Aydın E, Özgür C, Salman S, Kılıç Ş, Kubilay BD, Erkan M, Vatansever D, Akarçeşme ŞN, Karakabak LO, (2016) Meyve Suyu Endüstrisi Katı Atığından Elde Edilen Aktif Karbon ile Pestisit Giderimi. *12. Food Congress*. *pp:. 05-07.* Edirne.

Benek V, (2015) *Van Bölgesindeki Bazı Doğal Ponza Taşları Kullanılarak Bazı Ağır Metallerin Adsorbsiyonu*. (MSc Thesis), Graduate School of Natural and Applied Sciences,Van: Yüzüncü Yıl University.

Çay S, Uyanık A, (2002) Fabrika Atığı Çayların Ağır Metal Adsorbsiyonu İçin Hazırlanması. *XVI. National Chemistry Congress, pp. 109-109.* Konya.

Deng H, Lu J, Li G, Zhang G, Wang X, (2011) Adsorption of methylene blue on adsorbent materials produced from cotton stalk. *Chem. Engine. J*., **172**, 326– 334.

Dural MU, Cavas L, Papageorgiou SK, Katsaros FK, (2011) Methylene blue adsorption on activated carbon prepared from Posidonia oceanica (L.) dead leaves: Kinetics and equilibrium studies. *Chem. Engin. J*., **168**, 77–85.

Gerçel Ö, Seydioğlu G, (2015) Kiraz Çekirdeğinden Granül Aktif Karbon Üretimi. *J. Sci. & Tech., Eskişehir: Anadolu Un*., **16**(2), 189-193.

Hameed BH, Din ATM, Ahmad AL, (2007) Adsorption of methylene blue onto bamboo-based activated carbon: Kinetics and equilibrium studies. *J. Hazar. Mat.,* **141**, 819–825.

Kavitha D, Namasivayam C, (2007) Experimental and kinetic studies on methylene blue adsorption by coir pith carbon. *Biores. Tech*., **98**, 14-21.

Savcı S, Karaman Z, Yalvaç M, (2017) Reactive Red 45'in Antep Fıstığı Katı Atığı Üzerine Etkili Gideriminin Araştırılması. *J. Faculty Engin. & Arch. Adana: Çukurova Un.,***32**(4), 175-184.

Uçar B, (2009) *Tekstil Atık Sularındaki Reaktif Boyaların Farklı Katı Atıklar Kullanılarak Adsorpsiyonla Giderimi*. (MSc Thesis), Ankara University. Graduate School of Natural and Applied Sciences, Ankara.

Uslu AB, Elbağlı OG, Şen Y, Uzunoğlu D, Özer A, (2015) Acid Blue 121 Boyar Maddesinin Muz Kabuğuna Kesikli Sistemde Adsorbsiyonunun Araştırılması. *J. Sci. & Tech., Eskişehir: Anadolu Un*.„ **16**(2), 293-302.

Yaşar SB, Özcan M, (2004) Metilen mavisinin çözücü extraksiyonu ile sulu çözeltilerden geri kazanımı. Balikesir University Journal of the Institute of Science and Technology, 6, 50-58.

J. Int. Environmental Application & Science, Vol. 14(4): 183-192 (2019)

Research Paper

Isotherm, Kinetic and Thermodynamic Investigation into Methylene Blue Adsorption onto Pinecone Powder

Adnan Aldemir[1, *], Ali Rıza Kul[2], Hasan Elik[2]

[1]*Van Yüzüncü Yıl University, Faculty of Engineering, Chemical Engineering Department, 65080, Van, Turkey;*
[2]*Van Yüzüncü Yıl University, Faculty of Science, Chemistry Department, 65080, Van, Turkey*

Received September 18, 2019; Accepter December 3, 2019

Abstract: In this study, the usage of pine cone powder as an adsorbent for removing methylene blue from aqueous solution was investigated. Within this scope adsorption experiments were performed, and the results showed that the Freundlich isotherm model was a more convenient option compared to the Langmuir and Temkin models. The results also determined that the pseudo second order kinetic model demonstrated higher correlation coefficients (R^2) values compared to the pseudo first order and intra-particle diffusion models. Initial dye concentration was found to shift from 100 to 300 mg/L, while adsorption capacity onto the pine cone powder changed from 40.99 to 95.24 mg/g, 41.56 to 97.93 mg/g, and 43.51 to 101.41 mg/g for 298K, 308K and 318K, respectively. The thermodynamic parameters for the instant free energy (ΔG), enthalpy (ΔH), and entropy (ΔS) of this separation process were found by referring to -1595,11 J/mol, 2465,83 J/mol and 12,77J/mol, respectively. The negative ΔG° values revealed that this separation process was endothermic and natural.

Keywords: *adsorption, isotherm, kinetic, thermodynamic, pine cone, methylene blue*

Introduction

Various methods based on the chemical structure, colour and application are available to classify commercial dyes. As for the chemical structure classes, the dyes utilized industrially are the anthraquinone, azo, indigoid, phthalocyanine, sulphur, and triphenylmethyl (trityl) (Gupta & Suhas, 2009; Yagub *et al*., 2014). Quaternary salts are classified as basic dyes. Their cations have a positive charge mostly on nitrogen (N), carbon(C), oxygen(O) and sulphur(S) atoms while their anions are mostly Cl^-, SO_4^{-2}, HSO_4^-or $(COO^-)_2$ ions (Forgacs *et al*., 2004; Yagub *et al*., 2014).

Dyes have a stable and complex structure and a slow biodegradability. They are toxic to the organisms in the receiving waters and negatively affect the photosynthetic activities in such waters. The different dye classes and their health effects are given in (Kausar *et al*., 2018). Due to their harmful effects on the human beings, dyes must be removed from the aqueous solutions.

To date, several chemical and biological treatment methods, including electrocoagulation and chemical oxidation have been applied in the treatment of industrial wastewaters (Mahmodi *et al*., 2011; Debnath *et al*., 2017). Among these methods, the adsorption technique with relatively economical, efficient, flexible, and simple design has proved to ensure operational comfort in treating colorized wastewaters (Mtshatsheni *et al*., 2019). The performance of the adsorption technique is associated with the adsorbent materials. Activated carbon, a commonly used adsorbent, is very expensive, has high operation costs and requires regeneration after the treatment process (Jin *et al*., 2019). This limitation has to evoke a search for different adsorbents, such as biosorbents and waste materials to be used in the removal of dyes. Natural wastes have been used as adsorbents in the removal of dyes from wastewaters as they are low in cost, efficient, locally available materials and not hazardous to nature (Salleh *et al*., 2011; Crini, 2006).

Pine cones are important commercial and value and used extensively in many different industries (Martin-Lara et al., 2016). One pine cone consists of around 46.5% hemicellulose, 37.4% lignin, 18.8% cellulose, and 15.4% extractives (Ofomaja *et al*., 2010). Pine cone powder (PCP) has been used for remove the heavy metal pollutants such as lead, caesium, copper, nickel, and arsenic (Immaculate et al., 2018). There are only a limited number of studies that have been conducted on the dye adsorption capacity of these species (Mahmodi *et al.,* 2011). The present study investigated the dye adsorption capacity of PCP. Various adsorbents have been investigated for the adsorption of MB

*Corresponding: E-Mail: adnanaldemir@yyu.edu.tr; Tel: +904322251725Fax: +904324865413

onto aqueous solutions. As a result, some of them provided well-suited MB adsorption properties (Kul & Aldemir, 2019).

The interference between the adsorbent and adsorbate molecules is explained by way of adsorption isotherms. The adsorbate nature alters the amount adsorbed and the adsorbent affects the adsorption isotherm profile shape. In the present study, all of the above-mentioned isotherms were taken into account. The assumption with the Langmuir isotherm model, is that the adsorption onto the monolayer and all the active sites on the adsorbent surface are equal in terms of energy. The Freundlich isotherm model, on the other hand clarifies the multilayer adsorption behaviour. The kinetic mechanism of the adsorption process is explained by calculating different equations such as pseudo first order (PFO), pseudo second order (PSO) and intra-particle diffusion (IPD) models (Ofomaja *et al*., 2010).

In this study, the adsorption capacity of PCP onto MB was evaluated. Several parameters, important for dye removal were investigated within scope. MB was selected as the adsorbate due to it is being considered a toxic dye.

Materials and Methods

The Adsorbent (Pine Cone Powder)

The adsorption experiments were carried out using PCP obtained from *Pinus sylvestris* grown in the province Van in Turkey. After being collected the pine cones were washed multiple times using distilled water to remove any impurities. They were dried in an oven at 55 °C for 48h. The dried pine cones were later ground in a crusher. The resulting powders were sieved and the particles that measured less than 150 μm were gathered together in a plastic container to be used as adsorbents.

The Adsorbate (Methylene Blue)

In this study MB was used as the adsorbate. The formula of MB which has a molecular weight of 319.85 g/mol, is $C_6H_{18}N_3SCl*3H_2O$.The dye was purchased from Merck Chemicals Company (Germany) and used without any purification processes. The stock dye solution was prepared by dissolving 1 g of MB in 1000 ml of distilled water. The dye solutions (100-300 mg/L) used in the adsorption process were acquired by diluting the prepared stock dye solution with deionized water to the appropriate concentrations.

Adsorption Experiments

2 g of adsorbent treated with 500 ml of dye solution in a batch temperature-controlled water bath. Different initial concentrations of MB were available in the dye solution during 120 min while the pH was gradually adjusted with the addition of either H_2SO_4 solution or NaOH solution (0.1 M) to keep the constant pH values. All triplicate experiments were executed under the same conditions at temperatures of 298K, 308K and 318K. Consequently, average values were taken as the result after the entire data was calculated. Adsorption capacity was calculated with Eq. (1);

$$q_e = \frac{(Co - Ce)}{m} V \tag{1}$$

where V is the volume of the solution (L), C_0 and C_e are the initial and the equilibrium concentration of the dye (mg/L), respectively and m is the adsorbent mass (g). The data obtained in this study were tested by isotherm, kinetic and thermodynamic relationships to design the most appropriate MB removal conditions using PCP.

Results and Discussion

Adsorption Isotherm Studies

Many different models are used in identifying the adsorption of dyes onto solid surfaces. Three models were applicable to the descriptions of the experimental results obtained at three different temperatures. The parameters of these isotherm models were considered through regression by means of the linear isotherm equations (Mahmodi *et al*., 2011; Rida *et al*., 2013). The amount of the MB adsorbed for three temperatures are presented in Figure 1. The adsorption efficiency increases as the initial MB concentration rises.

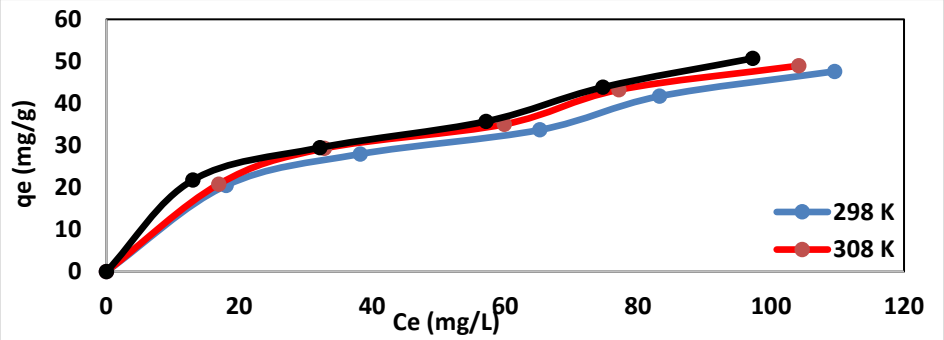

Figure 1. MB adsorption isotherms onto PCP at different temperatures

The Langmuir isotherm equation is given with Eq. (2);

$$q_e = \frac{q_m K_L C_e}{1 + K_L C_e} \tag{2}$$

where q_{max} is the maximum adsorption capacity (mg/g), C_e is the equilibrium concentration of the solution (mg/L), and K_L is a Langmuir constant. The values of q_m and K_L are determined by using the slope and intercept of the graph of C_e/q_e versus Ce. Figure 2 shows the isotherm results of MB adsorption onto PCP for 298K, 308K, and 318 K.

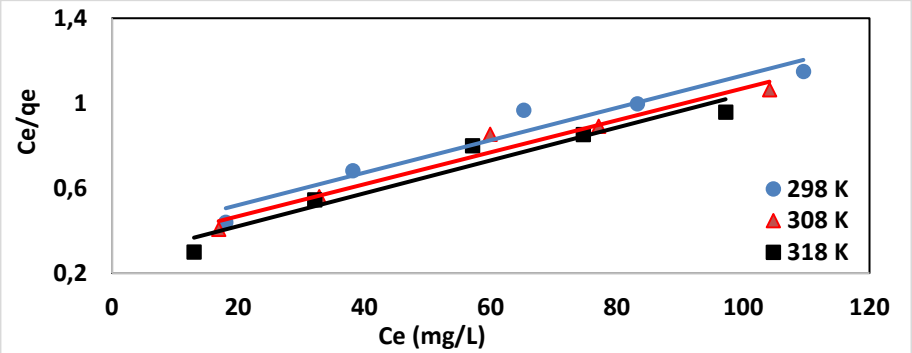

Figure 2. Langmuir isotherms of MB adsorption onto PCP for different temperatures

The Freundlich isotherm equation is given with Eq. (3);

$$q_e = K_F C_e^{1/n} \tag{3}$$

where K_F is a Freundlich constant associated with the adsorption capacity (L/g) and 1/n is an empirical parameter associated with the adsorption intensity. Figure 3 shows the Freundlich isotherm results of MB adsorption on PCP for 298K, 308K, and 318 K.

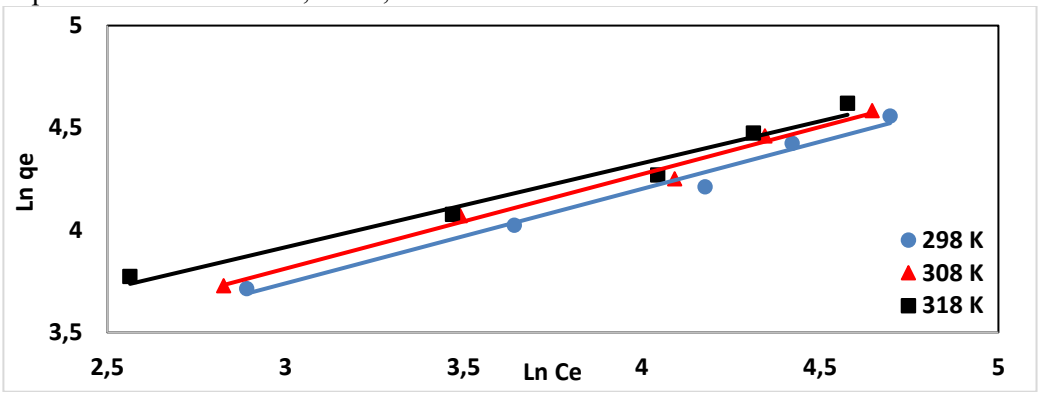

Figure 3. Freundlich isotherms of MB adsorption onto PCP for different temperatures

The Temkin isotherm equation is given with Eq. (4);

$$qe = \frac{RT}{b_T} \ln K_T + \frac{RT}{b_T} \ln Ce \tag{4}$$

where K_T and b_T are both related to the adsorption heat. Figure 4 shows the Temkin isotherm results of MB adsorption onto PCP for 298K, 308K, and 318 K.

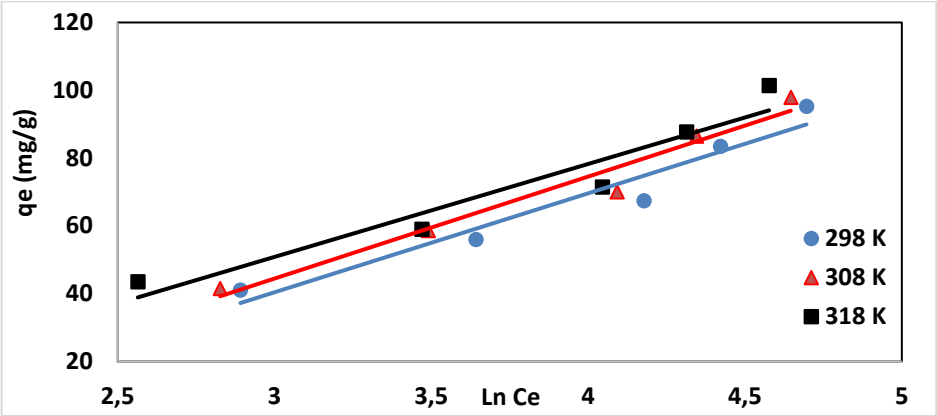

Figure 4. Temkin isotherms of MB adsorption onto PCP for different temperatures

The parameters calculated for MB adsorption onto PCP are presented in Table 1. With respect to the determined coefficients it was determined that the Freundlich model was more suitable than both the Langmuir model and the Temkin model. It was found that the values of K_F and n increased with the increase in temperature and that adsorption was accomplishable at higher temperatures. The R^2 values of all three isotherm models were high however the R^2 values of the Freundlich model were higher than those of the other two models. Table 2 shows the maximum adsorption capacity (q_m) of MB for different adsorbents while Table 3 shows pine cone adsorbent with different adsorbates calculated according to Langmuir isotherm model.

Table 1. Isotherm model parameters for MB adsorption on PCP at different temperatures

Temp	**Langmuir**			**Freundlich**			**Temkin**		
K	K_L (L / g)	q_m (mg/g)	R^2	n	K_F (L/g)	R^2	K_T (L/g)	b_T (J/mol)	R^2
298	0.0208	65.359	0.9436	0.4085	5.2683	0.9922	1.6162	169.734	0.9409
308	0.0236	66.667	0.9633	0.4617	5.6604	0.9961	1.5223	180.258	0.9606
318	0.0291	68.516	0.9386	0.5109	7.3251	0.9947	1.2718	192.841	0.9221

Effect of Temperature and Thermodynamics on Adsorption

The effect of temperature on MB adsorption was investigated by conducting experiments at three different temperatures. The experimental results showed that MB adsorption capacity decrease when temperature increased. This was caused by the adsorbed MB ions escaping which indicates the physical nature of the adsorption. Thermodynamic parameters are extremely important in detecting heat alteration in the adsorption process for the dye and PCP (Debnath *et al*., 2017). These parameters were calculated by using the following equations:

$$K_C = \frac{C_{Ads}}{Ce} \quad (5)$$

$$\Delta G^\circ = -RT \ln K_C \quad (6)$$

$$\Delta G^\circ = \Delta H^\circ - T\Delta S^\circ \quad (7)$$

$$\ln K_C = \frac{\Delta S^\circ}{R} - \frac{\Delta H^\circ}{RT} \quad (8)$$

where C_{Ads} is the dye amount (mg) adsorbed onto PCP per litter of the solution in equilibrium, the adsorbent per unit litter of the solution. Figure 5, shows the straight line, namely lnKc versus 1/T, obtained from the graphical representation in accordance with Eq. (8).The thermodynamic parameters are given in Table 4.

Table 2. Adsorption capacity of MB onto different adsorbents

Adsorbent	q_m (mg/g)	References
NaOH treated diatomite	27.8	(Cherifi et al., 2013)
Fe_3O_4 nanoparticles	38.2	(Gouamid et al., 2013)
Vegetal fiber activated carbons	33.7	(Caparkaya et al., 2008)
Date palm leaves powder	58.1	(El Sikaily et al., 2006)
The brawn algae	38.6	(Fu et al., 2000)
The green algae	40.2	(Dawood et al., 2012)
Dead fungus	18.5	(Ofomaja et al., 2010)
Marble dust	16.3	(Hamed et al., 2014)
PCP	68.5	This study

Table 3. Monolayer capacity of natural PCP on various adsorbates

Adsorbate	q_m (mg/g)	References
Acid Blue 7	37.4	(Mahmodi et al., 2011)
Acid Green 25	43.3	(Mahmodi et al., 2011)
Acid Black 26	62.9	(Mahmodi et al., 2011)
Congo Red	32.6	(Demirak et al., 2015)
Pb(II) metal	16.3	(Kul and Koyuncu, 2010)
Cu(II) metal	9.22	(Ofomaja et al., 2009)
NH_4	6.15	(Rafatullah et al., 2010)
2-nitrophenol	41.17	(Kupeta et al., 2018)
Methylene Blue	68.5	This study

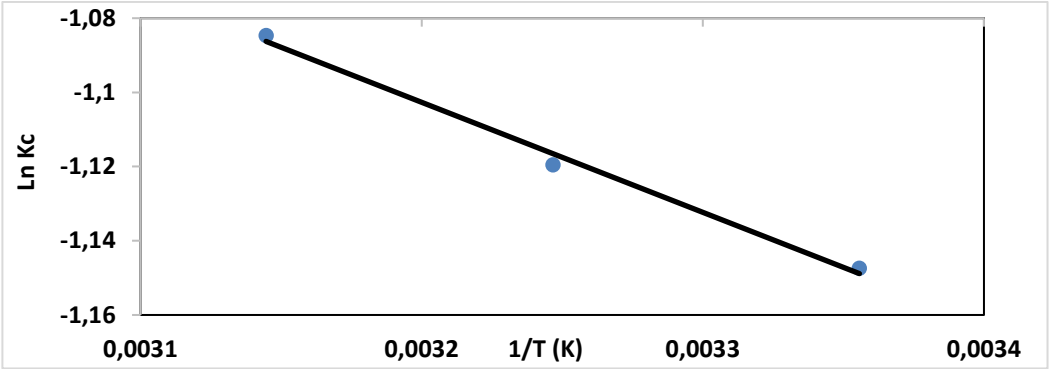

Figure 5. lnKc versus 1/T plot for MB adsorption onto PCP

The Gibbs free energy (ΔG°) absolute values of MB adsorption onto PCP were obtained as -1,3396 kJ/mol, -1,4673 kJ/mol, and -1,5951 kJ/mol for 298K, 308K, and 318K, respectively. The enthalpy (ΔH°) and entropy (ΔS°) values of MB adsorption onto PCP were found to be 2465.81 J/mol and 12.77 J/mol.K, respectively.

The values of ΔH° were found to be within the range of 1–60 kJ/mol which indicated physical adsorption. Physical adsorption can be the result of Van der Waals forces and/or weak charge transfer complexes between the adsorbate and adsorbent (Kupeta *et al*., 2018). From the results obtained, it can clearly be seen that physical adsorption is favourable for the adsorption of MB. The positive values of ΔH° proved the endothermic nature of the adsorption which governs the possibility of physical adsorption. The low value of ΔH° suggested that MB is physisorbed onto PCP while the negative values of ΔG° showed that the adsorption is spontaneous and extremely favorable. The positive values of ΔS° exhibited the increased disorder and randomness at the solid solution interface of MB with PCP adsorbent that causes various structural changes in MB and PCP (Miyah *et al*., 2018).

Table 4. Thermodynamic parameters of MB adsorption onto the PCP

Temp (K)	**Kc**	**ΔG°(kJ/mol)**	**ΔH° (kJ/mol)**	**ΔS°(J/mol.K)**	**R^2**
298	0.317	-1.3396			
308	0.327	-1.4673	2.4658	12.7703	0.993
318	0.337	-1.5951			

The Contact Time on Dye and Initial Dye Concentrations

As can be seen from Figures 6, 7 and 8, the removal of MB from the solutions is rapid in the initial period while this speed decreases in the final period in the near reach of the balance. At the start, the surface of adsorption is large and thus, the adsorption onto this surface is rapid. Figure 6, 7 and 8 show that the increase in the initial MB concentration leads to an increase in the adsorption capacity for all three temperatures. As the initial dye concentration increased from 100 to 300 mg/L, the dye adsorption capacity onto the PCP instead from 40.99 to 95.24 mg/g for 298K, 41.56 to 97.93 mg/g for 308K and 43.51 to 101.41 mg/g for 318K. These data prove that the initial dye concentration plays a crucial role in dye adsorption capacity and provides a driving power in the interaction between the adsorbent and the dye. MB adsorption on PCP has similarity herewith. Various studies in the literature have investigated the usage of different adsorbents and biosorbents, such as activated carbon, breadnut skin, hydrochar, rice husk, and sawdust for MB adsorption. When the results of these studies and those of the present study are compared it can be said that dye adsorption capacity of PCP is good and PCP may be the answer to a new inexpensive adsorbent usable for dye removal.

Figure 6, 7 and 8 are shows the changes of q_e (mg/g) versus time with nearly 50 min response times. Indeed, this can be explained by the fact that the migration of the dye solution can easily accessible to the vacant sites of the adsorbent in the initial period. Thus, a higher adsorption percentage is a result of the gradient concentration of the solid–liquid interface. The gradient concentration is extremely high at the beginning of contact between the solid and liquid phases. However, in the next period adsorption decreases due to the slower diffusion of the dissolved species through the adsorbent pores. The rapid removals of dyes facilitate the use of the decreased adsorbent amounts and thus ensure the efficiency and cost of separation (Miyah *et al*., 2018).

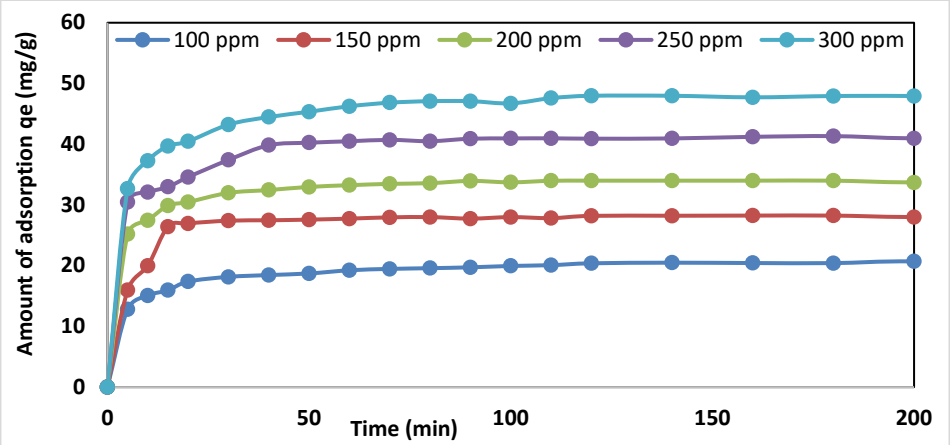

Figure 6. Effect of contact time and initial concentration on MB removal onto PCP at 298 K

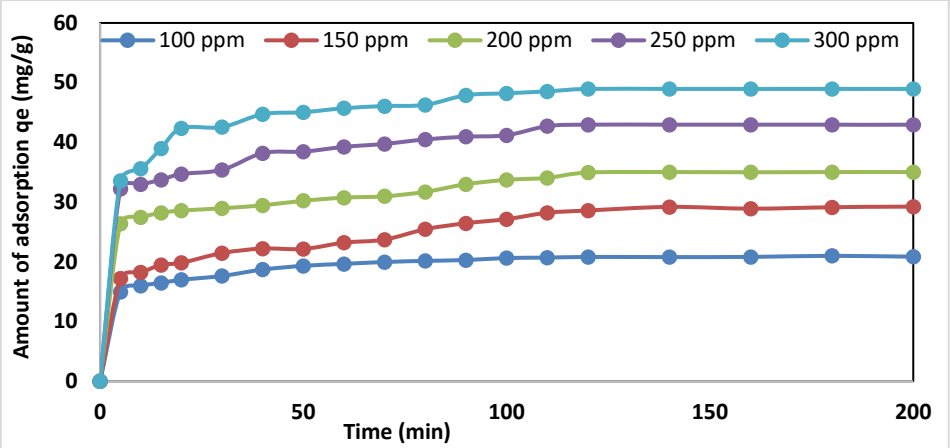

Figure 7. Effect of contact time and initial concentration on MB removal onto PCP at 308 K

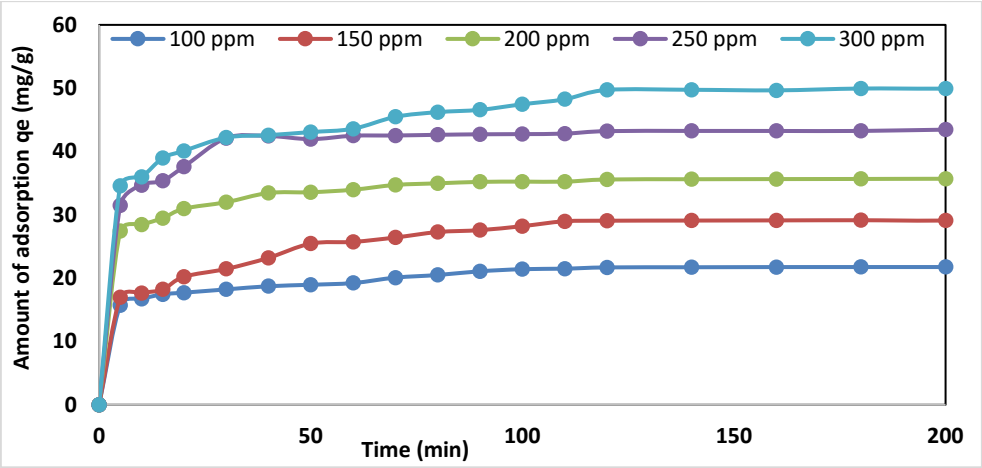

Figure 8. Effect of contact time and initial concentration on MB removal onto PCP at 318 K

Kinetics Studies for Adsorption

Kinetic models are used to evaluate the experimental results of the adsorption of adsorbates onto adsorbents. The adsorption kinetics of dyes is important when choosing the best test circumstances. Useful kinetic parameters for estimating adsorption rates provide vital knowledge to design and modelling adsorption processes (Jian *et al*., 2013). In the present study, MB was calculated by using three kinetic models, namely (PFO, PSO, and IPD). The most suitable model was chosen depending on the linear regression coefficient of the correlation coefficients of the R^2 values. All three models were examined in accordance with the experimental data at three temperatures and initial MB concentrations (Mahmodi *et al*., 2011).

The PFO kinetic model separates the kinetics equation according to the solution concentration and solid adsorption capacity. This model is most likely the first to characterize liquid-solid adsorption systems depending on solid capacity. It is utilized for studying the sorption in a liquid-solid system (Ghaedi *et al*., 2015). The equation of the model is given with Eq. (9);

$$\ln(q_e - q_t) = \ln q_e - k_1 t \tag{9}$$

where q_m (mg/g) is the adsorption capacity in equilibrium, q_t (mg/g) is the adsorption capacity at time t, respectively and k_1 (min^{-1}) is the rate constant of the PFO adsorption. To acquire the constants of this model the straight-line plots of $\ln(q_e\text{-}q_t)$ versus t are drawn. The constants are determined from the slope and intercept of the plot.

The fitness between the experimental data and the model-predicted values was expressed with the correlation coefficients (R^2) and the closeness of the experimental and theoretical adsorption capacity values. The PSO model was found to be successful in representing the kinetics of several adsorption systems (Hamed *et al*., 2014). The equation for this kinetic model, which is based on adsorption capacity is given with Eq. (10);

$$\frac{t}{q_t} = \frac{1}{k_2 q_e^2} + \frac{1}{q_e} t \tag{10}$$

where k_2 is the adsorption rate (g/mg.min), q_m is the adsorbate amount adsorbed onto the adsorbent in equilibrium (mg/g), q_t is the dye amount adsorbed at any time (mg/g).

The adsorption process can include several stages all with different adsorption rates. Every adsorption stage is governed by a different adsorption mechanism. An initial sharp region in intraparticle diffusion plots can emerge as a result of instantaneous adsorption or external surface adsorption caused by electrostatic attraction. This is followed by a second region in which intraparticle diffusion is accountable for restricting the adsorption rate. A third region occurs at the equilibrium state in cases where the intraparticle diffusion is restricted due to low adsorbate contents remaining in the solution (Allafchianet *al*., 2019).

The testing of intra-particle diffusion possibility as a rate limiting step was performed using the IPD model, the equation of which is given Eq. (11);

$$q_t = k_{ipd} t^{0.5} + C \quad (11)$$

where k_{ipd} is the IPD rate constant. A plot of q_t versus $t^{0.5}$ for different MB concentrations yielded two phases of the linear plots.

PFO, PSO, and IPD kinetic model parameters of MB adsorption on PCP are given in Table 5. The experimental results showed that the R^2 coefficients were higher than 0.99 and that the experimental and analyzed q_e values were very close to each other. Results are shows that this separation process is suitable for the PSO kinetic model. The experimental and calculated q_e values for 318 K were higher than those for 298K and 308K. According to the tables herein, it is obvious that the q_e values increased with the increase in MB concentration. The comparison of the kinetic constants showed that the constant values were closer to both temperatures and concentrations of the PSO model. This result revealed that MG adsorption kinetics onto PCP resulted from PSO.

Table 5. PFO, PSO and IPD kinetic model parameters for MB adsorption onto PCP

Kinetic Model	Temp (K)	Kinetic coefficients	100 (mg/l)	150 (mg/l)	200 (mg/l)	250 (mg/l)	300 (mg/l)
	298	$q_{e\ exp}$ (mg/g)	20.297	27.961	33.701	41.701	47.621
	308	$q_{e\ exp}$ (mg/g)	20.778	29.302	35.034	43.228	48.963
	318	$q_{e\ exp}$ (mg/g)	21.754	29.974	35.728	43.936	50.701
PFO kinetic model	298	k_1 (min^{-1})	0.0281	0.0418	0.0567	0.0321	0.0455
		q_{ecal} (mg/g)	7.975	5.438	12.591	21.713	21.211
		R^2	0.8097	0.7292	0.8696	0.8568	0.8854
	308	k_1 (min^{-1})	0.0243	0.0268	0.0465	0.0278	0.0442
		q_{ecal} (mg/g)	5.253	10.610	21.431	18.857	27.004
		R^2	0.8443	0.8325	0.8375	0.8124	0.8089
	318	k_1 (min^{-1})	0.0399	0.0248	0.0297	0.0174	0.0169
		q_{ecal} (mg/g)	14.430	16.029	9.953	7.278	17.326
		R^2	0.8518	0.8362	0.8662	0.7806	0.8009
PSO kinetic model	298	k_2 (min^{-1})	0.0335	0.0257	0.0209	0.0199	0.0185
		q_{ecal} (mg/g)	20.704	28.249	34.014	41.841	48.309
		R^2	0.9996	0.9998	0.9999	0.9998	0.9998
	308	k_2 (min^{-1})	0.0239	0.0181	0.0149	0.0147	0.0135
		q_{ecal} (mg/g)	21.097	30.488	35.842	44.053	49.751
		R^2	0.9997	0.9993	0.9987	0.9994	0.9997
	318	k_2 (min^{-1})	0.0196	0.0141	0.0106	0.0096	0.0031
		q_{ecal} (mg/g)	22.173	30.395	36.101	44.053	51.282
		R^2	0.9993	0.9988	0.9999	0.9999	0.9991
IPD kinetic model	298	k_{id} (mg/g.$min^{0.5}$)	0.7315	0.9251	1.0329	1.3567	1.6073
		C(mg/g)	11.578	17.409	21.871	25.298	28.792
		R^2	0.5292	0.4122	0.4004	0.4569	0.4752
	308	k_{id}(mg/g.$min^{0.5}$)	0.7492	1.2123	1.2809	1.5069	1.7196
		C (mg/g)	12.129	15.547	19.823	24.521	28.235
		R^2	0.5107	0.7418	0.5371	0.5363	0.5199
	318	k_{id}(mg/g.$min^{0.5}$)	0.7667	1.1427	1.2943	1.3904	1.8391
		C(mg/g)	12.323	13.066	22.131	27.167	27.022
		R^2	0.5405	0.7099	0.4488	0.4345	0.5851

Conclusions

This study investigated MB adsorption onto PCP. The data obtained demonstrate that MB adsorption increased with the increase in initial dye concentration, contact time, and temperatures. The dye adsorption capacity onto PCP changed from 40.99 to 95.24 mg/g, 41.56 to 97.93 mg/g, and 43.51 to 101.41 mg/g for 298K, 308K and 318K, respectively, while the initial MB concentration increased from 100 to 300 mg/l. For the removal of dye the equilibrium adsorption time was fixed to 100 min. Pine cones are significant to develop the processes of adsorption and separation. The high adsorption capacity of pine cones depends on chemical reactivity and the porosity of the functional groups on its surface. These functional groups which bind the molecules on the pine cones have been investigated in

previous studies. Although natural and modified PCP used in some previous studies as a biosorbent, the type of PCP used in this study is different.

The isotherm studies carried out the present study indicated that the Freundlich model presented a more suitable profile for MB adsorption onto PCP compared to the Langmuir and Temkin models. It was noted that the parameters of these three isotherm models increased with the increment in temperature and that adsorption was acceptable at higher temperatures. The R^2 values of all three isotherm models were found to be high. However, those of the Freundlich model were higher than the other two models. The monolayer adsorption capacity (q_m) of PCP was determined as 65.36, 66.67, and 68.52 mg/g for 298K, 308K, and 318K, respectively.

The kinetic studies determined that the rate-limiting step could be dye chemisorption. The R^2 coefficients were higher than 0.99 and the experimental and evaluated qe values very close to each other. The kinetic constants were near to the temperatures and the concentrations. The q_e values increased with the increase in MB concentration. The IPD constant (k_{id}) and monolayer concentration (C) values increased in line with the increase in temperature, revealing MB adsorption onto PCP.

The thermodynamic parameters demonstrate that MB adsorption onto PCP was endothermic. The absolute values of ΔG° decreased as temperature increased, proving that the separation process was constructive at low temperatures. The positive ΔS° value established an enhanced randomness in the solid–solute interface and the affinity of PCP for MB. In conclusion, all these results indicated that PCP may be used as an adsorbent for cationic dyes removal in wastewaters.

Information About Paper: *This study did not receive any specific grant from funding agencies in the public, commercial, or not-for-profit sectors. The authors declare that there is no conflict of interest regarding the publication of this paper.*

References

Allafchian A, Mousavi ZS, Hosseini SS, (2019) Application of cress seed musilage magnetic nanocomposites for removal of methylene blue dye from water, *Int. J. Biol Macromol.* **136**, 199-208.

Bedin KC, Martins, AC, Cazetta, AL, Pezoti, O, Almeida VC, (2016) KOH-activated carbon prepared from sucrose spherical carbon: Adsorption equilibrium, kinetic and thermodynamic studies for methylene blue removal. *Chem. Engin. J.*, **286**, 476-484.

Caparkaya D, Cavas L, (2008) Biosorption of methylene blue by a brown alga *Cystoseira barbatula* Kutzing. *Acta Chimia Slovakia*, **55**, 547-553.

Cherifi H, Fatiha B, Salah H, (2013) Kinetic studies on the adsorption of methylene blue onto vegetal fiber activated carbons. *Appl. Surf. Sci.*, **282**, 52-59.

Crini G, (2006) Non-conventional low-cost adsorbents for dye removal: A review. *Biores. Tech.*, **97**(9), 1061-1085.

Dawood S, Sen TK, (2012) Removal of anionic dye Congo red from aqueous solution by raw pine and acid-treated pine cone powder as adsorbent: equilibrium, thermodynamic, kinetics, mechanism and process design. *Water Res*, **46**(6), 1933-46.

Debnath S, Ballav N, Maity A, Pillay K, (2017) Competitive adsorption of ternary dye mixture using pine cone powder modified with β-cyclodextrin. *J. Molecular Liquids*, **225**, 679-688.

Demirak A, Keskin F, Şahin Y, Kalemci V, (2015) Removal of ammonium from water by cone powder as biosorbent. *Mugla J. Sci. & Tech.*, **1**(1), 5-12.

El-Sikaily A, Khaled A, El-Nemr A, Abdelwahab O, (2006) Removal of methylene blue from aqueous solution by marine green alga ulvalactuca. *Chemical Ecology*, **22**(2), 149-157.

Forgacs E, Cserhati T, Oros G, (2004) Removal of synthetic dyes from wastewaters: *A Rev. Environ. Int.*, **30**, 953-971.

Fu Y, Viraraghavan T, (2000) Removal of a dye from an aqueous solution by the fungus *Aspergillus niger*. *Water Quality Res.h J.*, **35**(1), 95-111.

Ghaedi M, Hajjati S, Mahmudi Z, Tyagi I, Agarwal S, Maity A, Gupta VK, (2015) Modeling of competitive ultrasonic assisted removal of the dyes – methylene blue and safranin-O using Fe3O4 nanoparticles. *Chem. Engine. J.*, **268**, 28-37.

Gouamid M, Ouahrani MR, Bensaci MB, (2013) Adsorption equilibrium, kinetics and thermodynamics of methylene blue from aqueous solutions using date palm leaves. *Energy Procedia*, (36), 898-907.

Gupta VK, Suhas, (2009) Application of low-cost adsorbents for dye removal – A review. *J. Environ. Manage.*, **90**, 2313-2342.

Hamed MM, Ahmed IM., Metwally SS, (2014) Adsorptive removal of methylene blue as organic pollutant by marble dust as eco-friendly sorbent *J. Ind. Eng. Chem.,* 20, 2370-2377.

Immaculate LA, Ouma EBN, Ofomaja AE, (2018) Thermodynamic, kinetic and spectroscopic investigation of arsenite adsorption mechanism on pine cone-magnetite composite. *J. Environ. Chem. Engine.*, **6**, 5409-5419.

Jian Z, Qingwei P, Meihong N, Haiqiang S, Na L, (2013) Kinetics and equilibrium studies from the methylene blue adsorption on diatomite treated with sodium hydroxide. *Appl. Clay Sci.*, **83**, 12-16.

Jin Y, Zeng C, Lü QF, Yu Y, (2019) Efficient adsorption of methylene blue and lead ions in aqueous solutions by 5-sulfosalicylic acid modified lignin. *Int. J. Biol. Macrom.*, **123**, 50-58.

Kausar A, Iqbal M, Javeda A, Aftab K, Nazli ZH, Bhatti HN, Nouren S, (2018) Adsorption Using Clay and Modified Clay: A Review. *Journal of Molecular Liquids*, **256**, 395-407.

Kul AR, Aldemir A, (2019) Comparison of Methylene Blue Adsorption Performance on Natural, Thermal and Acid Modified Kaolin: Isotherm, Kinetics and Thermodynamics Studies. *Fres. Environ. Bull.*, **28**(6), 4475-4483.

Kul AR, Koyuncu H, (2010) Adsorption of Pb(II) ions from aqueous solution by native and activated bentonite: Kinetic, equilibrium and thermodynamic study. *J Hazard Mater*, **179**, 332-339.

Kupeta AJK, Naidoo EB, Ofomaja AE. (2018) Kinetics and equilibrium study of 2-nitrophenol adsorption onto polyurethane cross-linked pine cone biomass. *J. Cleaner Produc.*, **179**, 191-209.

Mahmoodi NM, Hayati B, Arami M, Lan C, (2011) Adsorption of textile dyes on pine cone from colored wastewater: kinetic, equilibrium and thermodynamic studies. *Desalin.* **268**(1-3), 117-125.

Martín-Lara MA, Blazquez G, Calero M, Almendros AI, Ronda A, (2016) Binary biosorption of copper and lead onto pine cone shell in batch reactors and in fixed bed columns. *International J. Mineral Proces.* **148**, 72-82.

Miyah Y, Lahrichi A, Idrissi M, Khalil A, Zerrouq F, (2018) Adsorption of methylene blue dye from aqueous solutions onto walnut shells powder: Equilibrium and kinetic studies *Surfaces & Interf.,* **11** (1), 74–81.

Mtshatsheni KNG, Ofomaja AE, Naidoo EB, (2019) Synthesis and optimization of reaction variables in the preparation of pinemagnetite composite for removal of methylene blue dye. *South African J. Chem. Engin.*, **29**, 33-41.

Ofomaja AE, Naidoo EB, Modise SJ, (2009) Removal of copper(II) from aqueous solution by pine and base modified pine cone powder as biosorbent. *J Hazard Mater*, **168** (2-3), 909-17.

Ofomaja AE, Naidoo EB, Modise SJ, (2010) Biosorption of copper(II) and lead(II) onto potassium hydroxide treated pine cone powder. *J. Environ Manage*, **91**(8), 1674-85.

Ofomaja AE, Naidoo EB, (2010) Biosorption of lead(II) onto pine cone powder: Studies on biosorption performance and process design to minimize biosorbent mass. *Carbohydrate Polymers*, **82**(4), 1031-1042.

Rafatullah M, Sulaiman O, Hashim R, Ahmad A, (2010) Adsorption of methylene blue on low-cost adsorbents: a review. *J Hazard Mater*, **177**(1-3), 70-80.

Rida K, Bouraoui S, Hadnine S, (2013) Adsorption of methylene blue from aqueous solution by kaolin and zeolite. *Appl. Clay Sci.*, **83**, 99-105.

Salleh MAM, Mahmoud DK, WAW, AbdulKarim A, Idris A, (2011) Cationic and anionic dye adsorption by agricultural solid wastes: A comprehensive review. *Desalin.*, **280**(1-3), 1-13.

Yagub MT, Sen TK, Afroze S, Ang HM, (2014) Dye and its removal from aqueous solution by adsorption: a review. *Adv Collo. Inter.e Sci*, **209**, 172-84.

J. Int. Environmental Application & Science, Vol. 14(4): 193-198 (2019)

Research Paper

Sustainable Domestic Solid Waste Management in Jeddah, Saudi Arabia

Durmus Kaya*

Kocaeli University, Technology Faculty, Energy Systems Engineering, Kocaeli, Turkey

Received September 11, 2019; Accepted December 02, 2019

Abstract: In Saudi Arabia, as a result of rapidly developing population, urban development, demands for more prosperous life and technological developments, the amount of wastes generated, and the amount of these wastes are rapidly increasing. Methods used in today's conditions for removing these domestic wastes; irregular solid waste storage and solid waste storage. In this study, the establishment of a modern waste recovery facility instead of solid domestic waste storage and the technical and economic calculations of the energy production installation of this facility are examined. Such an integrated recycling system has been determined by means of technical and economic analysis of the average composition of the organic matter content of Jeddah (paper, plastic, glass, metal) and the amount of waste that can be disposed of waste disposal and power generation facilities. Based on these technical data; The main investment cost determined for the start of the facility is 201.096.000 USD. The annual income of the plant is 122.033.960 USD and the expense of the plant is 14.733.088 USD and the net income of the plant is predicted to be 107.300.872 USD. Finally, the simple repayment period for this investment was calculated as 1.87 years.

Keywords: *Household waste, obtaining energy from biogas and /or wastes, recycling*

Introduction

All kinds of environmental problems that we have to deal with today and the reasons and the actual sources of these problems are very different from each other. If we define the main causes of environmental problems; rapid migration from rural to urban, urbanization and poorly planned industrialization. Rapidly developing population, industrial development and distorted urbanization cause quite a lot of waste problems. Today, one of the most important environmental problems is the waste management generated by the various activities of the public. The problem of waste problems must be completely solved and managed. (Kaya *et al*., 2009, Kaya *et al*., 2008, Bascetincelik *et al*., 2009, Bascetincelik et al., 2009, Kaya et al., 2008, Recebli et al., 2015, Ozkaymak et al., 2016, Koymatcika *et al*., 2018, Abu-Qudais & Abu-Qdais, 2000, Morris & Waldheim, 1998).

Solid waste problems caused by human activities and methods used to solve these problems; domestic storage, waste storage, composting, recycling and incineration activities that are not carried out within a specific plan. In the Landfill Directive (1999/31 / EC) (Waste Management Action Plan, 2008-2012), one of the EU Landfill Directives has identified its technical requirements for the regular storage of wastes, and fully eliminates or minimizes the impacts of waste on the environment to carry out storage activities. The primary waste management method will be to minimize the waste generated by our separation at the waste source. Secondary method; recycling and / or composting methods will also be combined to produce bio-energy from wastes. Although methods such as incineration and solid waste management are acceptable workarounds for solid waste, these methods are at the bottom of the priority list. Bioenergy generation from waste and compost, recycling and re-use of resources are the highest solution types (Erdem *et al*., 2010, Ekinci *et al*., 2010, Yaldiz *et al*., 2011,).

In this study, technical and economical domestic and / or solid waste recovery, waste disposal and feasibility study of an energy production facility using these solid wastes were carried out. As a result, in an average household waste composition of Jeddah municipality, the amount of recyclable waste and the content of organic materials were found. In the light of this information; possible initial investment cost, estimated annual income, annual expenditure and estimated amortization period are determined.

Basic Materials and Applied Methods

Applied Steps: In the first stage, domestic waste comes from its sources to dissolution and treatment plants. This step follows the other step in which solid waste is reduced into dimensionally smaller pieces

* *Corresponding: E-Mail: durmuskaya@hotmail.com; Tel:+902623032287; Fax: +902623032203*

into organic and recyclable pieces. Organic parts are sent to be converted into biogas or fertilizer in fermentation units (wet or dry fermentation). Biogas is used to produce the electricity via gas engine and generator group is supplied to the city network, the rest can be used for various needs in the plant. In addition, some of the heat produced from biogas can be used for fermentation and heating, while the rest can be used for heating of residential areas, buildings, kindergartens, schools, hospitals, public places and heating greenhouses. The flowchart of solid waste recovery, waste disposal and energy generation facility from waste is shown in Figure 1.

Figure 1. Solid / domestic waste recovery, recycling and flow chart of the power plant.

In the recycling section, first all the metals are taken up magnetically and each of the waste such as plastic, paper, glass is separated into groups, the rest of which is also separated into another group. For plastic wastes, they are first separated according to their types and then converted to burrs, finally plastics that are converted to a granular form can be made into secondary raw materials for the economy. On the other hand, one of the methods used by glass manufacturers for energy saving is the recovery of used glass bottles. Broken glasses are melted together with other raw materials for recovery. The more intense glass is used in the furnace; the less heat is required for the process. When the glass products used in the melting furnace are melted, there is a 25% reduction in energy consumption. For recycled paper, the paper fibres are separated in water to be prepared in the paper slurry. If desired, fibre-free impurities and particles are removed from the mixture, as a result, the paper fibres prepared for processing may be used in the production of recycled paper.

Determination of the Amount and Composition of Solid or Household Wastes

The amounts of the Jeddah municipality recyclable wastes were obtained by using domestic solid wastes and the composition amounts of these wastes. In the calculation of waste amount, the population of Jeddah municipality was taken as 3.500.000 people, the amount of waste produced per day was considered as 1.5 kg and all calculations were made considering that the annual waste amount would be approximately 1.900.000 tons. The basic waste composition and the amount of recyclable waste for the calculations are shown in Table 1.

Table 1. Solid Waste compounds and amounts to be recycled referenced in calculations in according to product groups

The product group for Waste Composition	The Amount of Waste in according to product group (%)	Quantity of Recyclable Waste (Ton/Year)
Paper and carton	20	380,000
Plastic	15	285,000
Glass	2.9	55,100
Metal	1.9	36,100
Aluminium	0.80	15,200
Wood	1.98	37,620
Textile	1.93	36,670
Leather	0.3	5,700
Organic Waste	48	912,000
Other	7.14	136,610

Incomes

Paper Incomes: In this facility, 380,000 tons of paper waste of different types will be recycled annually. Considering that 1 ton of paper is 125 US Dollar in this recycling process:

$$\text{Annual Earnings} = \frac{380{,}000 \text{ tons of paper}}{\text{a year}} \times \frac{125 \text{ US Dollar}}{1 \text{ ton of paper}} = 47{,}500{,}000 \$$$

Plastic Incomes: In this facility, 285,000 tons of plastic waste of different types will be recycled annually. Considering that 1 ton of plastic is 95 US Dollar in this recycling process:

$$\text{Annual Earnings} = \frac{285{,}000 \text{ tons of plastic}}{\text{a year}} \times \frac{95 \text{ US Dollar}}{\text{a ton of plastic}} = 27{,}075{,}000 \$$$

Glass Incomes: In this facility, 55,100 tons of glass waste of different types will be recycled annually. Considering that 1 ton of glass is 60 US Dollar in this recycling process:

$$\text{Annual Earnings} = \frac{55{,}100 \text{ tons of glass}}{\text{a year}} \times \frac{60 \text{ US Dollar}}{\text{a ton of glass}} = 3{,}306{,}000 \$$$

Metal Incomes: In this facility, 36,100 tons of metal waste of different types will be recycled annually. Considering that 1 ton of metal is 240 US Dollar in this recycling process:

$$\text{Annual Earnings} = \frac{36{,}100 \text{ tons of metal}}{\text{a year}} \times \frac{240 \text{ US Dollar}}{\text{a ton of metal}} = 8{,}664{,}000 \$$$

Aluminium Incomes: In this facility, 15,200 tons of aluminium waste of different types will be recycled annually. Considering that 1 ton of aluminium is 1000 US Dollar in this recycling process:

$$\text{Annual Earnings} = \frac{15{,}200 \text{ tons of metal}}{\text{a year}} \times \frac{1.000 \text{ US Dollar}}{\text{a ton of metal}} = 15{,}200{,}000 \$$$

The Electrical Energy Incomes: We have assumed that the annual amount of organic waste is 912,000 tons and the daily use of these organic wastes is 2,500 tons. In the light of the information that we can obtain 140 m³ biogas from 1 ton of organic waste;

$$\text{The annual amount of produced biogas} = 912{,}000 \times 140 = 127{,}680{,}000 \text{ m}^3$$

$$\text{The annual production of electric} = 2.1 \times 127{,}680{,}000 = 268{,}128{,}000 \text{ kWh}$$

$$\text{Electric power of the facility} = \frac{268{,}128{,}000}{8{,}000} = 33{,}516 \text{ kWe}$$

Considering that one kWh of electricity is 7 $ cents and 8000 hours of work per year, the other detail calculations are as follows:

$$\text{Electrical Incomes} = 268{,}128{,}000 \text{ kWh} \times \frac{0.07 \text{ Dollar}}{\text{kWh}} = 18{,}768{,}960 \$$$

Thermal Energy Incomes: The annual thermal energy will be equal to the annual electricity amount.

$$\text{Thermal energy incomes} = 0$$

Carbon Trading: $\text{Carbon trading income} = \text{Built} - \text{in capacity (kW)} \times \text{Working hours} \times \text{Green certificate fee} \left(\frac{0.00 \text{ Euro}}{\text{kWh}}\right)$

$$\text{Carbon trading income} = 3{,}734.64 \text{ kW} \times 8{,}000 \text{ h} \times 0.00 \left(\frac{\text{USD}}{\text{kWh}}\right) = 0$$

Compost Incomes: An annual compost product of 304,000 tons will be obtained. This product is taken into account as 5 Euro per tonne

$$\text{Compost revenues} = \frac{304{,}000 \text{ a ton}}{\text{a year}} \times \frac{5 \text{ US Dollar}}{\text{a ton}} = 1{,}520{,}000 \$$$

$$\text{Total Revenues} = \frac{122{,}033{,}960 \$}{a \; year}$$

Spending

Facility Maintenance Spending: It is decided that the possible maintenance costs of the facility should be 2% of the total investment cost. Therefore,

$$\text{The maintenance spendings for one year} = 201{,}096{,}000 \times \frac{2}{100}$$

$$\text{The maintenance spendings} = 4{,}021{,}920\ \$$$

Insurance and Taxes: Insurance and taxes can be taken into account as 0.5% of the total investment cost. Thus, spending on annual insurance and taxes are 1,005,480 $.

Workmanship: Taking into account that an employee of 200 people and all expenses of each employee including tax and insurance is 1500 USD, the total labour expenses are 3.600.000 USD.

Transportation Spending

For transportation costs, 0.25 $ per ton is foreseen at the facility; therefore, the total annual expenditure is 475,000 $.

Domestic Consumption of Electricity Costs: 30% of the electricity generated from waste recovery in the facility was considered suitable for the consumption of the facility. Therefore, the total cost of electricity consumption of the facility is 5,630,688 USD.

Installation Cost

In this facility, where 1 kW power is 6000 USD and total investment cost is 201.096.000 USD, all income and expenses are listed above and also listed in Table-2 below.

Table 2. Incomes & Spending for the facility

Component of Facility	Calculation Technique	Example	Cost	Unit
Installation Sum	Built-in capacity (kW) * investment spending ($/kW)	3734.64 kWe×6,000 USD	201,096,000	Dollar ($)
		Spending		
Facility maintenance expenses	(Total investment spending) * % 2	18,673,200 $ 2%	4,021,920	$/yearly
Insurance and taxes	Total investment spending× % 0.5	18,673,200 $ × 0,5%	1,005,480	$/yearly
Workmanship	Person× 12 Months × 1.500 €	20 ×12×1500 $	3,600,000	$/yearly
Onsite transportation costs	Transportation spending	1,5 $/ton/yearly × 180,000 tons	475,000	$/yearly
Domestic consumption of electricity Costs	Production power×%30× Annual working hours × cost	3734.64×0,30×8,000×0.10	5,630,688	$/yearly
Annual total sum		14,733,068		$
		Incomes		
Electricity for sale	Built-in capacity (kW) × (%80) Working hours × The price of electricity	3734.64 kW × (8,000 h × 0.10 €/kWh	18,768,960	$/yearly
Carbon trading	Built-in capacity (kW) × Working hours × Green certificate fee	3734.64 kW × 8,000 h × × 0.01 €/kWh	0	$/yearly
Heat usage	Heat of cogeneration (kW) × Working hours × 0,01 €/kWh	3734,64 kW × 8,000 ×0.01 €/kWh	0	$/yearly

Organic fertilizer for sale	20,000 (t/a year) × 5 €/t	50,000 t/yearly × 5 €/t	1,520,000	$/yearly
Paper incomes	Sum for one year × 30 €/t	4,320 t/yearly × 30 €/t	47,500,000	$/yearly
Plastic incomes	Sum for one year × 100 €/t	6,840 t × 100 €/t	27,075,000	$/yearly
Glass incomes	Sum for one year × 17,5 €/t	3,780 ton× 17.5 €/ton	3,306,000	$/yearly
Metal incomes	Sum for one year × 125 €/t	3,060 ton×125 €/ton	8,664,000	$/yearly
The annual total incomes		122,033,960		$
The annual profit	(Incomes-Spending) /a year	(122,033,960-14,733,068) USD/a year	107,300,872	$
Amortization period (for one year)	Total investment sum / Annual profit	201,096,000/ 107,300,872	1.8741 (≈22,5 months)	a year

Conclusions

In this study, detailed feasibility studies of the waste recovery and storage project of Jeddah Municipality have been made in terms of technical and economic aspects and related cost analyses have been presented for the facility. In the light of all this information, the following findings are summarized.

*As a result of the establishment of a waste recovery or recycling facility instead of landfill, household wastes of a municipality will be separated at their source as much as possible and then become economical materials such as glass, metal, paper and plastic. Thanks to recycling, biogas and fermented fertilizer production will be realized from organic wastes. After these processes, electricity and heat can be produced from biogas and thus there will be no need for regular storage of municipal wastes.

*Thanks to the technology proposed in this study, separation of wastes can be achieved, recycled materials can be sold as a result of recycling, compost production can be provided from biogas and organic wastes, electricity and hot water will be produced from the biogas produced. Approximately 30% of the total electricity and heat generation produced in the facility can be used as energy within its own structure and the other 70% can be sold.

*The main investment sum of the facility is predicted to be 201.096.000 USD, the annual income of the facility is estimated to be 122.033.960 USD, the expense of the facility is 14.733.088 USD and the net revenue of the facility is predicted to be 107.300.872 USD. In this case, the repayment period for the investment was predicted as 1.87 years (≈ 22.5 months)

Acknowledgment: *With great thanks to King Abdulaziz University (KAU), Jeddah and Saudi Arabia who contributed to this study and the publication of the article.*

References

Erdem AM, Cubukcu EE, Erdogan D, (2010) Biomethanization Technology in Munucipial Solid Waste Management, 2sd International Waste Technologies Symposium and exhibition (IWES), 04-05th November, Istanbul, pp: 13-17, (in Turkish).

Kaya D, Cagman S, Coban V, Yagmur A, Eyidogan, M, Akgun F, Tiris M, (2009) Biogas production via dry fermentation Technology, *1st International Waste Technologies Symposium and exhibition (IWES*), 12-13th September, Istanbul, pp 63-66.

Kaya D, Kilic FC, Baban A, Dikec S, (2008) Administrative, institutional and legislative issues on agricultural waste exploitation in Turkey, *Renew. & Sustain. Energy Rev*., **12** (2), 417-436.

Bascetincelik A, Ozturk HH, Ekinci K, Kaya D, Kacira M, Karaca C, (2009) Strategy Development and Determination of Barriers for Thermal Energy and Electricity Generation from Agricultural Biomass in Turkey, *Energy Explor. & Explo*., **27**(4), 277-294.

Bascetincelik, A., Ozturk, HH, Ekinci K, Kaya D, Kacira M, Karaca C, (2009) Assessment of the Applicability of EU Biomass Technologies in Turkey, *Energy Explor.n & Explo*., **27**(4), 295-306.

Kaya D, Kilic FC, (2012) Renewable Energies and Their Subsidies in Turkey and some EU countries-Germany as a Special Example, *J. Int. Environ. Appl. & Sci.,* **7** (1), 114-127.

Ministry of Environment and Forest, General Directorate of Environmental Management, *Waste Manage. Action Plan,* 2008-2012.

Ekinci K, Külcü R, Kaya D, Yaldız O, Ertekin C, Öztürk HH, (2010) The Prospective of Potential Biogas Plants That Can Utilize Animal Manure in Turkey, *Energy Explor. & Explo*., **28** (3), 187-206.

Yaldiz, O, Sozer S, Caglayan N, Ertekin C, Kaya D, (2011) Methane Production from Plant Wastes and Chicken Manure at Different Working Conditions of One-Stage Anaerobic Digester, *Energy Sour., Part A: Recov., Util., & Enviro. Effect,* **33**(19), 1802-1813.

Recebli Z., Selimli S., Ozkaymak M., Gonc O., Biogas Production from Animal Manure, Journal of Engineering Science and Technology. 10, (**6)**, 722–729, 2015.

Ozkaymak M, Selimli S, Kaya D., Uzun U, (2016) Searching the fertility potential of iron and steel industry blast furnace slag, *World J. Engin.*, 13 (6), 482-486,.

Koymatcika C, Ozkaymak M, Selimli S, (2018) Recovery of iron particles from waste water treatment plant of an iron and steel factory, *Engine. Sci. & Tech., Int. J.*, **21**(3), 284-288,.

Abu-Qudais M, Abu-Qdais HA, (2000) Energy content of municipal solid waste in Jordan and its potential utilization, *Energy Conv. & Manga*., **41** (9), 983-991.

Morris M, Waldheim L, (1998) Energy recovery from solid waste fuels using advanced gasification technology, Wa*ste Management*, **18** (6-8), 557-564.